SEISMIC EVALUATION OF PORTAGE CREEK BRIDGE BASED ON AMBIENT VIBRATION TESTING

by

Yu Feng

B.Sc., Tianjin University, 2013

A THESIS SUBMITTED IN PARTIAL FULFILLMENT OF

THE REQUIREMENTS FOR THE DEGREE OF

MASTER OF APPLIED SCIENCE

in

THE FACULTY OF GRADUATE AND POSTDOCTORAL STUDIES

(Civil Engineering)

THE UNIVERSITY OF BRITISH COLUMBIA

(Vancouver)

April 2016

Abstract

Constructed in 1983, the Portage Creek Bridge is a three span highway bridge located in Victoria, British Columbia (BC), Canada. This bridge is a part of a smart seismic monitoring program, British Columbia Smart Infrastructure Monitoring System (BCSIMS), which funded by the British Columbia Ministry of Transportation and Infrastructure (MoTI), Canada. The BCSIMS aims to continuously monitor the seismic conditions of the selected bridges on lifeline highways in British Columbia, and as part of this goal, an ambient vibration test was carried out on the bridge in September 2014 in order to update/calibrate the finite element model of the bridge in SAP2000.

The updated model was then used to assess the seismic performance of the bridge in accordance with the Canadian Highway Bridge Design Code, 2015. Nonlinear time-history analysis was performed using a finite element model with concentrated plasticity, and results were compared with the performance criteria specified in the code. This thesis presents the overall procedure of the seismic evaluation, as well as the relevant theoretical background and discussion of analysis results.

Preface

The research work in this thesis is mainly an individual project under the supervision of Yavuz Kaya and Carlos Ventura. I developed the finite element model for seismic analysis and conducted all the data processing as well as the results discussion. The Ambient Vibration Testing described in Chapter 3 was carried out by a research group led by Yavuz Kaya who also provided a lot of advice for this research. The original idea for this research was proposed by Carlos Ventura and he also provided invaluable guidance and discussion throughout the study.

The contents of Chapter 3-5 in this thesis was presented at the 34th International Modal Analysis Conference (IMAC) and will be published in the book "*Dynamics of Civil Structures, Volume 2 - proceedings of the 34th IMAC, A Conference and Exposition on Structural Dynamics, 2016*", with the title "Finite Element Model Updating of Portage Creek Bridge". I prepared all the manuscript for this paper. Yavuz Kaya and Carlos Ventura edited the manuscript and provided a lot of guidance.

Table of Contents

List of Tables

List of Figures

Acknowledgements

First of all, I would like to thank my thesis supervisor Dr. Carlos Ventura, for providing me the opportunity to join his warm research group and work on this interesting research project. His continuous support and guidance helped me in all the time of research. He also granted my access to hardware and software to conduct the research, and helped me to secure the financial support for my study in UBC.

I would also like to thank my co-supervisor: Dr. Yavuz Kaya. He provided a lot of invaluable advice to the technical details for this research. I would never accomplish the thesis without his insightful comments and encouragement. The door to Yavuz's office was always open whenever I had questions about my research work.

My sincere thank also goes to my labmates in Earthquake Engineering Research Facility, especially to Xiang Li, Yuxin Pan, Felix Yao and Michael Fairhurst who have provided precious technical supports throughout this research project. They also inspired and motivated me during my life at UBC.

British Columbia Ministry of Transportation provided the funding for this research, as part of the BC Smart Infrastructure System (BCSIMS) project

Special thanks to my parents and all my friends in and out of UBC, without whom I would never accomplish all of this.

To My Parents

Chapter 1: Introduction

1.1. General

The BCSIMS is comprehensive seismic monitoring program that integrates the Strong Motion Network (SMN) and the seismic Structural Health Monitoring (SHM) network in British Columbia (BC). The program was initiated in 2009 and involves fifteen structures (fourteen bridges and one tunnel) that are currently being monitored in real-time. One of the main intentions of the SHM network is to mitigate the seismic risk in bridges in BC by continuously assessing the seismic condition of the bridges, and it is done using the tools and techniques that have been developed over the last six years.

The Portage Creek Bridge is located in Victoria on the Vancouver Island, BC, Canada at 48°27′53″N and 123°23′55″W geographic coordinates and is part of the BCSIMS project. The bridge is built in 1983 and was undergone a seismic retrofit by International School of Interdisciplinary Studies (ISIS) Canada in 2003 that included the implementation of Fiber Reinforce Polymer (FRP) wraps to strengthen the short columns.

As part of the BCSIMS project, seismic evaluation was performed for Portage Creek Bridge, based on nonlinear time history analysis with selected ground motions. Structural conditions were assessed in accordance with the new Canadian Highway Bridge Design Code (CSA S06-14) which was released in 2014, by Canadian Standard Association (CSA). It incorporated new provisions for seismic evaluation of existing bridges.

In order to make the seismic evaluation more reliable, Ambient Vibration Testing (AVT), which is a non-destructive vibration testing technique aiming to identify the dynamic characteristics of structures, was carried out by a research group in Earthquake Engineering Research Facility (EERF) at UBC. The finite element model used for seismic evaluation was calibrated based on the dynamic characteristics obtained from AVT.

1.2. Objective of the study

This research is part of BCSIMS project and has three main objectives:

1. Identify the dynamic characteristics (modal frequency, damping ratio, and mode shape) of Portage Creek Bridge based on the AVT results carried out in September, 2014.
2. Carry out seismic evaluation for Portage Creek Bridge in accordance with the new Canadian Highway Bridge Design Code, 2014 (CSA S06-14). Design guide about this new code and relevant engineering practice is still limited, so this research will provide engineers a reference for other projects on seismic evaluation of bridges in BC.
3. The structural information and evaluation results will be added to the BCSIMS bridge database and displayed on the Structure Information Page (SIP) on BCSIMIS website which makes the bridge status open to public.

1.3. Thesis organization

This thesis is organized in nine chapters. The current chapter is a brief introduction of research background and objective. The content of the research is arranged into the following chapters: Chapter 2 presents the description of the bridge including the general information of the bridge and a detailed description of the bridge geometry as well as the main structural members. Chapter 3 elaborates the procedure of Ambient Vibration Testing and introduces how the dynamic characteristics were obtained through modal analysis. Dynamic characteristics of the bridge are also presented in this Chapter 3. Chapter 4 to Chapter 6 present the details of finite element model for seismic evaluation, as well as the procedure of model updating. Chapter 7 elaborates the procedure of selecting ground motions for seismic analysis. A target spectrum was determined first and ground motion records were selected from EERF strong motion database and scaled to match the target spectrum. Chapter 8 presents the seismic evaluation procedure indicated in CSA S06-14. Since the provisions about seismic evaluation are very general in the code and are not easy to be practiced, a practical methodology for seismic evaluation is proposed in this chapter based on the code provisions. Chapter 9 & 10 present the analysis methods and results, as well as the conclusion of seismic evaluation.

Chapter 2: Description of Bridge

2.1. Overview

Portage Creek Bridge, designed and owned by BC Ministry of Transportation, is a disaster-route bridge located in city of Victoria, BC, Canada. It crosses Interurban Road at McKenzie Avenue, as shown in figure 2-1.

(a) (b)

Figure 2-1: Location (a) and view (b) of Portage Creek Bridge

The bridge was designed in 1982, which is long before the introduction of current seismic design standards. Dynamic analysis was performed and seismic retrofit was carried out by ISIS Canada in 2003 to make the bridge meet the seismic design requirement in that era. Most of the bridge was retrofitted by conventional materials and methods. An innovative retrofit technique-Fiber Reinforce Polymer Wraps (FRPs) was applied to strengthen the short column for shear without increasing the moment capacity. (Huffman et al. 2006) With the structural aging and introduction of new seismic design provisions over past decade, the bridge is in need of a re-assessment of seismic performance to determine whether a further retrofit is needed.

2.2. Superstructure

The superstructure of the bridge is concrete-steel hybrid structure (with concrete decking and steel girder), with a total length of 125m. Reinforced concrete deck is supported by 3 steel girders and 4 steel stringers. (Figure 2-3) Girders and stringers are connected by steel beams spaced at every 5 meters. (Figure 2-4) Since the bridge is located in seismic zone and requires a high resistance to lateral load, steel bracings are assigned

to the superstructure to provide additional lateral force resistance (Figure 2-3). The deck has a slope of 5.33% and a roadway width of 16m (52ft) with two 1.78m (6’6’’) sidewalks and aluminum railings. Cross-section of the concrete deck has a uniform thickness of 222.45mm along the bridge. Steel girders have I-shape cross section with web height of 2514.6mm. Web thickness, flange width and thickness are changing over the length of the bridge: the web thickness is ranging from 12.7mm (1/2in) to 15.875mm (5/8in); flange thickness is ranging from 25.4mm (1in) to 50.8mm (2in); and flange width is ranging from 457.2mm (18in) to 762mm (30in). Floor beams at the south and north end of the bridge have web section of 914.4mm×9.525mm (Height × Thickness) and flange section of 254mm×19.05mm (Width × Thickness). For other floor beams, the webs are same as those of the end beams while the flange section is 355.6mm×19.05mm. Stringers and bracings adopt the standard beam section of W21×55 and WT7×21.5, respectively. Detailed section sizes are shown in Appendix.

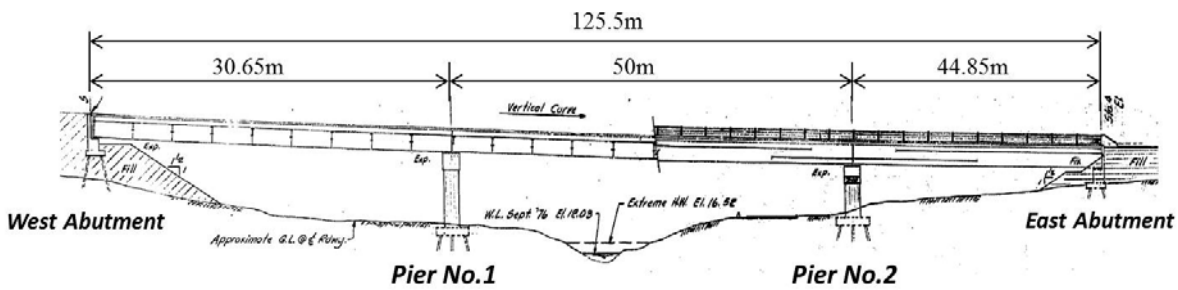

Figure 2-2: Elevation of Portage Creek Bridge

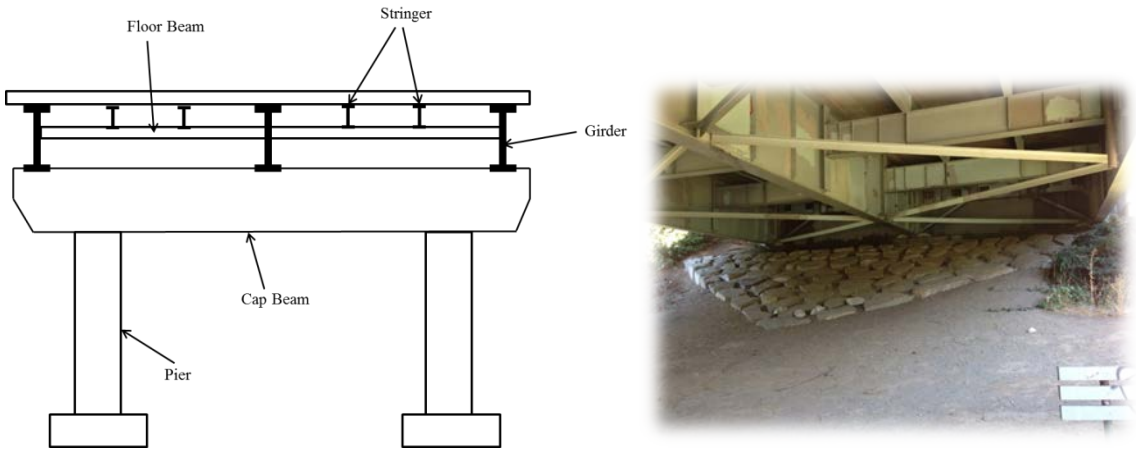

Figure 2-3: Cross-section of Portage Creek Bridge and location of bracing

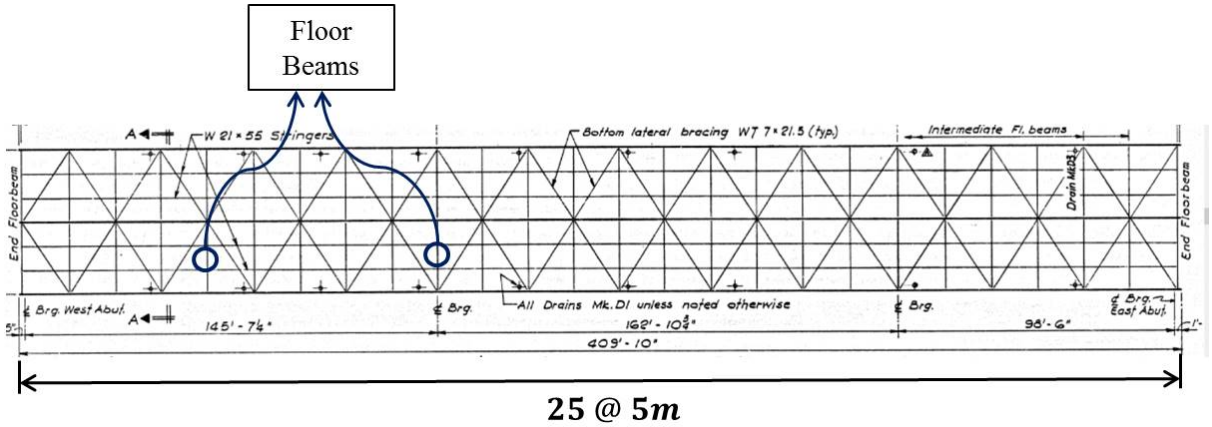

Figure 2-4: Spacing of floor beams

2.3. Substructures

Two sets of double-pier bents support the superstructure at 30.65m and 80.65m from the west end of the bridge, which divide the bridge into 3 spans. (Figure 2-2) All the piers have the same circular section with diameter of 1676.4mm. (Figure 2-5) Twenty-two 33M longitudinal reinforcement bars are evenly spaced around the section with cover thickness of 50.8mm (2in). 15M transverse reinforcement bars are spirally spaced at 76.2mm (3 in), as shown in figure 2-4. Pier No.1 has a height of 8.5m and pier No.2 is 5.8m in height (figure 2-2). Piers and steel girders are connected by reinforced concrete cap beams with 177.8mm×152.4mm rectangular cross section (figure 2-5). The cap beams have the same cross sections at Pier No.1 and Pier No.2. At the west and east end, the bridge is supported by reinforced concrete abutment. The bridge is founded on concrete footings with steel batter piles. The concrete footings have a uniform thickness of 1524mm (5ft). Arrangement of piles is shown in Figure 2-5. The piles adopt H-shape steel section HP12×53. The outer piles (piles around the perimeter of the footing) have a batter of 3:12 Pile batter for all other piles are 2:12.

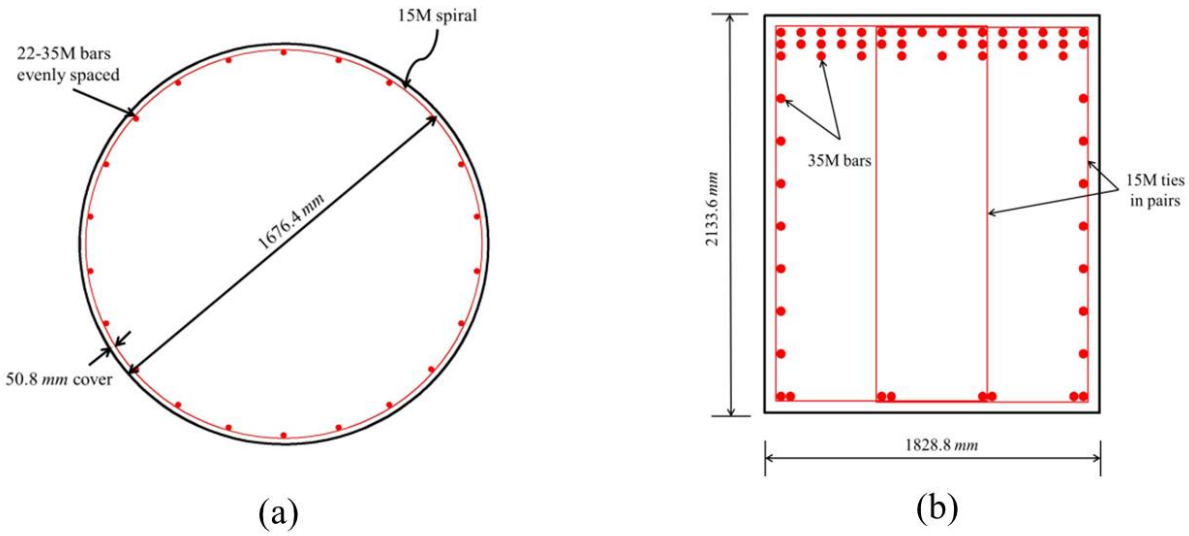

Figure 2-5: Cross-sections of (a) piers and (b) cap beams

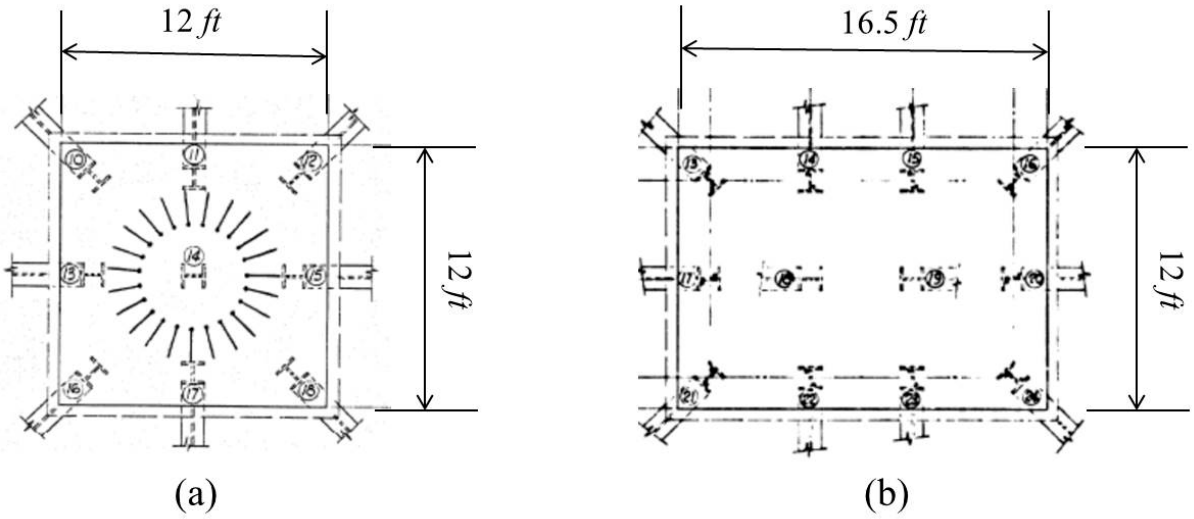

Figure 2-6: Arrangement of pile group for pier No.1 (a) and pier No.2 (b)

2.4. Bearing

Steel girders are connected to cap beams and abutments by elastomer bearings. The bearings are designed to dissipate energy during earthquake and hence improve seismic resistance of the bridge. Expansion bearings are adopted at west abutments, pier No.1 and pier No.2. Fix bearings are used at east abutment. Typical expansion bearing is shown in Figure 2-7. More bearing details are shown in Appendix. It can be seen that the vertical movement is totally restricted due to the existence of steel bolt. For longitudinal direction (the

direction parallel to the bridge layout line), the movement is allowed within a distance varying for different bearings (from 3 inches to 7 inches, see Appendix). For transverse direction (the direction perpendicular to bridge layout line), the movement is also allowed because the width of slotted hole (1.625 inches) is larger than the diameter of bolt (1.25 inches).

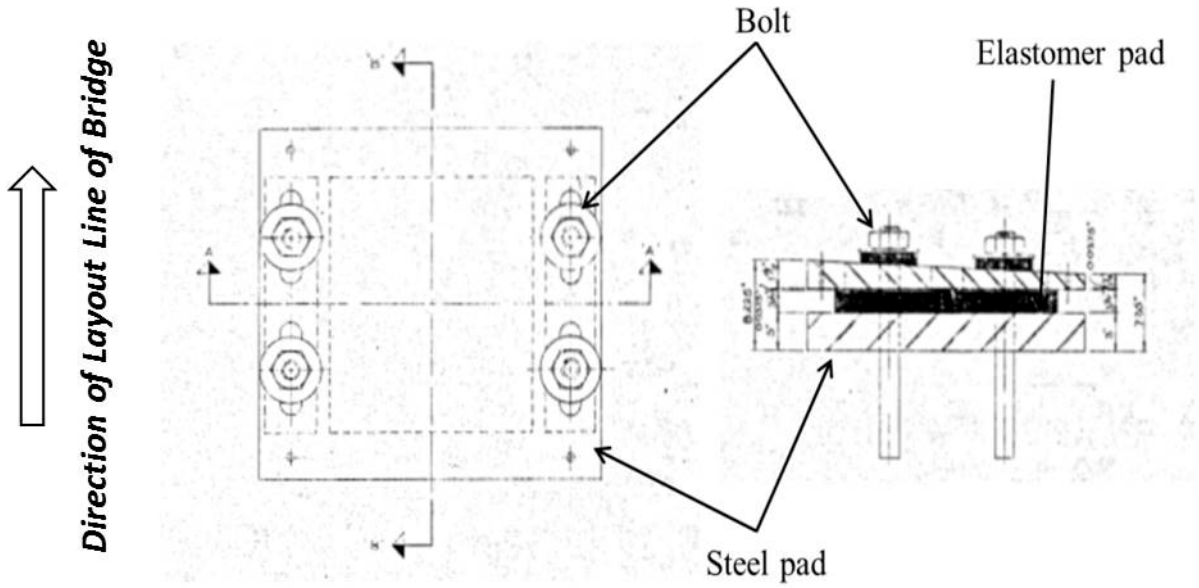

Figure 2-7: Typical expansion bearing

Chapter 3: Description of Ambient Vibration Test

3.1. Introduction to ambient vibration test and TROMINO

Ambient Vibration Test (AVT) is a non-destructive test aiming to record dynamic response of structure when no severe excitation is applied. Data collected from AVT could be processed to obtain modal information of tested structure, which is crucial in many research areas including seismic rehabilitation of existing structures and finite element model updating, etc.

Structural vibration sensor called TROMINO (figure 3-1) is used to carry out the AVT of Portage Creek Bridge. TROMINO sensor is widely used in Earthquake Engineering Research Facility (EERF) at the University of British Columbia to study dynamic characteristics of existing structures. The original idea behind TROMINO was to produce a truly portable system sensitive enough to capture the average noise level in the range of frequency of engineering interest. In fact, the sensor also allows one to measure the large and potentially dangerous vibrations in buildings and structures. TROMINO is an almost pocketable instrument with miniaturization (10×14×8cm) and lightweight (1.1 kg), ultra-low energy consumption and total absence of external cables, which leaves the wave field virtually unperturbed.

This sensor is a combination of two sets of 3 orthogonal high-resolution electrodynamic sensors: high gain and low gain velocimeters, and one set of 3 orthogonal digital accelerometers with frequency range from 0.1 to 300 Hz. (MoHo s.r.l 2011) TROMINO is powered by two 1.5V alkaline batteries and could keep working for 80 hours at sampling rate of 128 Hz.

Since the sensors are recording vibration independently at different locations of a structure, synchronization between sensors needs to be ensured during the test. For TROMINO, there are two ways of synchronizing the sensors: GPS and radio. There is an internal GPS in each sensor. When GPS synchronization is selected, internal clock of sensors will be adjusted to consist with the clock of GPS satellite. An external GPS receiver can be connected to the sensor to strengthen the signal receiving capacity. Radio is another option to synchronizing the sensors, which allows all the sensors to start and stop at the same time. An external radio receiver is needed to ensure wireless connection between sensors, as shown in Figure 3-1.

Figure 3-1: TROMINO sensor with radio receiver

3.2. Test setup

AVT was carried out on Sunday, September 7th, 2014. Radio synchronization was selected for this test. TROMINO sensors were placed on the sidewalk heading to the east end of the bridge with the radio receiver on the concrete railing, as shown in figure 3-1.

32 testing points are selected at different locations, with 30 points on the bridge and 2 points around the pier. The test was divided into 5 groups (i.e. 5 setups). 8 sensors were used for each setup and one of them is reference sensor placed at the mid-span of the bridge and remains unmoved when changing setups. Sensor locations of the 5 setups are highlighted in figure 3-2. The test last from 14:25 pm to 17:34 pm, with acquisition length of 30 min for each setup and a sampling rate of 128 Hz. Table 3-1 summarizes the start and stop time for each setup.

Table 3-1: Start and stop time for each test setup

Setup No.	Start Time	Stop Time
1	14:25:35	14:57:01
2	15:01:09	15:32:34
3	15:41:49	16:12:37
4	16:18:01	16:48:18
5	17:02:50	17:34:49

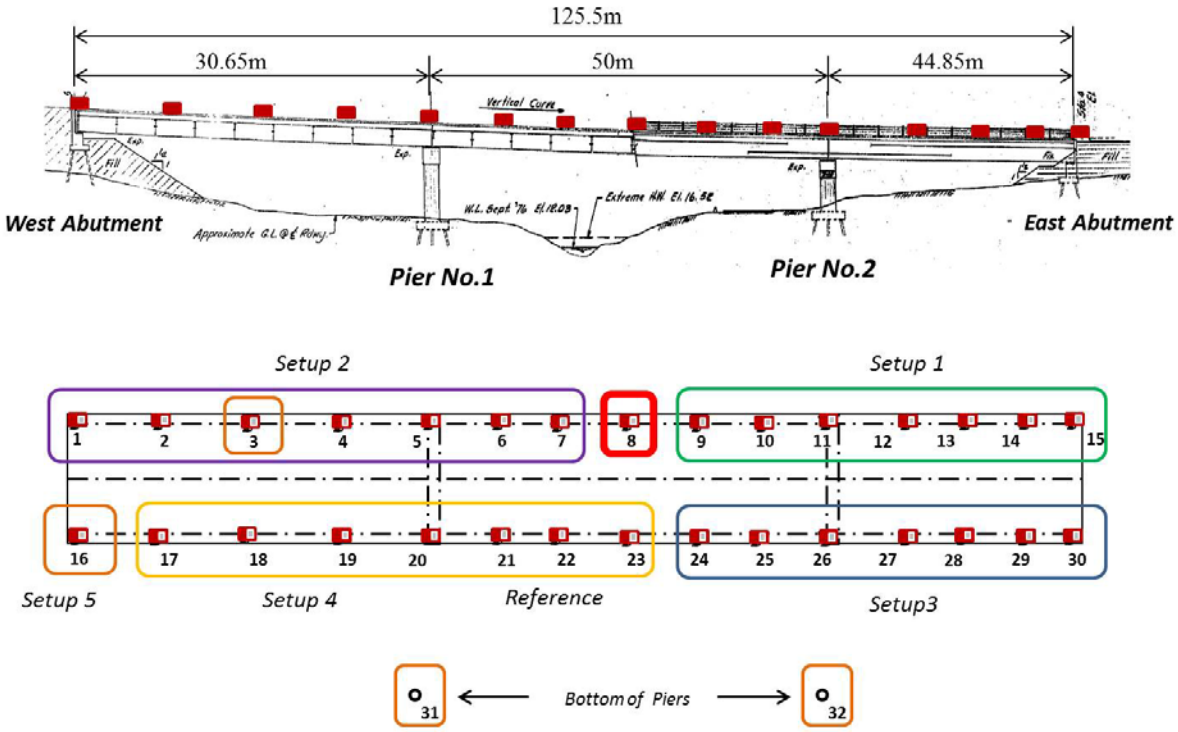

Figure 3-2: Locations for all test setups

3.3. Data output and synchronization

Raw data collected by TROMINO cannot be read directly by modal analysis program. Also, the recorded data have different start and end time for each set so they need to be synchronized before further data analysis. Grilla software was used to convert the raw data to readable format and synchronize the data at the same time. Only recorded data from the channel of high-gain velocity can be synchronized by Grilla, so it was used for the modal analysis. Figure 3-3 shows the typical plot of recorded data from the channel of high-gain velocity, for setup 3.

3.4. Modal analysis

3.4.1. Literature review of modal identification techniques

Modal parameters can be identified from the data collected in AVT through a variety of modal identification techniques. Classical technique for modal identification is referred to as the basic frequency domain technique (BFD), or the peak picking technique. The classical technique is to simply process the data using a discrete Fourier transform, and use the fact that well separated modes can be directly estimated from the

power density spectrum at the peak. However, the classical technique is based on the assumption that the modes of the structure are well separated, which is difficult to be satisfied in real case. In the case of close modes, this technique is difficult to detect the closes. Furthermore, it is impossible to estimate damping through the classical technique and the frequency estimates are limited by the frequency resolution of spectra density estimate. (Brincker, Zhang, and Andersen 2000)

Frequency domain decomposition (FDD) is an extension of classical frequency domain technique. It removes most of the disadvantages of the classical technique but keeps the user-friendliness. The FDD technique approximately decomposes the dynamic response into several independent SDOF systems and performs singular value decomposition of the spectral density matrices. Then the natural frequencies can be roughly identified through peak-picking and mode shapes can be estimated using the singular vector matrices. The theoretical background of FDD techniques can be expressed by

$$G_{yy}(jw) = \overline{H}(jw)G_{xx}(jw)H(jw)^T \qquad (\text{Eq.}\, 3-1)$$

where $G_{xx}(jw)$ is the $r \times r$ Power Spectral Density (PSD) matrix of the input, r is the number of inputs, $G_{yy}(jw)$ is the $m \times m$ PSD matrix of the responses, m is the number of responses, $\overline{H}(jw)$ is the $m \times r$ Frequency Response Function (FRF) matrix, and "—" and superscript T denote complex conjugate and transpose, respectively. (Brincker, Zhang, and Andersen 2000)

After the FDD, equivalent single degree of freedom 'spectral bells' are identified for each mode. Then, the resulting auto-correlation function can be used to reevaluate the frequency by counting the number of zero crossings in a finite time interval, by inverse fast Fourier transform (IFTT) of the spectral bell. Damping ratios are also estimated using the logarithmic decrement of the auto-correlation function. (Brincker, Ventura, and Andersen 2001) This step is also referred to as enhanced frequency domain decomposition (EFDD).

3.4.2. Pre-processing of signals

In order to assure the quality of the data, the recorded data should be checked in both time domain and frequency domain before they can be analyzed for system identification purpose. Possible problems for the

data include over-saturated signals, dead signals and accidental hit, etc. During this test, sensor NO.8 was found to be kicked in setup3 (figure 3-3), so that set of data was removed from further analysis.

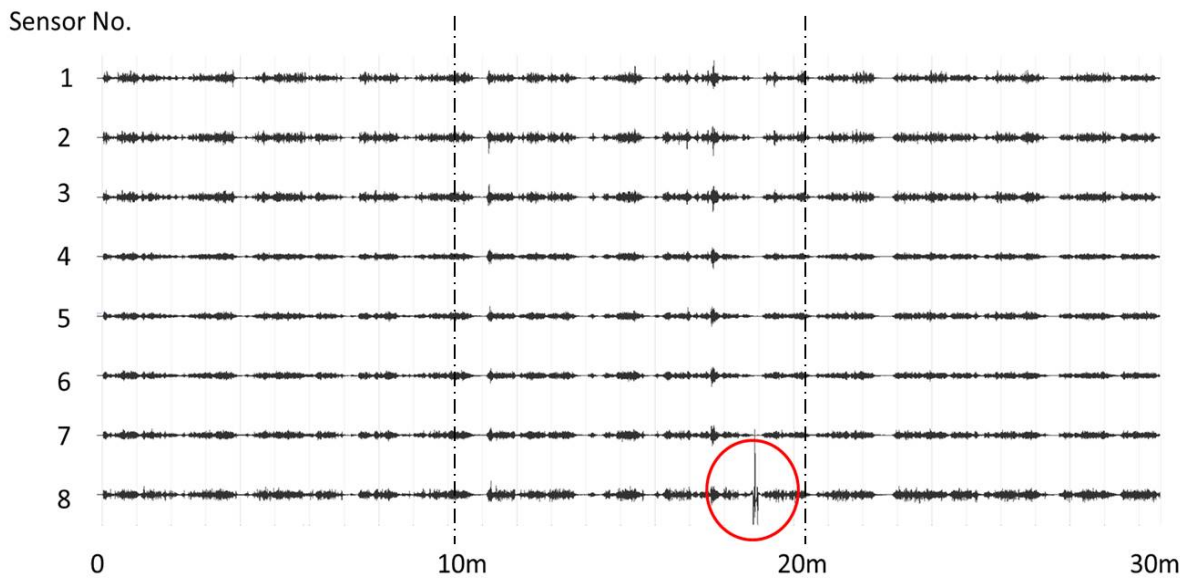

Figure 3-3: Recoded signal in setup3

3.4.3. Modal identification using ARTeMIS modal

Commercial software ARTeMIS (Structural Vibration Solutions 2001) was used in this project to perform data processing, system identification and visualization of mode shapes. Analysis model was built in ARTeMIS with 96 (32×3) channels for data input, as shown in figure 3-4. The recorded data from AVT were input to corresponding channels.

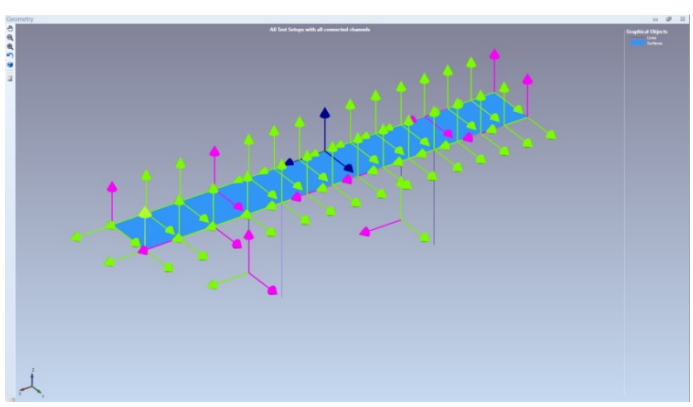

Figure 3-4: ARTeMIS mdoel

ARTeMIS has powerful capabilities for signal processing which includes detrending, decimation and filtering

of data. Trend is a slow, gradual change in some property of a set of data. It is necessary to remove the trend from the tested data, which is known as detrending or baseline correction, because the analysis result might be overwhelmed by the non-zero mean and the trend terms. (Wu et al. 2007) Decimation and filtering could process the data to targeting frequency range because only a specific frequency range of data is desired in modal analysis. In this study, filtering was applied with the frequency range from 1Hz to 20Hz which is the estimated modal frequency range of the finite element model. The frequency range of finite element model is presented in Chapter 5.

After signal processing, singular value decomposition was then applied to estimate frequency contents of the structure. ARTeMIS provides various techniques for singular value decomposition. Each technique will create different plots of spectral densities. Natural modes were then estimated through manually selecting the peak of the spectrum. Results from Frequency Domain Decomposition (FFD) technique and Enhanced Frequency domain Decomposition (EFDD) are presented below.

Frequency Domain Decomposition (FDD)

The FDD technique approximately decomposes the dynamic response into several independent SDOF systems and performs singular value decomposition of the spectral density matrices. Modal frequencies and mode complexity are identified from peak-picking approach shown in figure 3-4. The modal frequencies for first 10 modes are summarized in table 3-2.

Table 3-2: Identified frequencies using FDD technique

Mode No.	Mode Description	Frequency [Hz]	Complexity [%]
1	1st Translational Mode in Vertical Direction	2.375	16.971
2	1st Torsional Mode	2.938	39.831
3	2nd Translational Mode in Vertical Direction	3.313	18.377
4	2nd Torsional Mode	3.875	31.704
5	3rd Torsional Mode	4.688	27.899
6	4th Torsional Mode	5.813	7.583
7	3rd Translational Mode in Vertical Direction	6.75	7.236
8	4th Translational Mode in Vertical Direction	7.313	7.531
9	5th Translational Mode in Vertical Direction	7.75	3.582
10	5th Torsional Mode	8.375	37.894

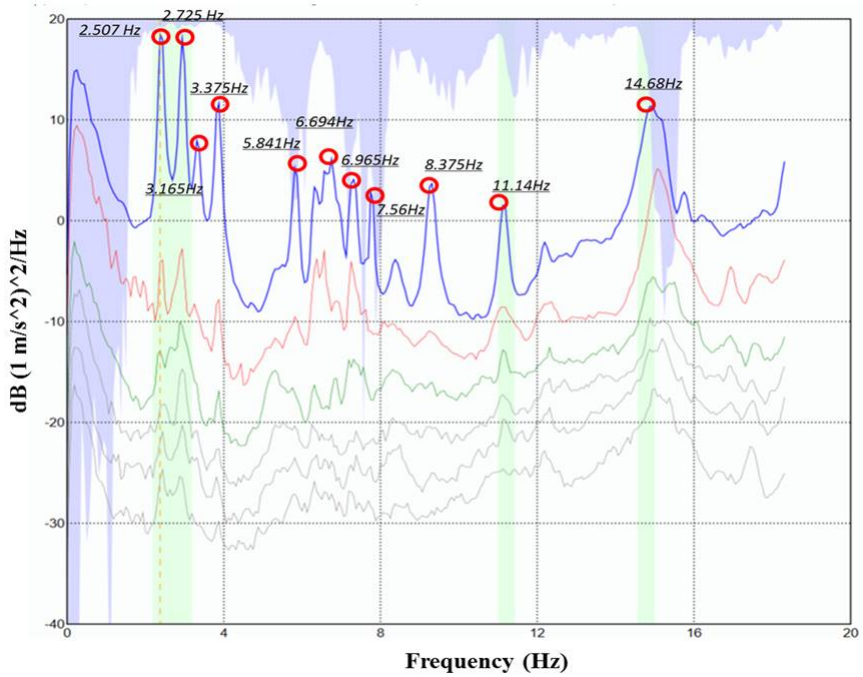

Figure 3-5: Singular values of spectral densities calculated by FDD technique

Enhanced Frequency Domain Decomposition (EFDD)

The EFDD technique includes 2 steps. The first step is to perform FDD and identify mode shapes, and the second step is to use the identified mode shapes to identify the SDOF Spectral Bell functions and estimate frequency and damping ratio from that. Modal frequencies, modal damping and mode complexity are identified from peak-picking approach shown in figure 3-5. The modal frequencies for first 10 modes are summarized in table 3-3.

Table 3-3: Identified frequencies using EFDD technique

Mode No.	Mode Description	Frequency [Hz]	Damping [%]	Complexity [%]
1	1st Translational Mode in Vertical Direction	2.507	3.19	13.641
2	1st Torsional Mode	2.725	3.189	37.196
3	2nd Translational Mode in Vertical Direction	3.165	3.15	17.196
4	2nd Torsional Mode	3.375	3.154	32.459
5	3rd Torsional Mode	4.688	0	27.899
6	4th Torsional Mode	5.841	1.175	6.536
7	3rd Translational Mode in Vertical Direction	6.694	2.404	4.289
8	4th Translational Mode in Vertical Direction	6.945	2.862	5.571
9	5th Translational Mode in Vertical Direction	7.556	0.881	4.412
10	5th Torsional Mode	8.425	1.629	37.894

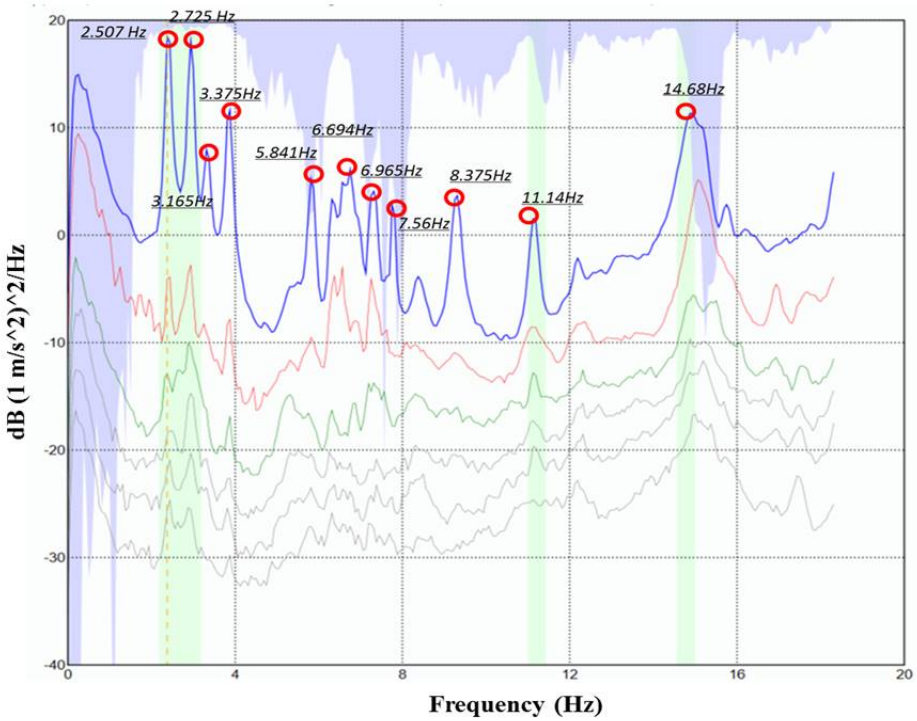

Figure 3-6: Singular values of spectral densities calculated by EFDD technique

The estimated frequencies are slightly different between FDD and EFDD techniques due to the different theoretical model they are using. However, the identified mode shapes from the two techniques are identical. The mode modes will be presented in Chapter 5.

Chapter 4: Elastic Finite Element Model

An elastic finite element model was created in Sap2000 to estimate the modal properties of Portage Creek Bridge. Modeling details and preliminary results are presented in this section.

4.1. Material properties

Geometry and material properties of the structure were provided in the structural drawing. Since this chapter does not consider the nonlinear properties of the bridge, only the modulus of elasticity, shear modulus and density will be discussed. Modulus of elasticity of concrete was calculated based on the design strength and empirical equations shown in Eq.4-1 (CSA S06-14). The structural drawings of Portage Creek Bridge indicate the minimum compressive strength of concrete should be 4000 psi (28MPa) for columns and 3000 psi (21MPa) for cap beams. The detailed property of deck concrete is not contained in the structural drawing, so its strength was estimated as 20 MPa in terms of the recommendation in Section 14.7.4 of CSA S06-14. Concrete and steel densities were adopted as 24.0kN/m^3 and 77kN/m^3, respectively, as recommended in Table 3.4 of CSA S06-14. All material properties will be updated in future work based on the experimental results.

$$E = (3000\sqrt{f_c'} + 6900) \cdot \left(\frac{\gamma_c}{2300}\right)^{1.5} \qquad (\text{Eq.}\, 4-1)$$

where E is the modulus of elasticity of concrete; f_c' is the compressive strength of concrete; γ_c is the mass density of concrete.

Table 4-1: Material properties

	Modulus of Elasticity (MPa)	Density (kN/m^3)
Concrete for Deck and Caps	21677	24.0
Concrete for Column	24281	24.0
Structural Steel	200000	77.0
Rebar Steel	200000	77.0

4.2. Shell element

Shell is a three or four-node area object used to model membrane and plate-bending behavior. There are two types of shell element in sap2000: Thick shell and thin shell. Thick shell formulation follows

Mindlin/Reissner (Mindlin 1951), which accounts for transverse shear deformation in plate-bending behavior while thin shell formulation follows a Kirchhoff (Love 1888) application which neglects shear behavior.

Shear deformation tends to be significant when plate thickness is greater than approximately 1/5 to 1/10 of the span of plate-bending curvature. (Habibullah and Wilson 1996) However, it is recommended by Sap2000 user's manual that thick-plate formulation (figure 3-1) is more accurate in practice though slightly stiffer, even for thin-plate bending problems in which shear deformation is negligible.

Bridge decking and foundation footings were modeled as shell element in this model. Changing of decking thickness was considered in this model as shown in figure 4-1. All the shell elements werer modeled as thick-shell which means that shear behavior is accounted for in the analysis.

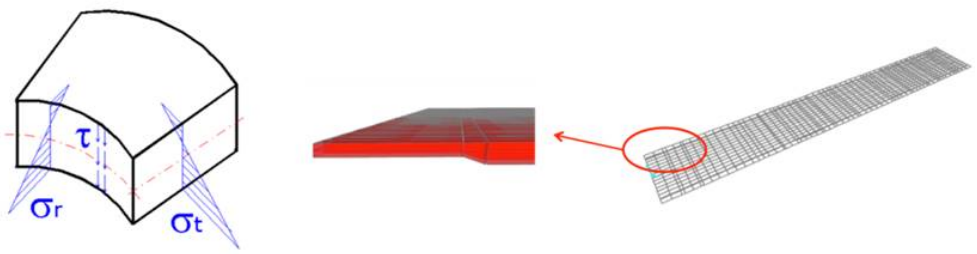

Figure 4-1: Shell element for concrete decking

4.3. Frame element

In Sap2000, a general, three-dimensional beam-column formulation is used for frame element, which includes the biaxial bending effects, torsion, axial deformation and biaxial shear deformation, as illustrated in figure 4-2. (Habibullah and Wilson 1996) They are used to model beams, columns, braces, and truss elements in planar and 3D systems.

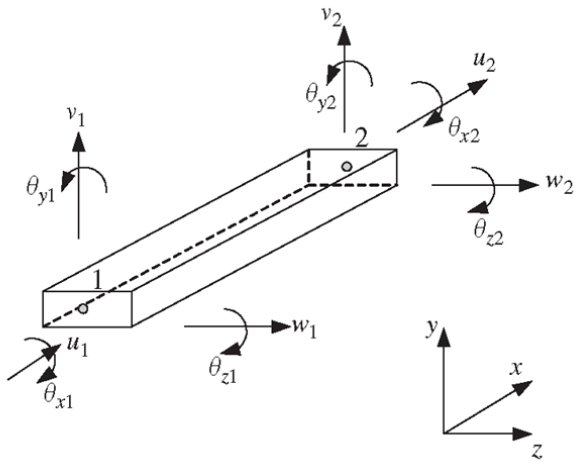

Figure 4-2: Frame element formulation

Frame elements in this model includes steel girder, stringer, bracing, concrete bents and piers (Figure 4-3). Steel elements are either bolted or welded together. Concrete piers and cap beams are poured together at the connection. Therefore, all the Connections between frame elements are assumed to be fixed at all DOFs.

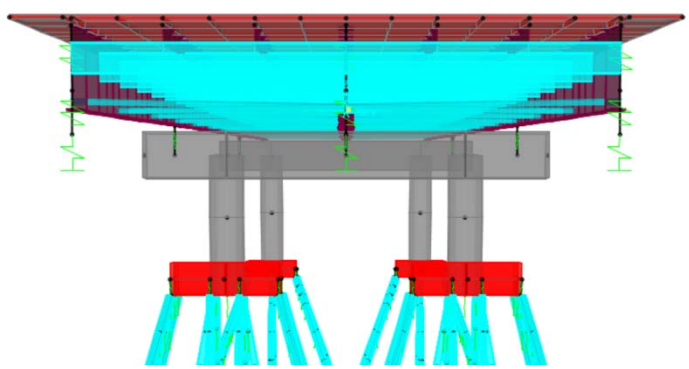

Figure 4-3: Extrude view of frame elements in Sap2000

4.4. Link element

Link elements are utilized to model specialized structural behavior between two nodes. Linear, nonlinear and frequency-dependent properties can be assigned to each of the six deformational DOFs of the link elements (U1 to U6). Each link element can be viewed as an element with multiple internal springs, including axial, shear, torsion and pure bending spring (figure 4-4).

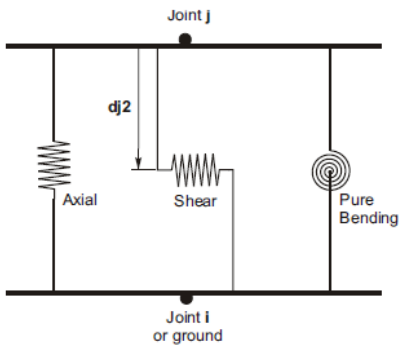

Figure 4-4: Numerical model for link element

In this study, link elements are mainly used to model the elastomeric bearings and foundation. Also, in the case where thickness of structural members cannot be ignored, link elements with extra-large stiffness are used to represents the effects of member thickness, as shown in figure 4-5.

4.4.1. Bearings

Bridge bearing is a common device in modern bridge structure which provide resting surface between bridge decking and piers. The purpose of the bearings is to allow controlled movement of the superstructure and hence reduce the stress involved in the structural members. The movement includes thermal expansion and displacement caused by earthquake or wind.

The most common form of bearing in modern bridge structure is elastomeric bearing, which is also the bearing utilized in Portage Creek Bridge. It mainly consists of two steel plates with an elastomer pad between them. For this bridge, steel bolts are used to restrict movements of bearings in vertical direction and movements in translational directions are allowed at small level (See Section 2-4).

In order to model the bridge bearings in detail, material properties and results from hysteresis test of the bearing are needed. In general, the manufacture is responsible to provide the necessary information to the analyzer. However, the bridge was designed and constructed in 1982 and the company, which produced the bearings, had closed down 10 years ago. It is impossible for author to get the detailed bearing properties from the manufacture, so elastic stiffness of expansion bearings in transverse directions is estimated according to

Eq.4-2 (Akogul and Celik 2008) and bearing nonlinearity are neglected in this model.

$$k_{eff} = \frac{G_{eff}A}{H_r} \qquad (\text{Eq.}\, 4-2)$$

where G_{eff} is the effective shear modulus of the elastomer pad; A and H_r are cross-sectional area and thickness of elastomer pad, respectively.

Bearing stiffness for all other directions can be assumed to be infinite large based on the drawings of the bearing (Figure 2-7) Bearings are assigned between steel girders and substructure (abutments, piers), as shown in figure 4-5. Link 1 (link element) is fixed link which represents the thickness of steel girder. Link 2 is the link element for expansion bearing.

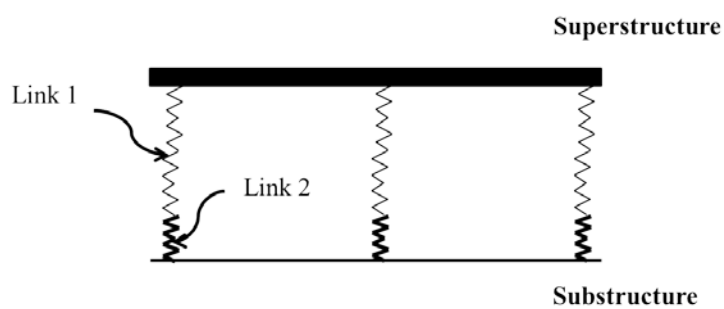

Figure 4-5: Link elements for bearings

4.4.2. Foundation

In modeling soil, the most intuitive approach to structural engineer is to use a spring to approximate soil behavior as a simplification. This soil-spring model is referred as Winkler model. (Kerr 1964) Though user-friendly in practice, there are some limitations for Winkler approach, which are summarized below. (Das 2015)

- No prediction of soil movements at a distance from the foundation element is given.
- No shear transmission between adjacent springs, therefore no prediction of differential settlement.
- Difficulty determining spring stiffness leading to uncertainty in predicted total or average settlements.

Due to these limitations, Winkler models are reasonable only if the main quantities of interest are structural loads effects rather than the soil movements. The main purpose of this research is to evaluate seismic behavior of structural system, so the Winkler model is enough to represent the effect of soil on foundation. Pile foundation was adopted for Portage Creek Bridge. Winkler model for pile foundation is simplified in figure 4-6. The pile model in Sap2000 can be seen in figure 4-7.

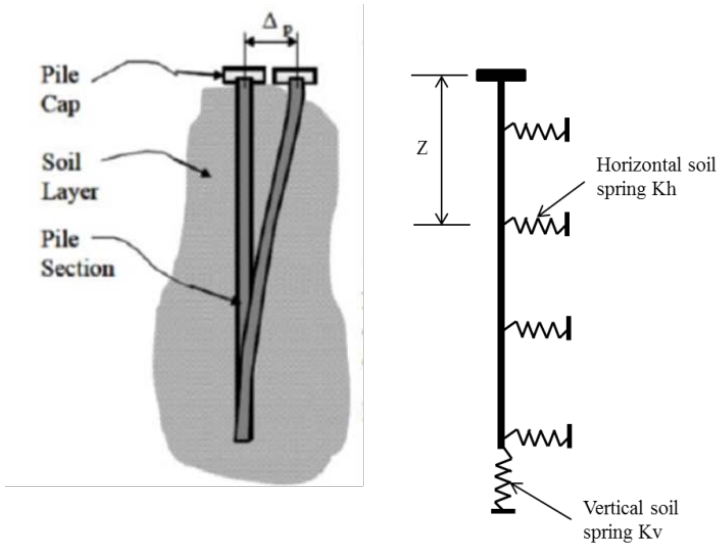

Figure 4-6: Numerical model for pile foundation

In general, stiffness for soil spring should be determined based on the p-y curve from field test. P-y curve defines the relationship between the soil reaction p (load per unit length of the pile, Unit: kN/m) and the lateral displacement y (Unit: mm) along the pile. (Dj Amar 2013) However, the author failed to get an opportunity to carry out the field test, thus the stiffness of horizontal soil spring is estimated per empirical equation suggested by Das:

$$K_h = k_h \Delta_z \qquad (\text{Eq.}\, 4-3)$$

where Δ_z is the distance between soil springs; k_h is the modulus of subgrade reaction, which are calculated per Eq.4-4 & 4-5 for sand and clay, respectively.

$$k_{h,sand} = n_h z \qquad (\text{Eq.}\, 4-4)$$

$$k_{h,clay} = \frac{E_s}{1-\mu_s^2} \qquad (\text{Eq.}\, 4-5)$$

where n_h is constant of modulus of horizontal subgrade reaction, representative values of which are

summarized in Table 4-2; z is the distance from soil spring to the pile cap; E_s is modulus of elasticity of soil (Table 4-3) and μ_s is Poisson's ratio of the soil. For sands, the coefficient of subgrade reaction shows a linear variation with depth while the subgrade reaction for cohesive soil (clay) is assumed to be approximately constant along the depth. Since the piles are drilled into bedrock, the vertical soil spring can be assumed to be infinite stiff.

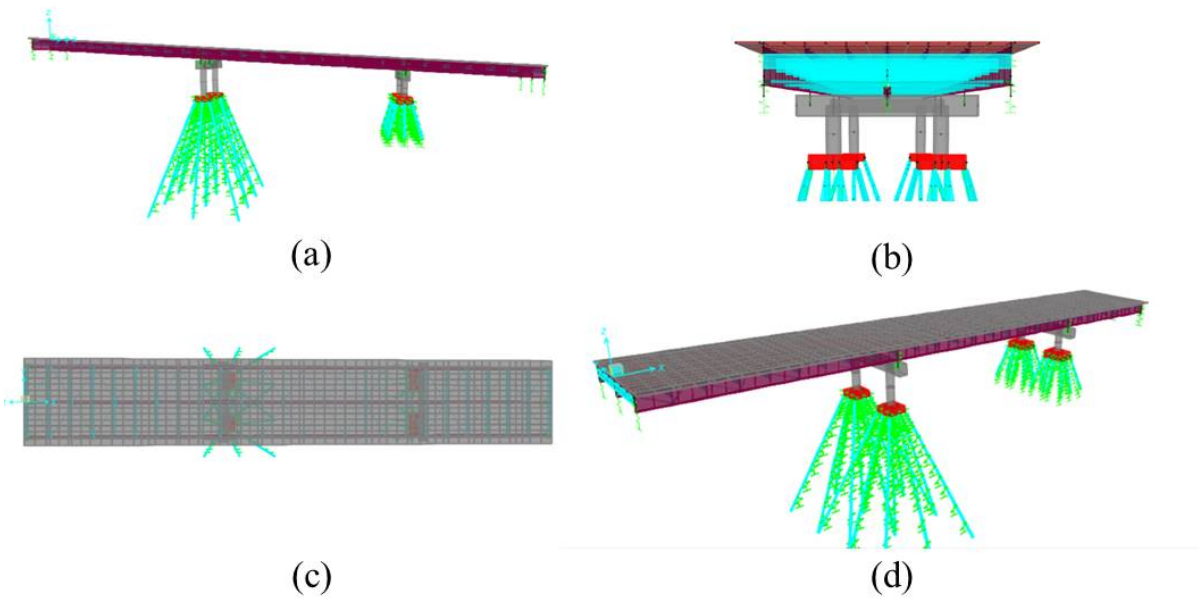

Figure 4-7: (a) Front view (b) side view (c) top view and (d) 3D view of finite element model

Table 4-2: Representative value of nh

Soil	n_h (kN/m^3)
Dry or moist sand	
Loose	1800-2200
Medium	5500-7000
Dense	15000-18000
Submerged sand	
Loose	1000-1400
Medium	3500-4500
Dense	9000-12000

Table 4-3: Typical values of modulus of elasticity for different types of soil

Type of Soil	E_s (N/mm^2)
Clay	
Very soft	2-15
soft	5-25
Medium	15-50
Hard	50-100
Sandy	25-250
Glacial till	
Loose	10-153
Dense	144-720
Very dense	478-1440
Loess	14-57
Sand	
Silty	7-21
Loose	10-24
Dense	48-81
Sand and gravel	
Loose	48-148
Dense	96-192
Shale	144-14400
Silt	2-20

Chapter 5: Finite Element Model Updating

5.1. Introduction

The finite element model described in Chapter 4 is intended to model the dynamic characteristics of structures for future structural assessment. However, inaccuracy of finite element model may exist because of unknown material properties, poorly known boundary conditions and simplification of the model. For this model, uncertainties will mainly arise from roughly modeled bearing and foundation behaviors, poorly known material properties and boundary conditions. These uncertainties will cause the predicted dynamic response to be different from the measured response of a structure. Model updating is to make the results from numerical model match the measured results by adjusting the parameters of finite element model.

Many model-updating techniques have been proposed in recent years. (Levin and Lieven 1998; Marwala 2002; Marwala 2010) All these techniques may be split according to the type of measured data used and the model parameters updated. The measured data may be dynamic response during earthquake, natural frequencies and mode shapes.

5.2. Identification of corresponding mode

Ambient vibration test has been carried out for Portage Creek Bridge as described in Chapter 3. Natural frequencies and mode shapes have been identified from ARTeMIS model via peak-picking approach. However, not all the identified modes have corresponding mode in finite element model. The first step of model updating is to determine the corresponding modes between experimental and numerical results.

Bridge structures generally have a relatively low level of ambient vibration comparing with the buildings, especially for short bridge like Portage Creek Bridge, which makes test results sensitive to the noise induced by vehicles or unexpected incidence during the test. Most of modes identified from ARTeMIS model have irregular mode shape, which means most modes do not have perfect mode shape in certain direction and the irregularity makes it difficult to find perfectly matching modes in finite element model. Therefore,

corresponding modes are determined based on two criteria: Close natural frequency and same category of mode shapes (vertical, translational, torsional). The identified corresponding modes are listed in Table 5-1. The mode shapes for the first mode are presented in figure 5-1. More mode shapes can be seen in figure

Table 5-1: Comparison between numerical and experimental results

Mode No.	Frequencies from FEM (Hz)	Frequencies from ARTeMIS (Hz)	Description
1	2.416	2.507	Vertical
2	2.664	2.725	Translational
3	3.275	3.165	Vertical
4	3.308	3.375	Torsional
5	7.031	6.96	Vertical
6	7.897	7.56	Vertical
7	8.377	8.375	Torsional
8	11.235	11.14	Vertical

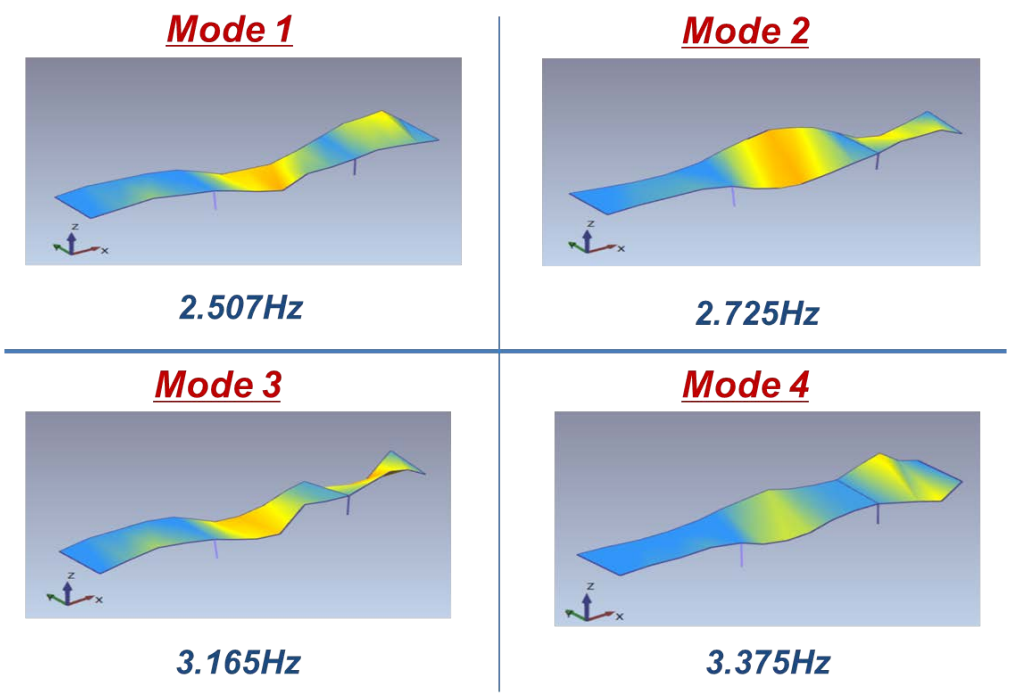

Figure 5-1: Mode shapes of the first 4 modes

5.3. Sensitivity analysis

The key to success in model updating is the choice of parameters. The parameters should be selected where

uncertainties are likely to arise. Table 5-2 summarizes the preliminarily selected parameters for model updating. E is the modulus of elasticity of the materials; ρ is the material density; k is the stiffness for link element.

Table 5-2: Parameters for finite element model updating

Element	**Deck**		**Girder**		**Column**		**Foundation**	**Expansion Bearing**
Type	E	ρ	E	ρ	E	ρ	k	k

Manually model updating is basically a trial and error approach, but sensitivity analysis can be performed to provide a direction for model updating. Finite element model is not equally sensitive to all the parameters listed in Table 5-2 and sensitivity analysis is aimed to find the most significant parameters for the model and hence improve the efficiency of model updating procedure. Results of sensitivity analysis for parameters in Table 5-2 are shown in Figure 5-2 to 5-11.

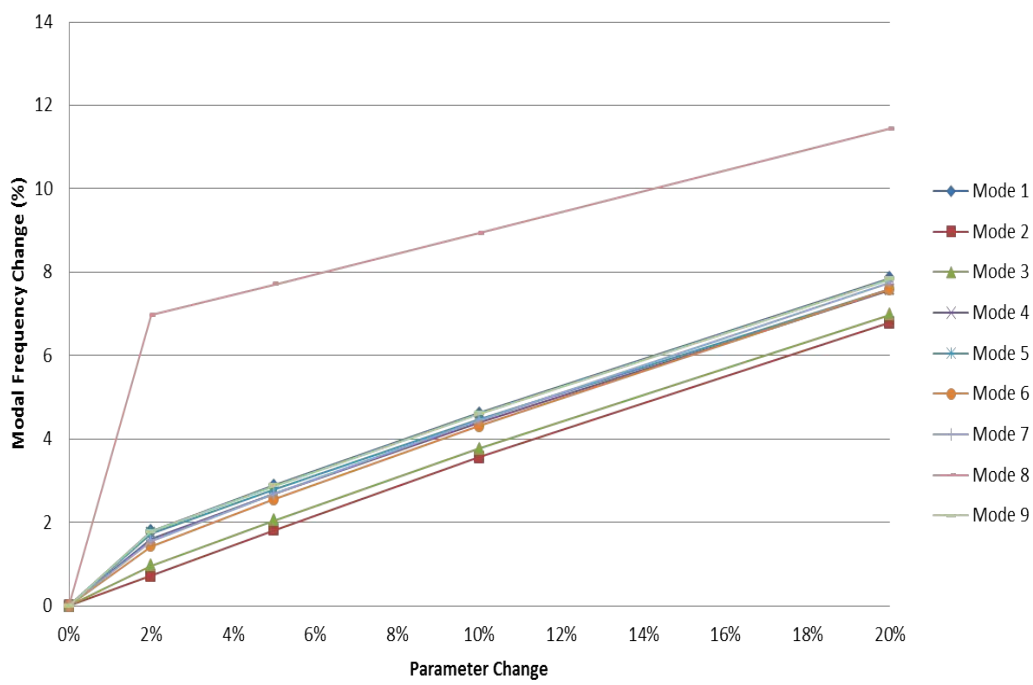

Figure 5-2: Sensitivity of elastic modulus of deck concrete

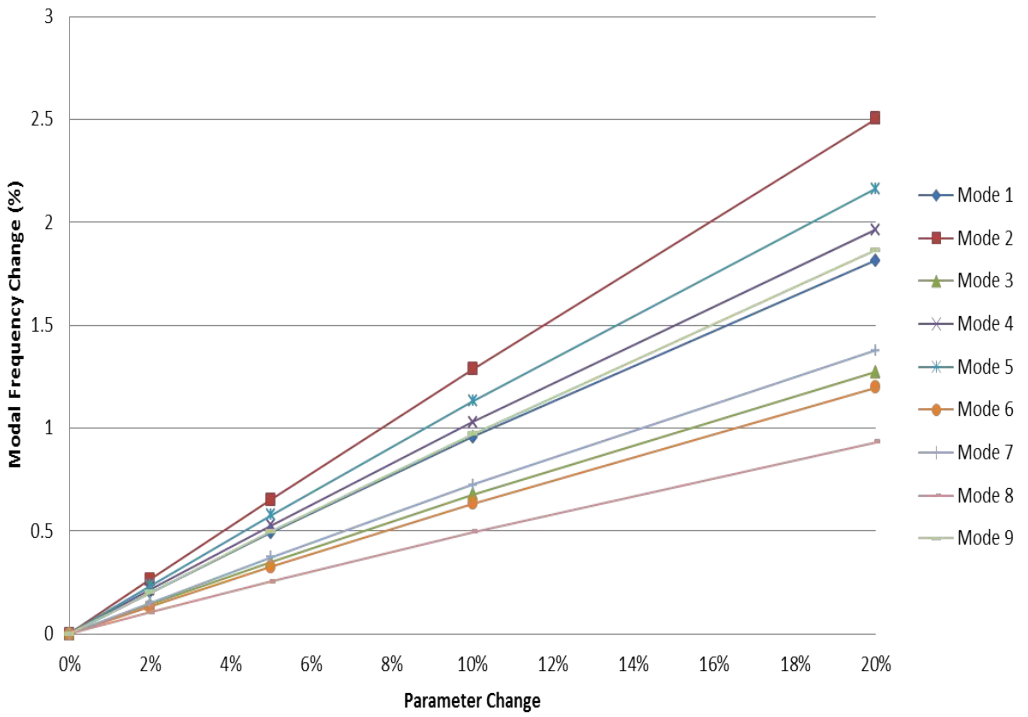

Figure 5-3: Sensitivity of density of deck concrete

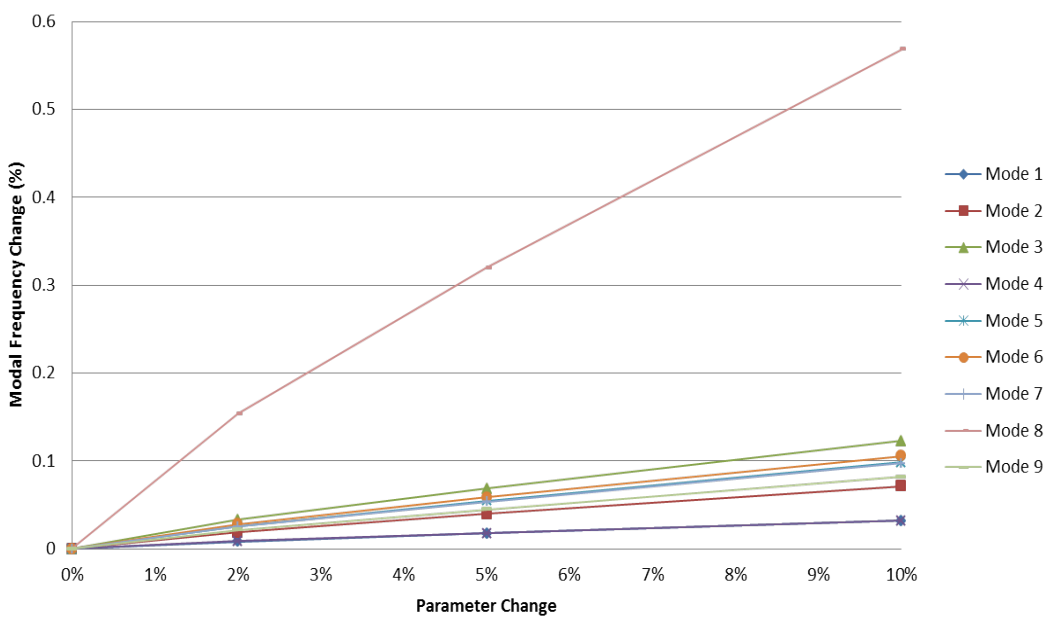

Figure 5-4: Sensitivity of elastic modulus of column concrete

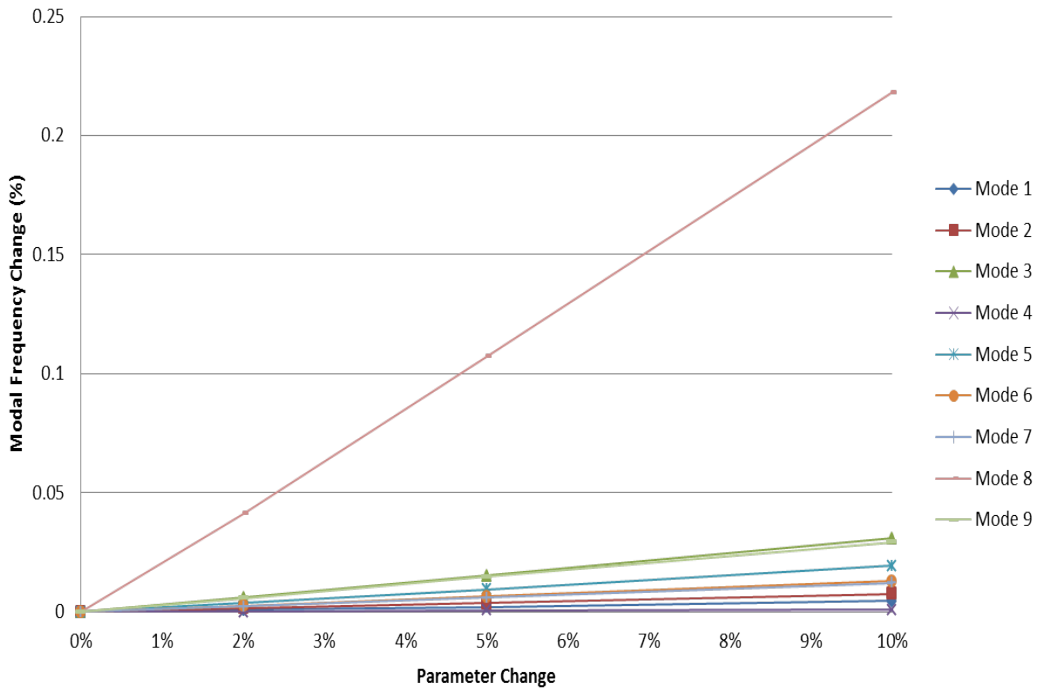

Figure 5-5: Sensitivity of density of column concrete

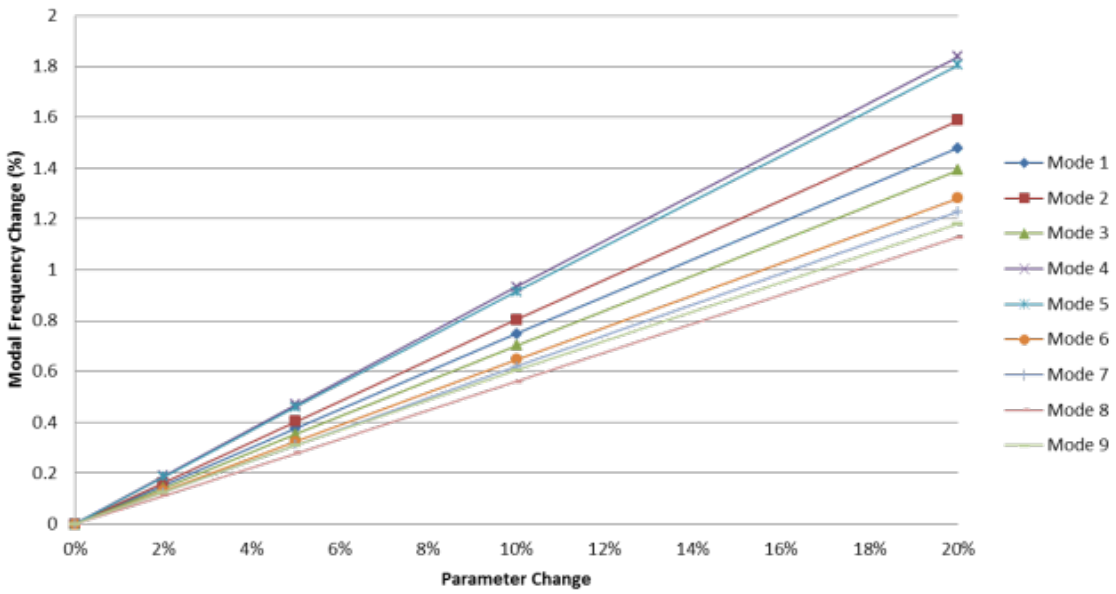

Figure 5-6: Sensitivity of elastic modulus of girder steel

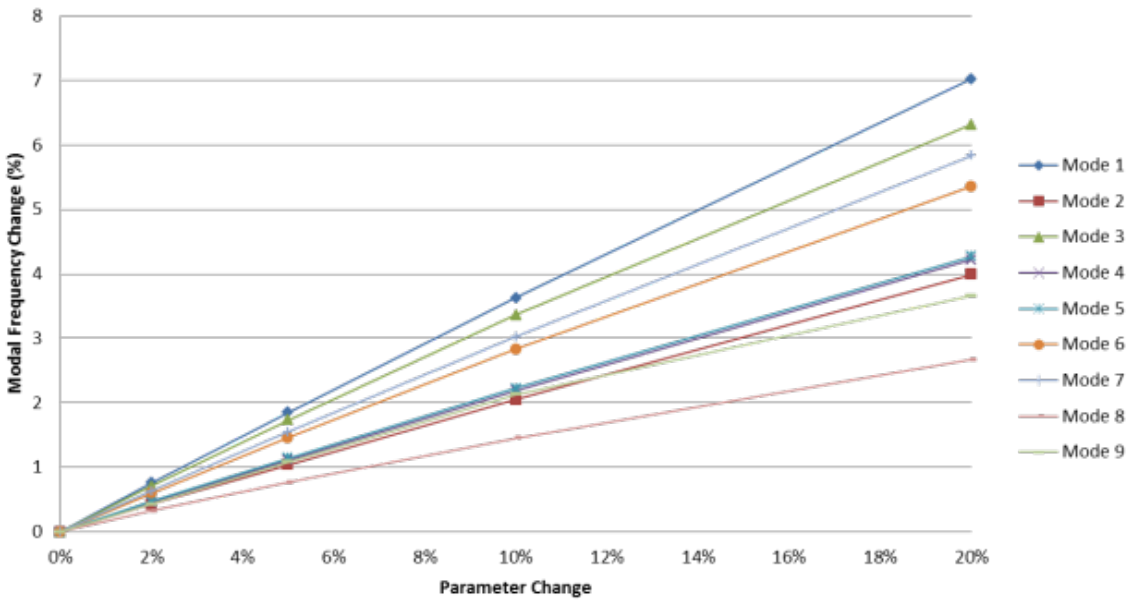

Figure 5-7: Sensitivity of density of girder steel

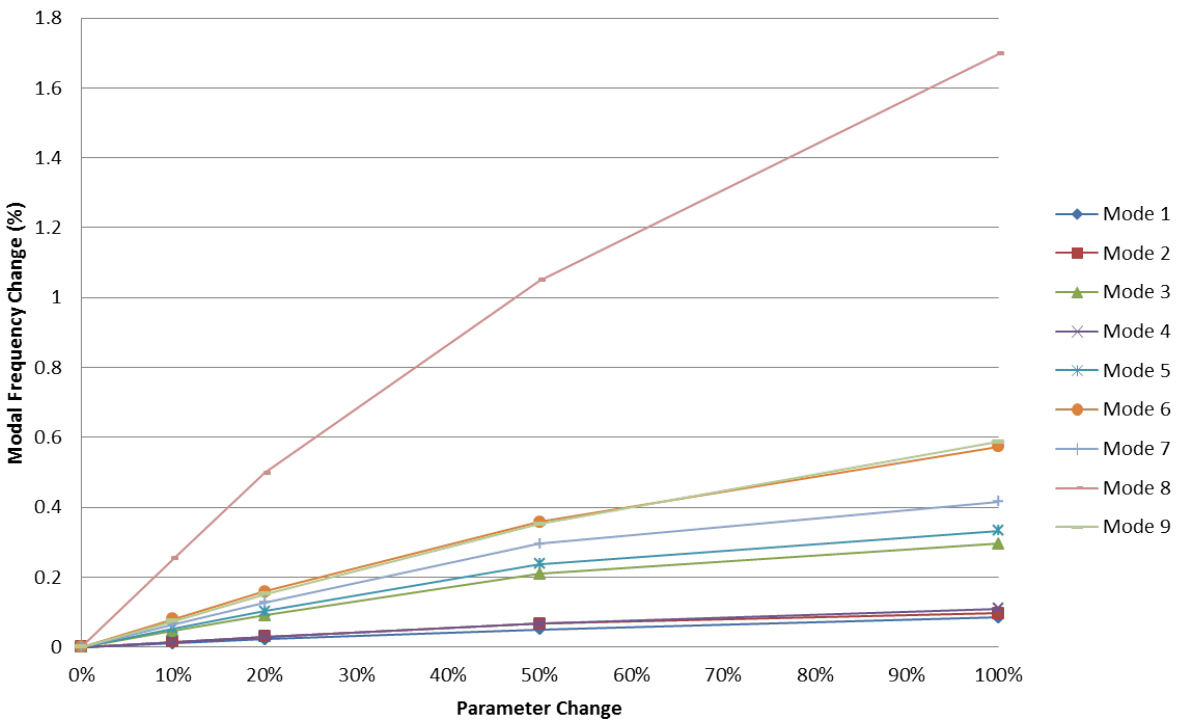

Figure 5-8: Sensitivity of stiffness of foundation spring

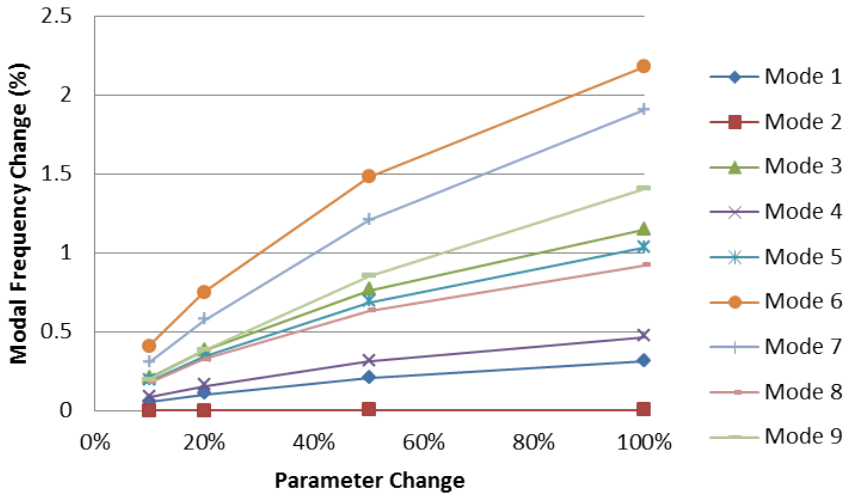

Figure 5-9: Sensitivity of bearing stiffness in transverse direction

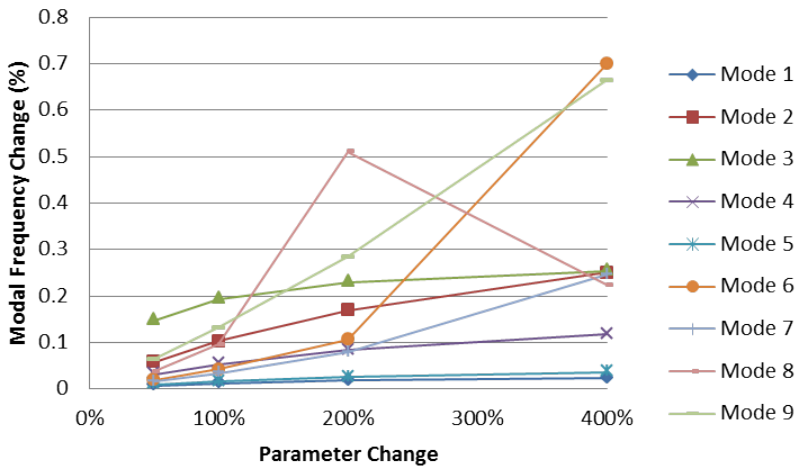

Figure 5-10: Sensitivity of bearing stiffness in longitudinal direction

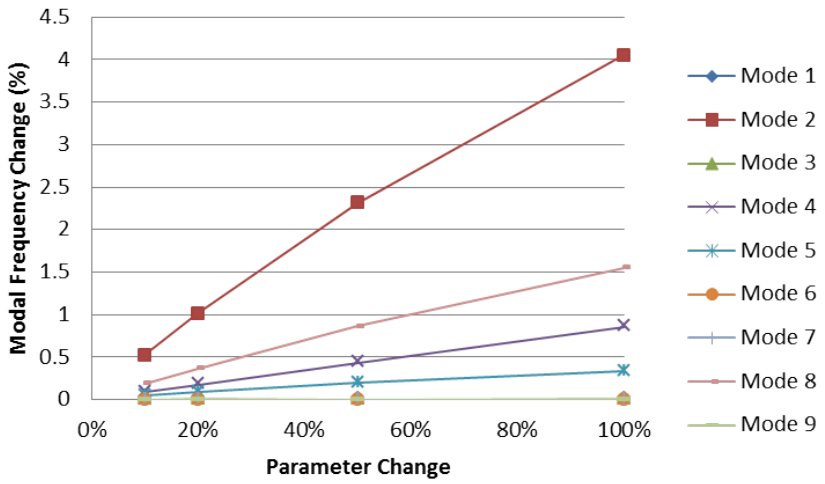

Figure 5-11: Sensitivity of bearing stiffness in vertical direction

It can be found that the finite element model is quite sensitive to the material properties of concrete deck and steel girder but not very sensitive to the properties of concrete columns. All the modes have similar sensitivity to the material properties of the bridge, so it did not help a lot when the author wants to change frequencies of some modes and leave the rest unchanged. For the link element, different modes show different sensitivities to the link stiffness, and some links are shown to be significant for certain modes. For instance, 8th mode from finite element model is quite sensitive to the stiffness of foundation spring; (Figure 5-8) 2nd mode is very sensitive to the bearing stiffness in vertical direction. (Figure 5-11)

5.4. Model updating and results

Model updating was performed manually based on the findings from sensitivity analysis. A better match between numerical model and experimental results was achieved as shown in Table 5-3, with a maximum difference of 5.41% for the 6th mode. Changes in parameters are listed in Table 5-4 and Table 5-5 for material properties and bearing properties, respectively. Stiffness of foundation springs remains unchanged after model updating. Elastic modulus of deck concrete was increased by about 20% which means that the recommendation for estimating elastic modulus in CSA S06-14 is very conservative for Portage Creek Bridge. Stiffness for bearings were significantly increased by more than 100%, which means the equations proposed by Akogul (Akogul and Celik 2008) were not applicable to the bearings in Portage Creek Bridge.

Table 5-3: Comparison between numerical and experimental results

Mode No.	FEM before (Hz)	FEM after (Hz)	ARTeMIS (Hz)	Diff after (%)
1	2.416	2.442	2.507	2.59%
2	2.664	2.763	2.725	1.39%
3	3.275	3.258	3.165	2.94%
4	3.308	3.356	3.375	0.56%
5	7.031	7.090	6.96	1.87%
6	7.897	7.969	7.56	5.41%
7	8.377	8.499	8.375	1.48%
8	11.235	11.368	11.14	2.05%

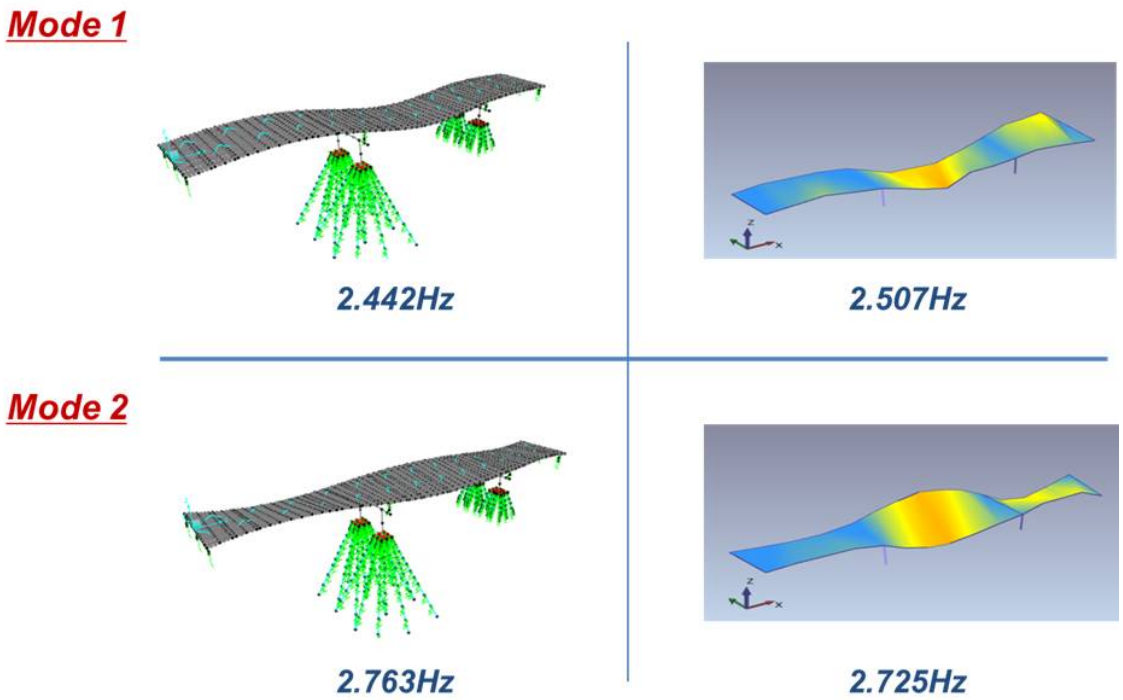

Figure 5-12: Comparison of mode shapes between numerical and experimental results (Mode 1&2)

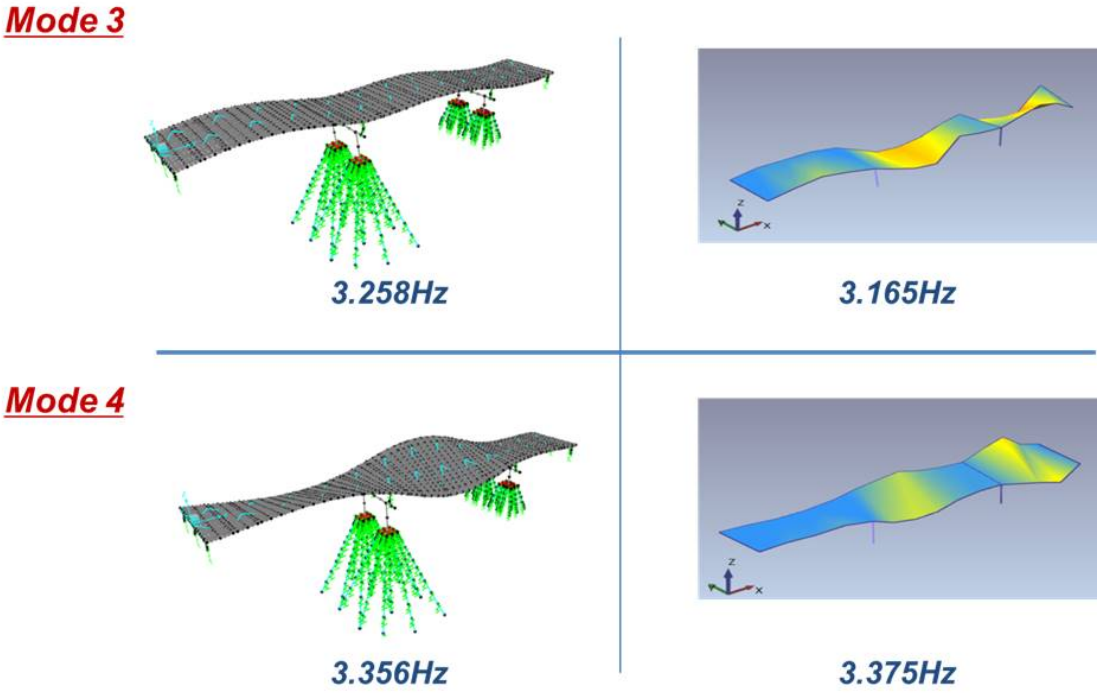

Figure 5-13: Comparison of mode shapes between numerical and experimental results (Mode 3&4)

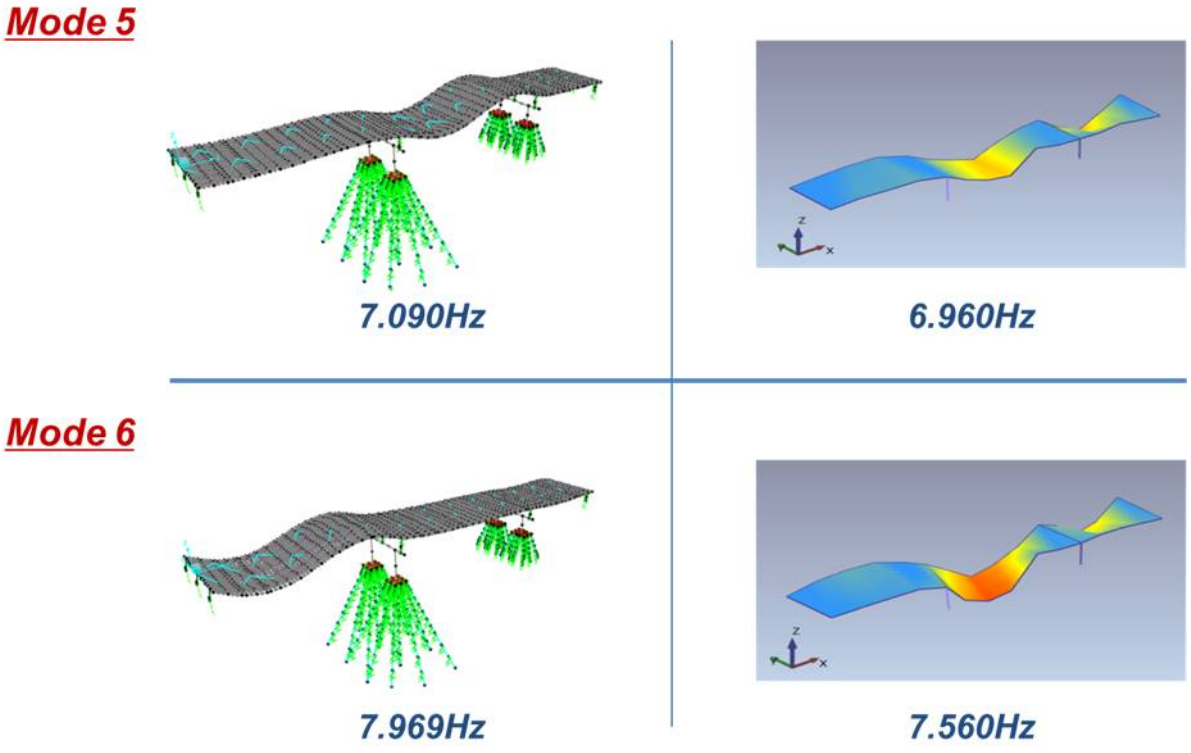

Figure 5-14: Comparison of mode shapes between numerical and experimental results (Mode 5&6)

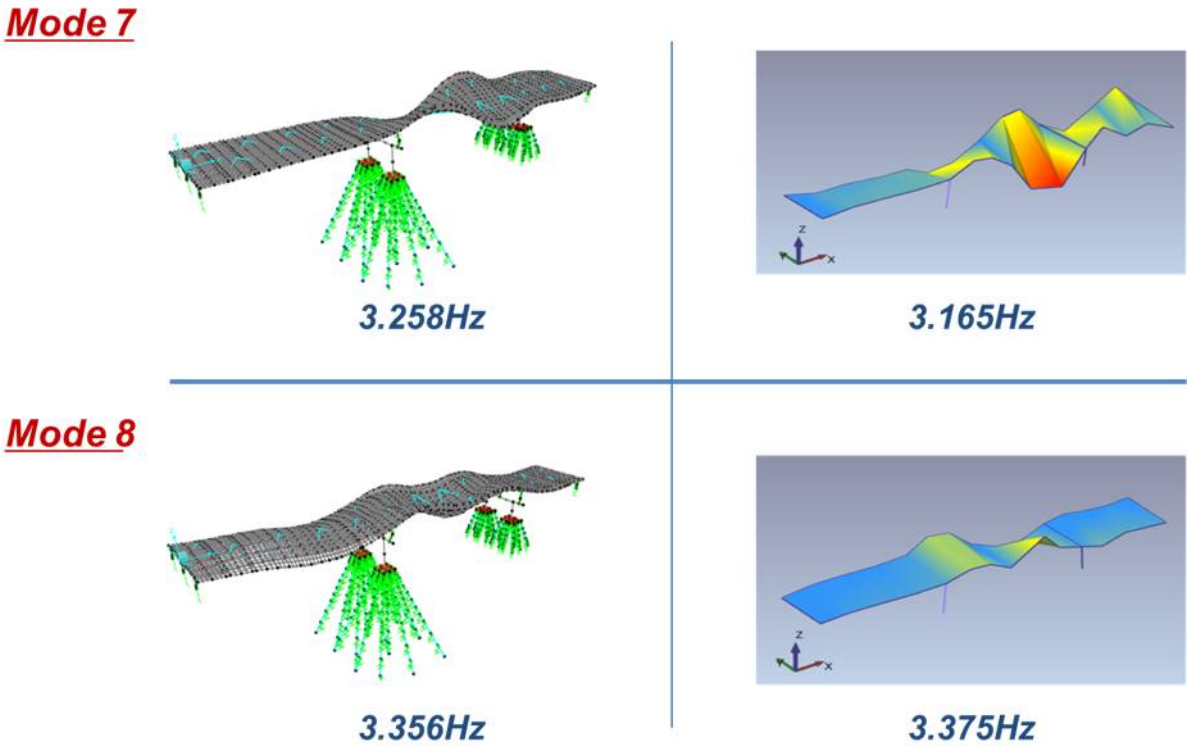

Figure 5-15: Comparison of mode shapes between numerical and experimental results (Mode 7&8)

Table 5-4: Parameter changes in material properties

Element	Deck		Girder		Column	
type	*E* (MPa)	ρ (kN/m^3)	*E* (MPa)	ρ (kN/m^3)	*E* (MPa)	ρ (kN/m^3)
Before	21677	24.0	200000	76.9	24281	24.0
After	27800	23.5	unchanged	unchanged	24400	unchanged

* *E* is the modulus of elasticity of the materials; ρ is the material density

Table 5-5: Parameter changes in bearing properties

		U1	U2	U3	U4	U5	U6
P1-EXT	**before**	fixed	4126.523	4126.523	fixed	fixed	fixed
	after	1000000	10000	10000	unchanged	unchanged	unchanged
P1-INT	**before**	fixed	6752.492	6752.492	fixed	fixed	fixed
	after	1000000	13000	13000	unchanged	unchanged	unchanged
P2-EXT	**before**	fixed	3126.154	3126.154	fixed	fixed	fixed
	after	1000000	10000	10000	unchanged	unchanged	unchanged
P2-INT	**before**	fixed	4689.231	4689.231	fixed	fixed	fixed
	after	1000000	13000	13000	unchanged	unchanged	unchanged

*P1-EXT represents bearing under exterior girder at Pier No.1; All units in kN/m; See section 4.1 for the definition of U1 to U6

Chapter 6: Nonlinear Structural Behaviors

6.1. Overview

Nonlinear structural behavior can be obtained from section analysis, which is aimed to find out the stress-strain relationships of sections. Section analysis is a critical step in the procedure of seismic evaluation of structures. On the one hand, the results from section analysis (moment-curvature relationship, P-M interaction) could be used to define nonlinear finite element model; on the other hand, it could provide a relatively accurate estimation of member capacities for seismic evaluation. This chapter only presents the section analysis for piers and cap beams which are expected to undergo inelastic response during earthquake.

6.2. Material model

Elastic material properties (elastic modulus and density) have been defined in Chapter 4 and calibrated based on ambient vibration testing results. However, nonlinear behaviors of materials have to be defined in order to perform nonlinear static and dynamic analysis required by Canadian Highway Bridge Design Code. A variety of mathematical models have been developed to simulate the nonlinear stress-strain relationships of concrete and structural steel over decades. (Tedesco et al. 1997; Malvar et al. 1997; Turgay et al. 2009) In this study, a theoretical stress-strain model proposed by Mander (Mander, Priestley, and Park 1988) was adopted for both confined and unconfined concrete and a simplified bilinear model with strain hardening was used for structural steel. Besides, since the bridge was retrofitted by Glass Fiber Reinforcement Polymer (GFRP) at Pier No.2, a theoretical model developed by Lam and Teng. (Lam and Teng 2003)

6.2.1.Mander model

Mander proposed a unified stress-strain model for confined concrete applicable to both circular and rectangular shaped transverse reinforcement, as illustrated in Figure 6-1.

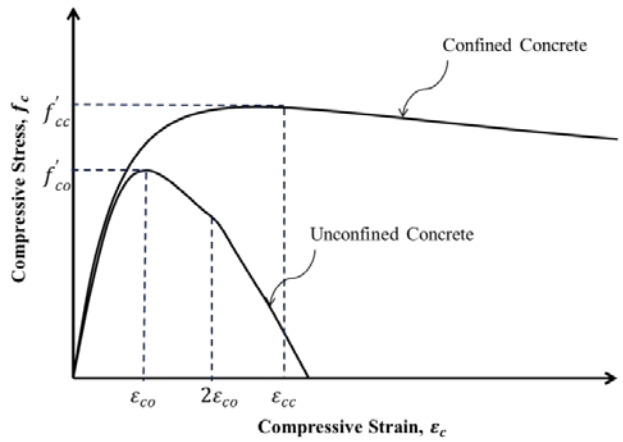

Figure 6-1: Stress strain model for confined and unconfined concrete

For a slow strain rate and monotonic loading, the compressive stress of concrete, f_c is given in Eq.6-1.

$$f_c = \frac{f'_{cc}\left(\frac{\varepsilon_c}{\varepsilon_{cc}}\right)r}{r-1+\left(\frac{\varepsilon_c}{\varepsilon_{cc}}\right)^r} \qquad (\text{Eq.}\,6-1)$$

where f'_{cc} is the compressive strength of confined concrete which can be taken as $1.3f'_{co}$; ε_c is the longitudinal compressive concrete strain; ε_{cc} is given by Eq.6-2.

$$\varepsilon_{cc} = \varepsilon_{co}\left[1 + 5\left(\frac{f'_{cc}}{f'_{co}} - 1\right)\right] \qquad (\text{Eq.}\,6-2)$$

where f'_{co} and ε_{co} are the unconfined concrete strength and corresponding strain, respectively and ε_{co} can be assumed to be 0.002 according to Richart et al; (Richart, Brandtzaeg, and Brown 1928) r is defined by Eq.6-3.

$$r = \frac{E_c}{E_c - E_{sec}} \qquad (\text{Eq.}\,6-3)$$

where E_c is the elastic modulus of concrete; E_{sec} is given by Eq.6-4.

$$E_{sec} = \frac{f'_{cc}}{\varepsilon_{cc}} \qquad (\text{Eq.}\,6-4)$$

For unconfined concrete, the equations above are also applicable in the region where $\varepsilon_c < 2\varepsilon_{co}$. The stress-strain behavior out of the region is assumed to be a straight line which reaches zero at the spalling strain which can be assumed to be 0.005. (Caltrans 2010)

As mentioned in Chapter 2, the structural drawings of Portage Creek Bridge indicate the minimum compressive strength of concrete should be 4000 psi (28MPa) for columns and 3000 psi (21MPa) for cap

beams. According to CSA S06-14, the expected compressive strength of concrete, f'_{ce} shall be taken as $1.25f'_c$, where f'_c is the specified compressive strength of concrete. The expected material properties are summarized in Table 6-1. The stress-strain relationship of concrete can be obtained based on Eq.6-1 to Eq.6-4, as shown in figure 6-5.

Table 6-1: Nonlinear parameters of concrete

	f'_{ce} (MPa)	f'_{cc} (MPa)	E_c (MPa)	ε_{co}	ε_{cu}	ε_{sp}
Piers	35	44.01	24400	0.002	0.012	0.005
Caps	26.25	34.71	27800	0.002	0.015	0.005

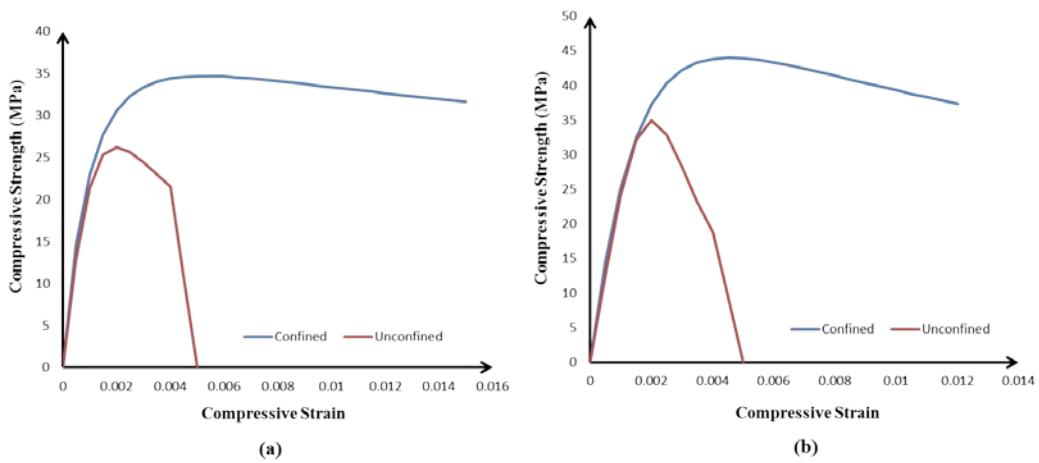

Figure 6-2: Stress-strain relationship of concrete for (a) cap beams and (b) pier No.1

6.2.2. FRP-confined concrete model

FRP jackets have been widely used to enhance seismic performance of structures in engineering practice. It is widely accepted that the shear capacity of RC columns can be considerably increased due to the application of FRP jackets, but the exact behavior of retrofitted member has not been found. (Asaei et al. 2012)

Numerous researches have tried to find out the effects of FRP jackets on structural member over the last recent decades and a large number of experimental studies proved that FRP confinement would affect the post-yielding behavior of concrete while its contribution to elastic modulus of structural members can be ignored. (Asaei et al. 2012) Many researchers proposed their methods to predict the behavior of concrete after confinement using FRP, such as Lam and Teng (Lam and Teng 2003), Turgay (Turgay et al. 2009) and

Fahmy (Fahmy and Wu 2010). However, the approach proposed by Lam and Teng is considered to be the most conventional technique, which can be illustrated in Figure 6-3.

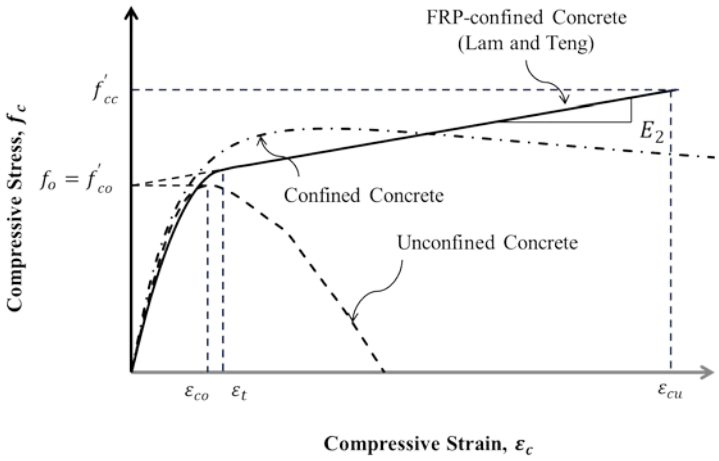

Figure 6-3: Stress strain model for FRP-confined concrete

The stress-strain model of FRP-confined concrete proposed by Lam and Teng consists of a parabolic portion and a linear portion which are given by the following expressions.

$$f_c = E_c\varepsilon_c - \frac{(E_c - E_2)^2}{4f_o}\varepsilon_c^2 \qquad \text{for } 0 \le \varepsilon_c \le \varepsilon_t \qquad (\text{Eq.}\,6-5)$$

$$f_c = f_o + E_2\varepsilon_c \qquad \text{for } \varepsilon_t \le \varepsilon_c \le \varepsilon_{cu} \qquad (\text{Eq.}\,6-6)$$

where f_o is intercept of the stress axis by the linear second portion. The parabolic first portion meets the linear second portion with a smooth transition at ε_t, which is given by

$$\varepsilon_t = \frac{2f_o}{(E_c - E_2)} \qquad (\text{Eq.}\,6-7)$$

where E_2 is the slope of the linear second portion, given by

$$E_2 = \frac{f'_{cc} - f_o}{\varepsilon_{cu}} \qquad (\text{Eq.}\,6-8)$$

where f'_{cc} is the compressive strength of confined concrete, given by Eq.6-9; ε_{cu} is the ultimate strain of FRP-confined concrete, given by Eq.6-10.

$$f'_{cc} = \left(1 + 3.3\frac{f_l}{f'_{co}}\right)\cdot f'_{co} \qquad (\text{Eq.}\,6-9)$$

$$\varepsilon_{cu} = \left[1.75 + 12\left(\frac{f_l}{f'_{co}}\right)\cdot\left(\frac{\varepsilon_{h,rup}}{\varepsilon_{co}}\right)^{0.45}\right]\cdot\varepsilon_{co} \qquad (\text{Eq.}\,6-10)$$

where f_l is the equivalent maximum confining pressure, given by

$$f_l = \frac{2E_{frp}\cdot t\cdot\varepsilon_{h,rup}}{D} \qquad (\text{Eq.}\,6-11)$$

where E_{frp} and t are the elastic modulus and thickness of FRP jacket; D is the diameter of confined section; and $\varepsilon_{h,rup}$ is the rupture strain of FRP, given by

$$\varepsilon_{h,rup} = \frac{f_{tfrp}}{E_{frp}} \qquad (\text{Eq. } 6-12)$$

where f_{tfrp} is the tensile strength of FRP jackets.

5 layers of GFRP were wrapped on the entire Piers No.2 (short piers) in order to enhance the shear capacity of the pier. (Huffman et al. 2006) Location and properties of the FRP jackets are illustrated in figure 3. The stress-strain relationship of the FRP-confined concrete can then be defined in terms of above equations, as shown in figure 6-5.

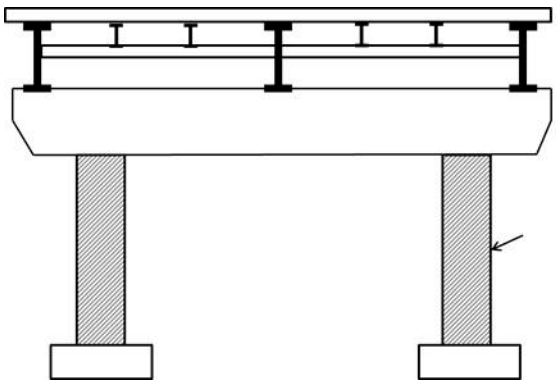

Types	GFRP
Thickness per layer	1.3 mm
Tensile strength	552 MPa
Modulus	27.6 GPa
No. of layers	5

Figure 6-4: Location and properties of FRP jackets

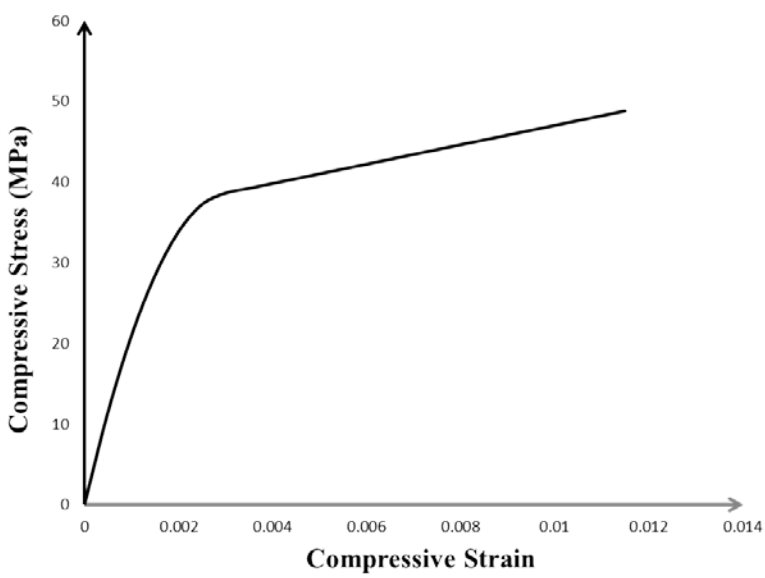

Figure 6-5: Stress-strain relationship of FRP-confined concrete

6.2.3.Reinforcing steel model

The mathematical model for reinforcing bar is a simplified bilinear model with strain hardening, as illustrated in figure 6-6.

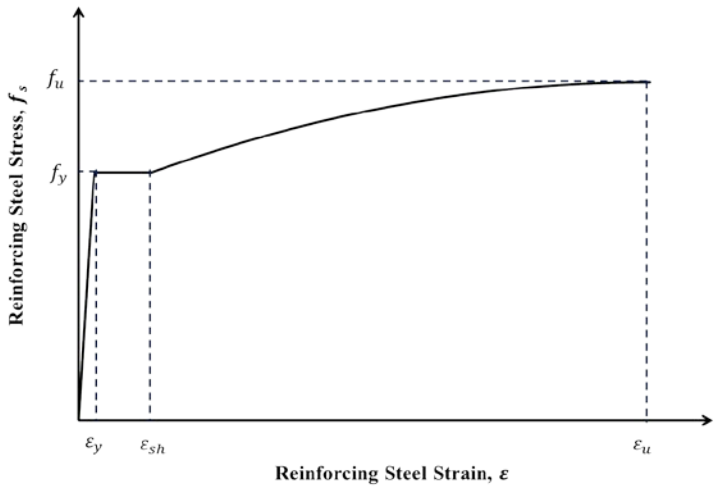

Figure 6-6: Stress-Strain model for reinforcing steel

The stress-strain relationship of reinforcing steel is given by:

$$f_s = E \cdot \varepsilon \qquad \text{for } \varepsilon < \varepsilon_y \qquad (\text{Eq.}\, 6-13)$$

$$f_s = f_y \qquad \text{for } \varepsilon < \varepsilon_y \qquad (\text{Eq.}\, 6-14)$$

$$f_s = f_u - (f_u - f_y) \cdot \left(\frac{\varepsilon_{su} - \varepsilon}{\varepsilon_{su} - \varepsilon_{sh}}\right) \qquad \text{for } \varepsilon < \varepsilon_y \qquad (\text{Eq.}\, 6-15)$$

where E is the elastic modulus; f_y and ε_y are yielding stress and strain, respectively; f_u and ε_{su} are ultimate stress and strain, respectively; ε_{sh} is the strain at strain hardening. (Caltrans 2010)

The structural drawing indicates that the reinforcing steel should conform to Canadian Standard Association (CSA) specification G30.12M grade 400 which indicates a minimum tensile strength of 400 MPa. (CSA A23.3-04) For seismic evaluation of existing bridges, effective nominal resistance using the expected material strength shall be used to determine the flexural resistance of ductile substructure elements, assuming the material resistance factor to be 1.0 in accordance with CSA S06-14. The expected material strength, $f_{y,e}$ of reinforcing bars shall be taken as

$$f_{y,e} = R_y f_y \qquad (\text{Eq.}\, 6-16)$$

where $R_y = 1.2$ for ductile substructure elements with response modification factor larger than 3; f_y is the minimum specified yield strength of reinforcing bars. Material parameters for reinforcing steel are

summarized in table 6-2.

Table 6-2: Material parameters for reinforcing steel

E (MPa)	f_y (MPa)	f_u (MPa)	ε_y	ε_{sh}	ε_{su}
200000	480	655	0.0024	0.015	0.09

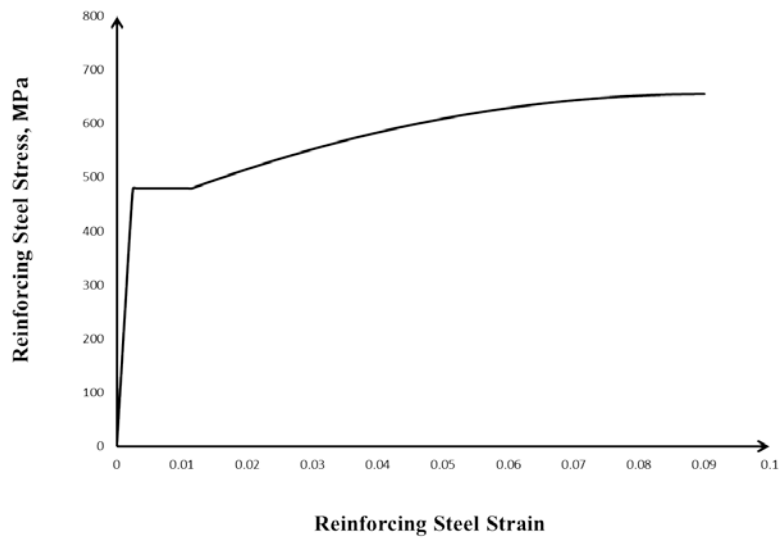

Figure 6-7: Stress –strain relationship for reinforcing steel

6.3. Section analysis

With the material model described above, nonlinear behaviors of ductile structural elements can be predicted through section analysis. There are a lot of commercial software that are capable of performing section analysis, such as X-Section, Xtract and Response 2000. (Aviram, Mackie, and Stojadinović 2008) Also, Sap2000 has a built-in section analysis program called Section Designer. In this study, Xtract by Imbsen (Chadwell and Imbsen 2004) was adopted due to its user-friendly modeling tools and convenient way of output.

Moment-curvature curve of ductile structural elements can be obtained from section analysis, which derives curvatures associated with a range of moments for a cross section under monotonic loading. The moment-curvature curve can be idealized with a bilinear model to estimate the moment capacity of the members which will be used for seismic evaluation of the bridge. Figure 6-8 shows a typical

moment-curvature curve as well as the idealized bilinear model of it.

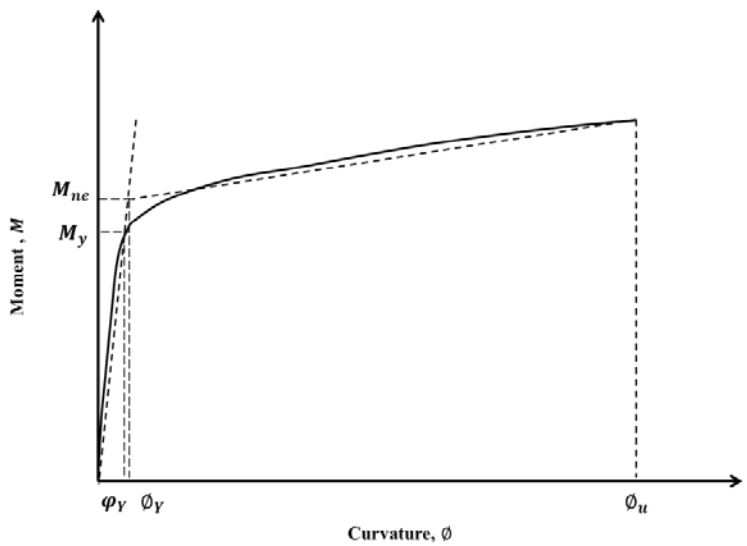

Figure 6-8: Typical moment-curvature curve and idealized bilinear model

The linear portion of the idealized bilinear model should pass through the point marking the first reinforcement bar yields $(M_y, \emptyset_y)$ and the expected nominal moment capacity $(M_{ne}, \emptyset_y)$. The nominal moment capacity represents the end of elastic behavior of the section when the concrete compressive strain reaches 0.003. (Caltrans 2010) According to Section 4.11.8 of CSA S06-14, the nominal member moment capacity should be used for seismic evaluation of existing bridges.

Section analysis was performed for the piers and cap beams which are the members expected to be ductile during earthquake. The section model for piers is shown in figure 6-9. Since the axial forces of piers are expected to vary in time-history analysis, moment-curvature analysis was performed at different levels of axial forces. The interactions between nominal moment capacity and axial force are shown in figure 6-10. Since the pier sections are symmetric in geometry, only the positive values are shown in the figure.

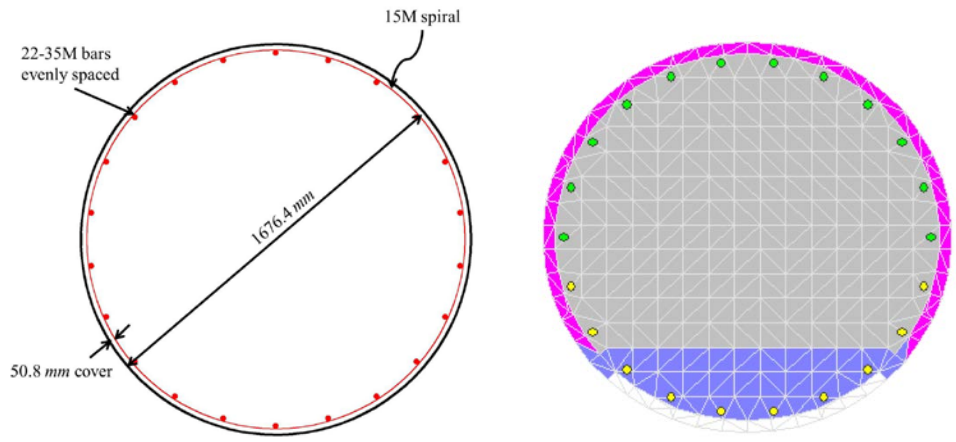

Figure 6-9: Pier section model in Xtract by Imbsen

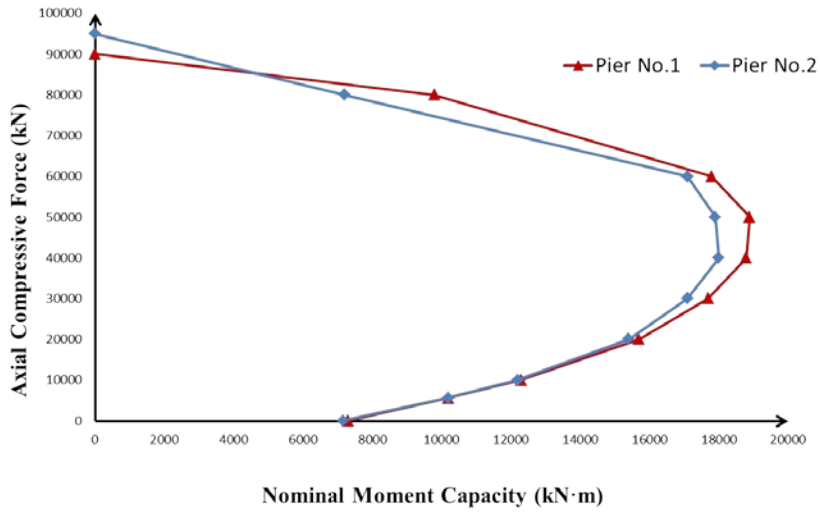

Figure 6-10: P-M interaction of piers

Since Pier No.2 of the bridge has been retrofitted by GFRP, it can be concluded from figure 6-10 that the FRP confinement will not affect the member moment capacity under small to moderate axial forces.

For the cap beams, the axial force can be ignored so the P-M interaction is no longer needed. The moment-curvature analysis should be performed under both positive and negative moment loading because the beam section is asymmetric in the loading direction while positive and negative moments are all expected to emerge during earthquake. The section model for cap beams is shown in figure 6-11 and the moment curvature relationship is illustrated in figure 6-12. Nominal moment capacity of cap beams can be determined accordingly to be 34600kN•m in negative direction and 14400kN•m in positive direction.

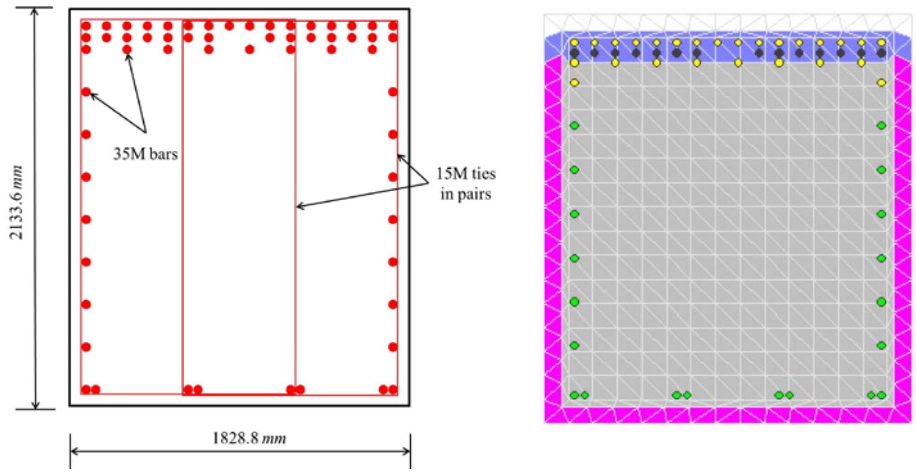

Figure 6-11: Cap beam model in Xtract by Imbsen

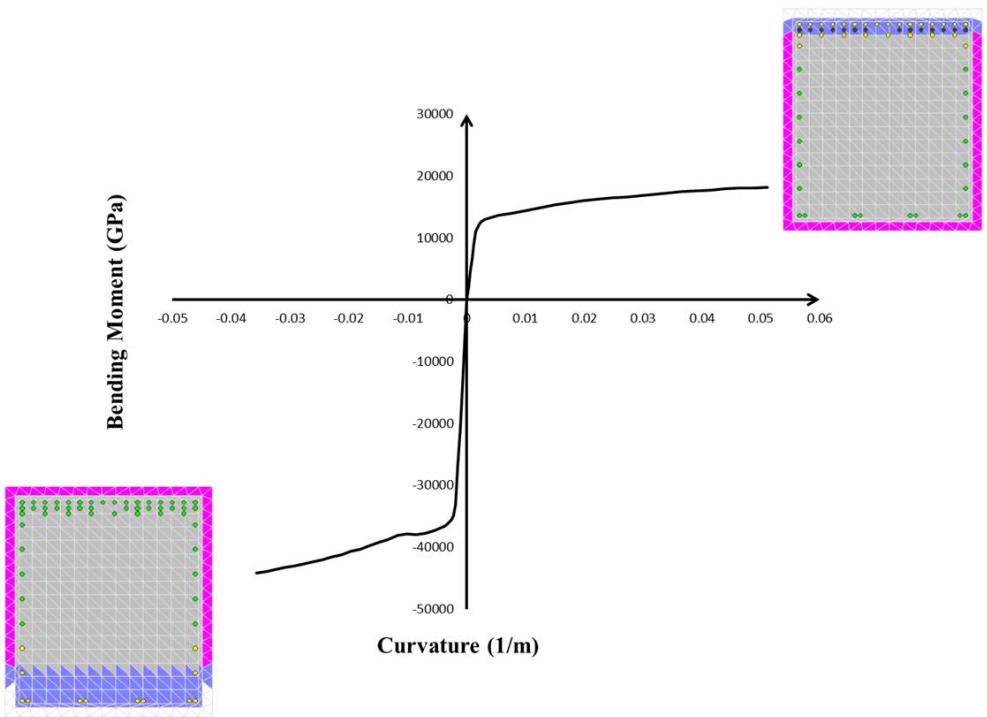

Figure 6-12: Moment-curvature relationship of cap beam section

Chapter 7: Selection of Ground Motions

Seismic input is needed to be defined in order to perform time-history analysis. This chapter presents the methodology to define the input ground motions for nonlinear time-history analysis. The definition of seismic input mainly includes two stages: seismic hazard analysis and selection and scaling of ground motions.

7.1. Seismic hazard analysis

In this study, the site seismic hazard is mainly on the basis of probabilistic analysis. The probabilistic seismic hazard analysis (PSHA) has three stages: 1) definition of spatial distribution of earthquake in source zones; 2) attenuation relationships which will be adopted to estimate the ground motion models for specific geologic conditions; 3) development of site-specific hazard results by integrating the hazard contributions from all source zones over all magnitudes and distances (McGuire,2004). The goal of PSHA is to quantify the probability of exceeding various ground-motion levels at specific site. The PSHA results were used as a reference to select and scale ground motion records.

The seismic hazard analysis was executed following the methodology adopted by the Geological Survey of Canada (GSC) in Open File 4459. (Adams and Halchuk 2003) The software EZ-FRISK (McGuire 1995) was used to perform the PSHA. The ground motion hazard was defined through a Uniform Hazard Spectrum (UHS) which is constructed by enveloping the spectral amplitudes at all periods that are exceeded with a given probability. (Venture 2011) UHS with probabilities of exceedance of 1%, 2%, 5%, 10% and 50% in 50 years, as shown in Figure 7-1. According to CSA S06-14, the UHS with 2% probability of exceedance in 50 years will be used as target spectrum for selecting ground motions.

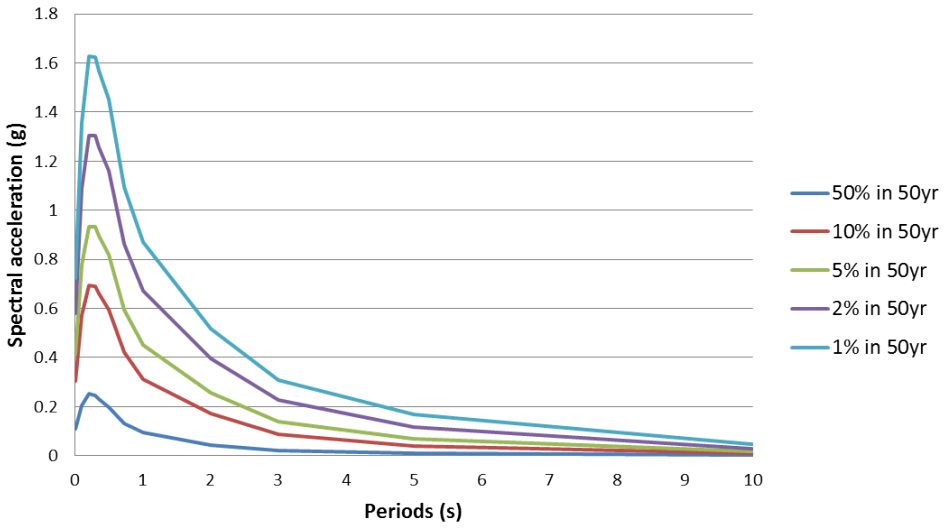

Figure 7-1: Uniform hazard spectrum at the location of bridge

7.2. Seismic hazard deaggregation

The deaggregation of seismic hazard is an effective way to identify the earthquake events that most significantly contribute to selected seismic hazard level. It provides a probability distribution of earthquake magnitude and distance that contribute to the hazard for specific spectral period and ground motion amplitude. For the site of Portage Creek Bridge, deaggregation was carried out at the fundamental lateral period of the bridge, 0.3s, for hazard level of 2% in 50 years. The results are presented in figure 7-2. It can be observed from the figure that there are three 'groups' of ground motion records which correspond to the three types of earthquake. The group with moderate to strong magnitude (5Mw-7.5Mw) and short distance (0-40km) represents the crustal earthquake. The one with strong magnitude (6Mw-7.5Mw) and long distance (50km-150km) stands for the subcrustal earthquake and the rest one represents the subduction earthquake, as shown in figure 7-2.

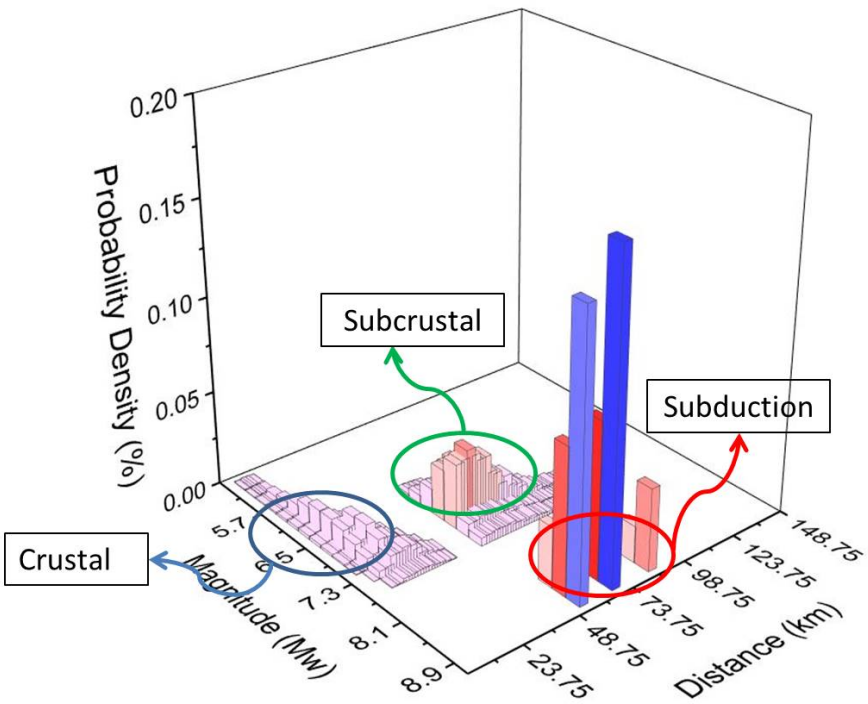

Figure 7-2: Magnitude-Distance deaggregation of hazard level 2% in 50 years at Vancouver Island

7.3. Selection and scaling of ground motions

The results of deaggregation indicate the magnitude and distance (distance from earthquake source) combinations that most significantly contribute to the hazard. Each type of earthquake corresponds to certain range of magnitude and distance, as presented in previous section. The ground motions were selected from the ground motion database developed by researchers in Earthquake Engineering Research Facility (EERF) in UBC, based on the seismic hazard deaggregation results. Table 7-1 indicates the range of magnitudes and distances which were used for selection of ground motion for different types of earthquake records.

Table 7-1: Range of magnitudes and distances for selecting ground motions

Ground motion category	Magnitude (Mw)	Distance (km)
Crustal	5.0-7.5	0-25
Subcrustal	6.0-7.5	50-150
Subduction	8.0-9.0	50-100

Traditional approach for selection of ground motion is to search the ground motion database for earthquake

records which are within the magnitude and distance range of interest. A large amount of eligible records, in general, will be returned from the database and it is the researcher's duty to choose several records from them as needed. The selected records will be scaled in order that the geometric mean response spectrum of them could match the target UHS (2% in figure 7-1). The geometric mean spectral acceleration is defined as

$$S_{a,geomean} = \sqrt{S_{a,1}^2 + S_{a,2}^2 + \cdots + S_{a,n}^2} \qquad (\text{Eq. } 7-1)$$

where $S_{a,n}$ is the spectral acceleration of individual ground motion record. However, a good match does not always happen after scaling of selected records. When the match is not satisfied, researchers need to redo the selection and scaling within the eligible records until a good match is achieved, which is very time-consuming. Mr. Fairhurst, a PHD student in the EERF, has developed a Matlab program to perform the algorithm described above automatically. With the help of this program, selection, scaling and optimization of ground motions were accomplished within a few minutes and a perfect match between geometric mean spectrum of selected records and target spectrum was achieved as shown in figure 7-9 to 7-11. Fifteen ground motions were selected in total with five records for each type of ground motion.

According to Canadian Highway Bridge Design Code (2015), eleven or more sets of ground motion records shall be used for time-history analysis of bridges but no more than two sets of records shall be selected from the same historical earthquake. (CSA S06-14) Twelve ground motion records were selected and Table 7-2 summarizes the station, epicentral distance, magnitude and PGA of each selected record. Figure 7-3 to 7-8 shows the acceleration responses and response spectra of selected records.

Table 7-2: Selected ground motion records

No.	Earthquake	Station	PGA (g)	Magnitude (Mo)	Distance (km)	Type
1	**Chi Chi (1999)**	CWB	0.302	6.2	6.2	Crustal
2	**Morgan Hill (1984)**	CDMG STATION 57217	0.711	6.2	0.53	
3	**Northridge (1994)**	CDMG STATION 24611	0.124	6.7	39.29	
4	**Northridge (1994)**	USC STATION 90046	0.201	6.7	31.48	
5	**Geiyo (2001)**	EHM0050103241528	0.109	6.4	59.85	Subcrustal
6	**Geiyo (2001)**	YMG0180103241528	0.229	6.4	59.32	
7	**Miyagi (2005)**	IWT0100508161146	0.173	7.2	118.97	
8	**Miyagi (2005)**	MYG0160508161146	0.162	7.2	130.78	
9	**Hokkaido (2003)**	HKD0940309260450	0.131	8	110.81	Subduction
10	**Maule (2010)**	llolleo1002271_L	0.325	8.8	120.68	
11	**Tohoku (2011)**	IBR0081103111446	0.307	9	127.7	
12	**Tohoku (2011)**	TCG0161103111446	0.394	9	100.90	

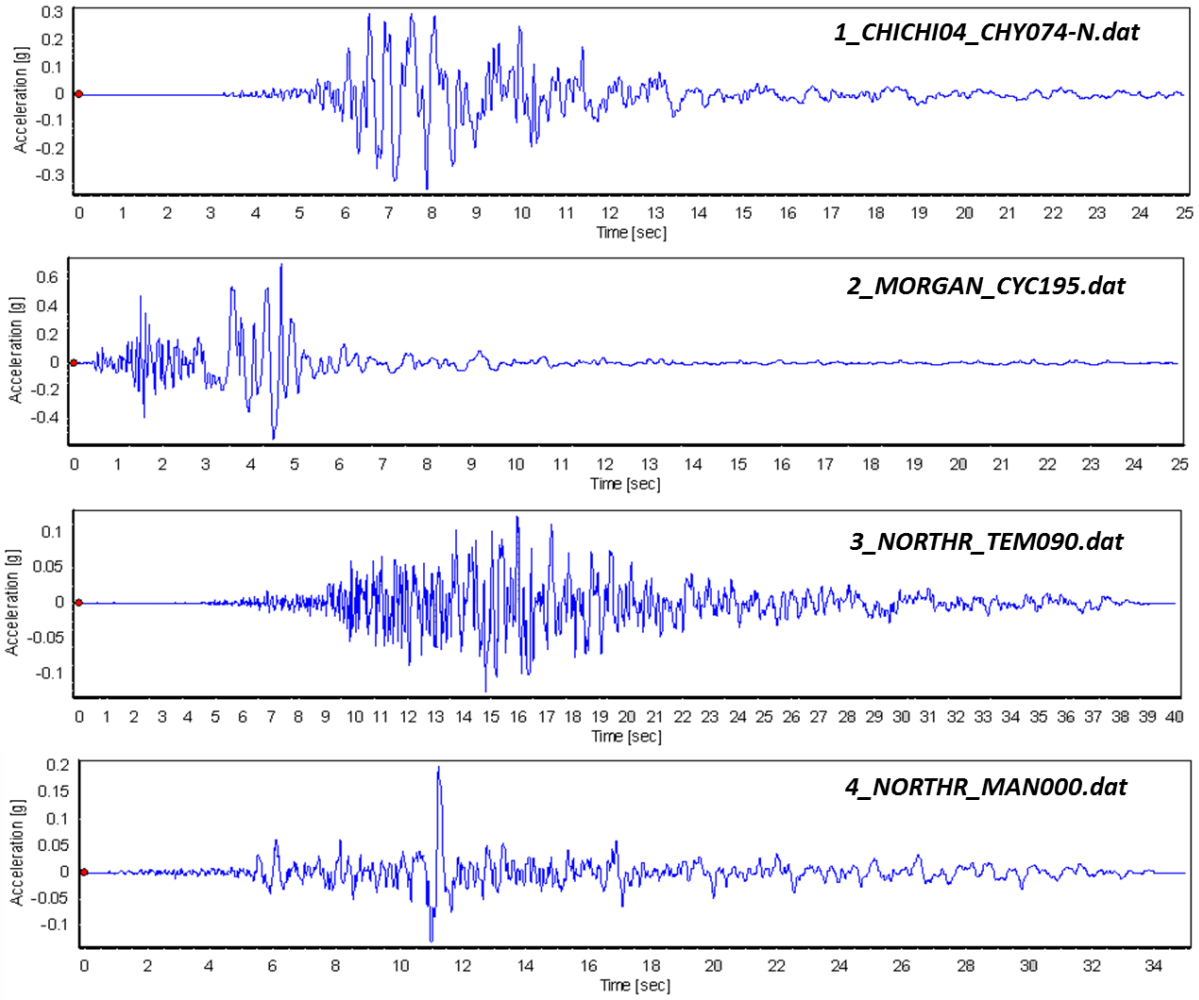

Figure 7-3: Selected crustal earthquake records (No.1-4 in Table 7-2)

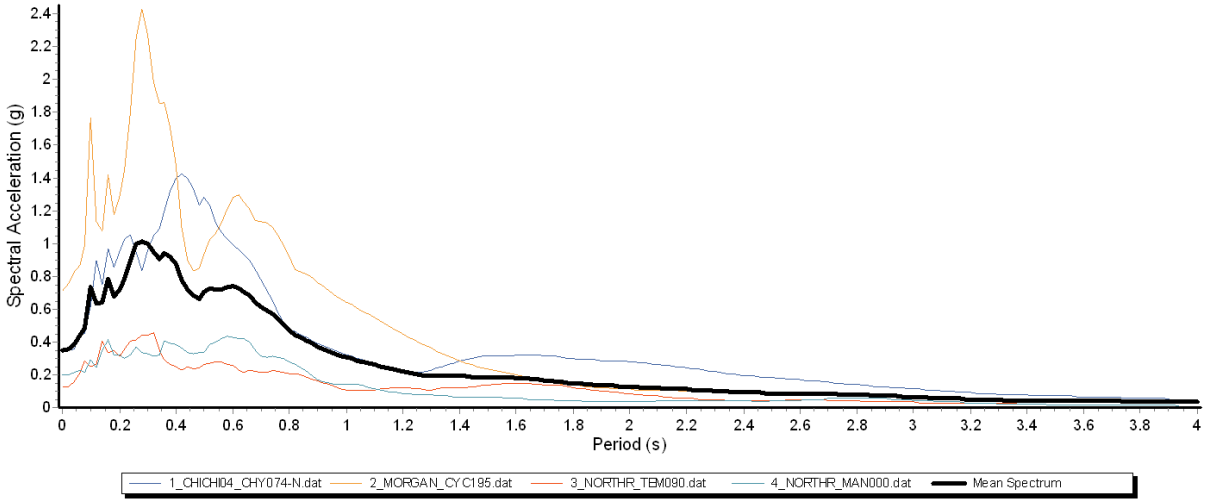

Figure 7-4: Response spectra of crustal earthquake records with 5% damping

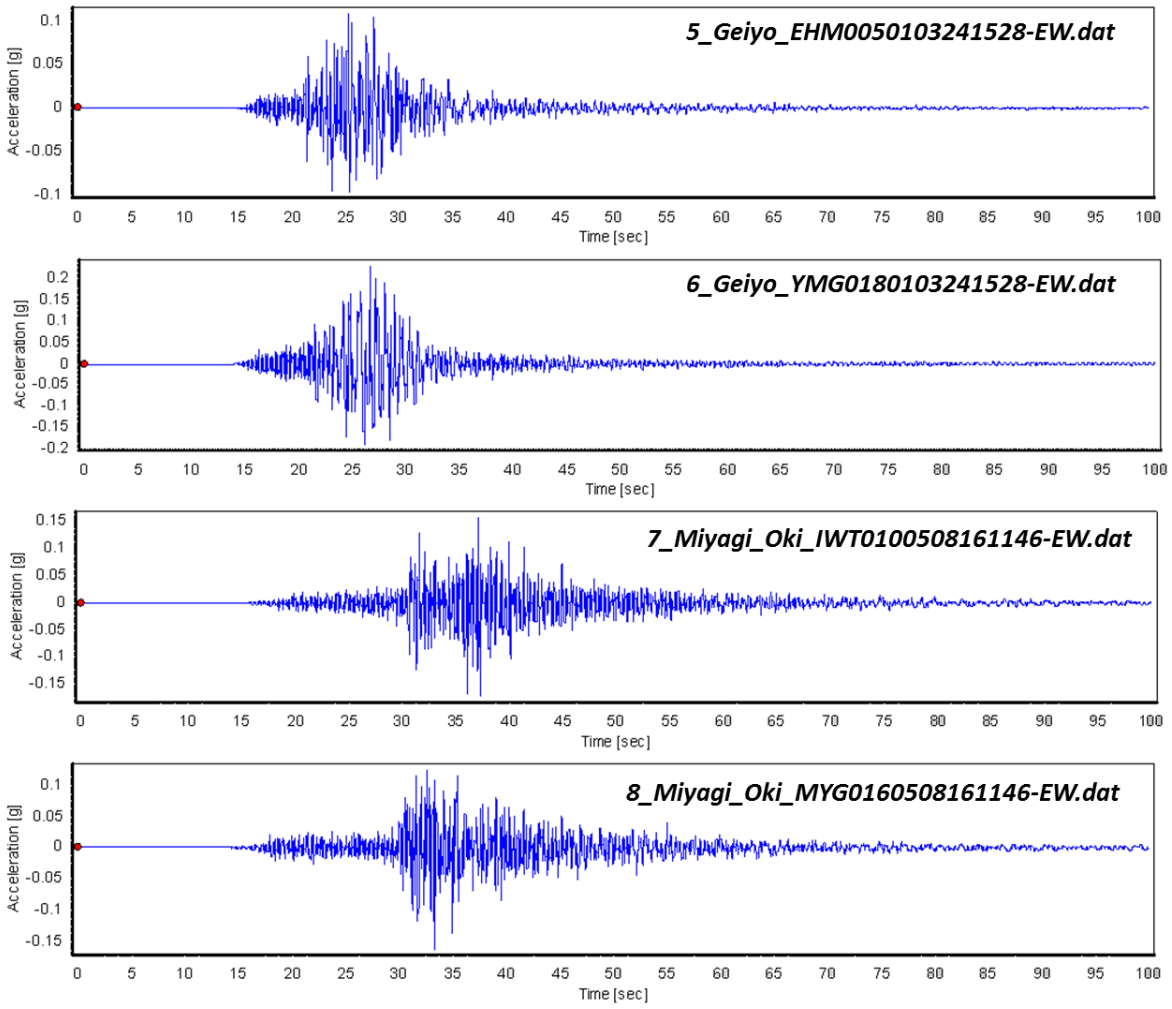

Figure 7-5: Selected subcrustal earthquake records (No.5-8 in Table 7-2)

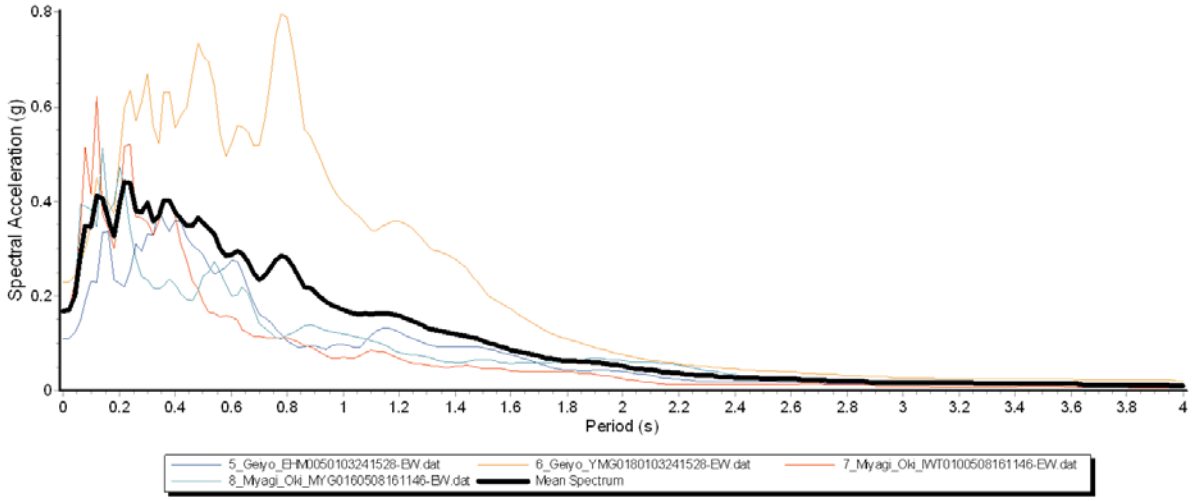

Figure 7-6: Response spectra of subcrustal earthquake records with 5% damping

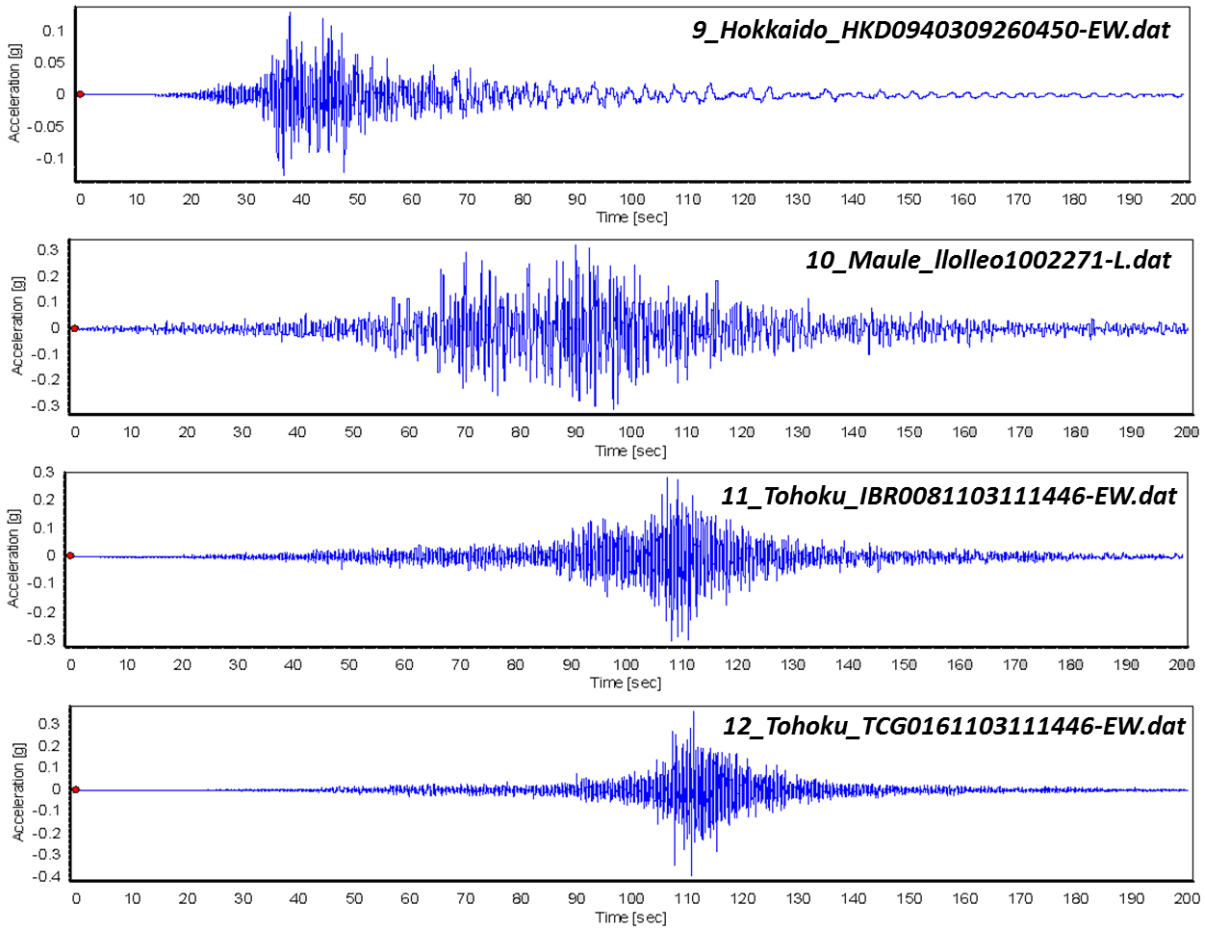

Figure 7-7: Selected subduction earthquake records (No.9-12 in Table 7-2)

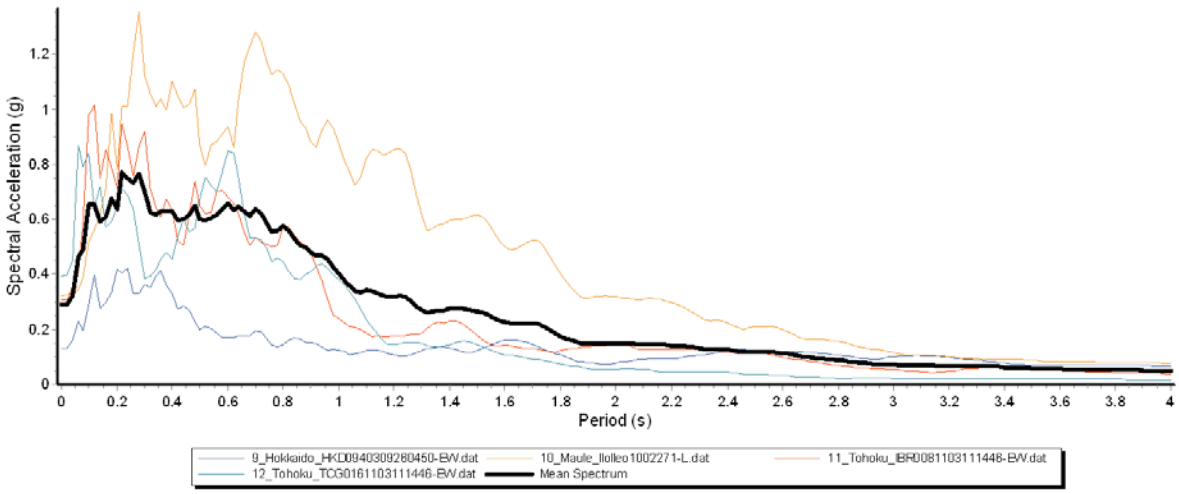

Figure 7-8: Response spectra of subduction earthquake records with 5% damping

7.4. Scaling of ground motions

The selected ground motion records were scaled to match the target response spectrum in the period range of 0.2T to 1.5T. (Venture 2011) The scaling is based on the geometric mean response spectrum of selected records. Target spectrum is Uniform Hard Spectrum (UHS) for a hazard level of 2% in 50 years. (CSA S06-14) The scaling of records was performed for each type of earthquake individually. Each set of earthquake record was linearly scaled by different scale factors, as listed in Table 7-3. The scaled geomean spectrum of selected records are shown in Figure 7-9 to 7-11 for crustal, subcrustal and subduction earthquake, respectively.

Table 7-3: Scale factors for selected ground motion records

Crustal		Subcrustal		Subduction	
Records No.	Scaling Factor	Records No.	Scaling Factor	Records No.	Scaling Factor
1	1.37	5	4.46	9	4.87
2	0.75	6	2.09	10	1.16
3	3.39	7	4.65	11	1.83
4	3.69	8	4.56	12	2.37

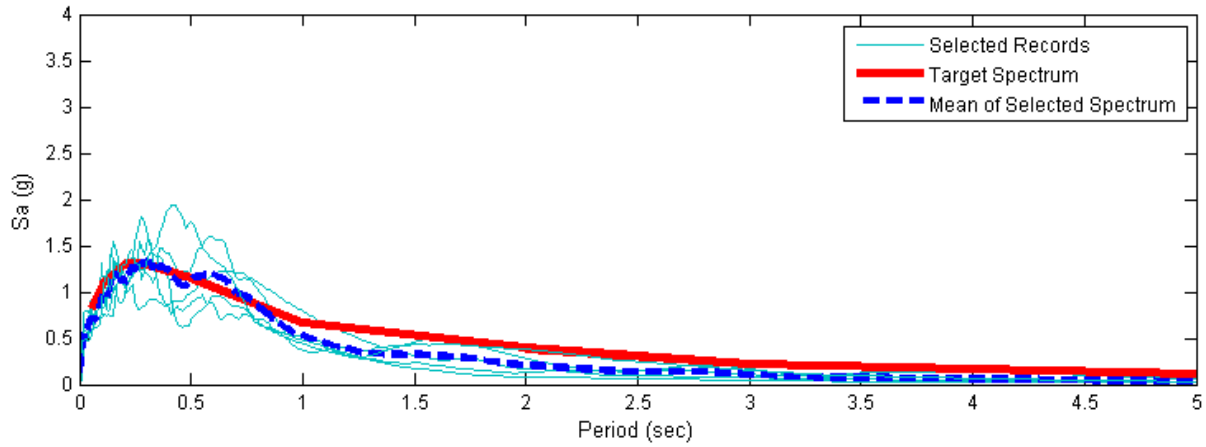

Figure 7-9: Geometric mean response spectrum for scaled crustal earthquake records

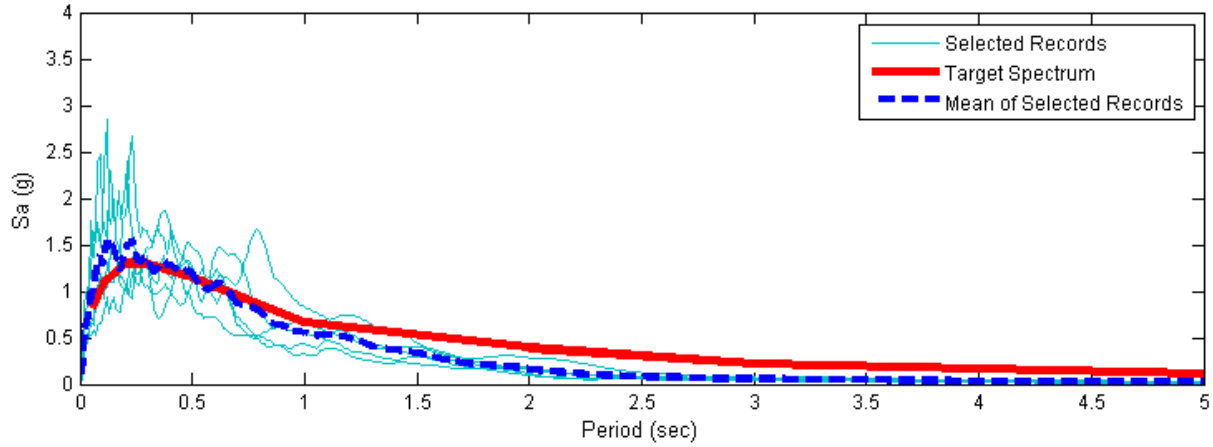

Figure 7-10: Geometric mean response spectrum for scaled subcrustal earthquake records

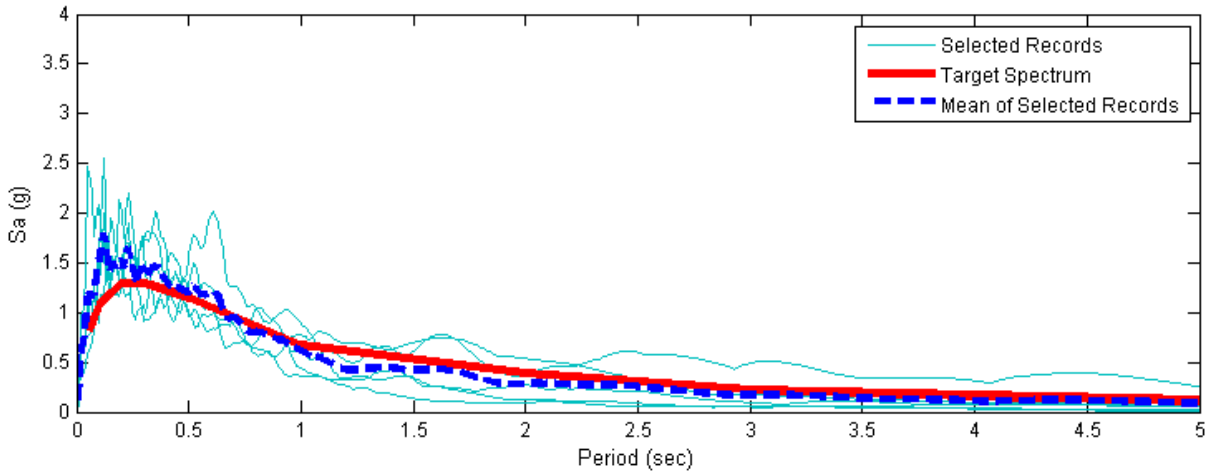

Figure 7-11: Geometric mean response spectrum for scaled subduction earthquake records

Chapter 8: Methodology of Seismic Evaluation

8.1. General

Requirement of member capacities, analysis methods and performance criteria have significantly changed in the code over the past decades. Therefore, seismic evaluation of Portage Creek Bridge, which was designed in 1982, is necessary to be conducted in accordance with current bridge design code, i.e. CSA S06-14, to make sure an acceptable seismic performance in potential earthquake.

Before performing seismic analysis, the analysis requirements were determined based on the bridge classifications in CSA S06-14. Bridges are categorized in terms of importance, seismic performance and regularity in the bridge code. The procedure for determining bridge category is presented below:

First of all, the importance category shall be decided based on social/survival, economic and security/defense requirements. There are three importance categories which are lifeline bridges, major-route bridges and other bridges. Potage Creek Bridges, according to previous research work by Huffman et al (Huffman et al. 2006), is a lifeline bridge. Secondly, the seismic performance category can be determined according to section 4.4.4 in CSA S06-14. Each bridge shall be assigned to one of the three seismic performance categories, based on site-specific spectral acceleration with 2% probability of exceedance in 50 years, the fundamental period of the bride as well as the importance category. For a lifeline bridge with fundamental period of 0.4s and S(0.2) = 1.3, Portage Creek Bridge is in the 3rd seismic performance category. The regularity of bridges can be evaluated according to section 4.4.5.3.2 of the bridge codes. This bridge shall be considered regular based on the criteria.

The seismic analysis requirement can be determined accordingly based on the bridge categories. For Portage Creek Bridge, elastic dynamic analysis (EDA), inelastic pushover analysis and nonlinear time history analysis are all required for seismic evaluation, according to Table 4.12 of CSA S06-14.

8.2. Performance criteria for performance-based design approach

According to Table 4.12 of CSA S06-14, performance-based design is required for Portage Creek Bridges given its importance and seismic performance categories.

Performance level shall be determined first in performance-based design approach. There are four performance levels specified in Table 4.16 of CSA S06-14, which are Immediate, Limited, Service Disruption and Life Safety. Performance criteria about service requirements and expected damages are described in the code for each performance level. Performance levels shall be satisfied under earthquake for different return periods. For Portage Creek Bridge, the first performance levels shall be satisfied for return periods of 475 years and 975 years, which means an immediate return to occupancy is expected during small to moderate earthquake. During severe earthquake with return period of 2475 years, the second performance level is required which means limited damage shall occur but the damage is repairable without requiring bridge closure. The service requirement and expected damage of performance level 1& 2 are detailed in Table 8-1.

Table 8-1: Performance level 1&2 in CSA S06-14

Performance Level	Service	Damage
Immediate	Bridge shall be fully serviceable for normal traffic and repair work does not cause any service disruption	**General:** Bridge shall remain essentially elastic with minor damage that does not affect the performance level of the structure **Concrete Structures:** Concrete compressive strains shall not exceed 0.004 and reinforcing steel strains shall not exceed yield. **Steel Structures:** Steel strains shall not exceed yield. Local or global buckling shall not occur. **Connections:** Connections shall not be compromised. **Displacements**: Pounding shall not occur. Residual displacement, settlement, translation or rotation, of the structure or foundations, including retaining and wing walls, shall be negligible, and not compromise the performance level. **Bearings and Joints:** Shall not require replacement except for possible damage to joint seals.

		Restrainers: No observable damage or loss of displacement capacity to restraining systems or connected elements shall occur. **Foundations:** Foundation movements shall be limited to only slight misalignment of the spans or settlement of some piers or approaches that does not interfere with normal traffic, provided that no repairs are required.
Limited	Bridge shall be usable for emergency traffic and be repairable without requiring bridge closure. At least 50% of the lanes, but not less than one lane shall remain operational. If damaged, normal service shall be restored within a month.	**General:** There may be some inelastic behavior and moderate damage may occur; However, primary members shall not need to be replaced, shall be repairable in place and shall be capable of supporting the dead load plus full live load. **Concrete structures:** Reinforcing steel tensile strains shall not exceed 0.015. **Steel structures:** Buckling of primary members shall not occur. Secondary members may buckle provided that stability is maintained. Net area rupture of primary members at connections shall not occur. **Connections:** Primary connections shall not be compromised. **Displacements:** Permanent offset shall not compromise the service and repair requirements of the bridge. No residual settlement or rotation of main structure shall occur. There may be some movement of wing walls, subject to performance and reparability. **Bearings and joints:** Elastomeric bearings may be replaced. If finger joints are damaged, they shall be repairable. **Restrainers:** Restraining systems shall not be damaged. **Foundations:** Foundation movements shall be limited to only slight misalignment of the spans or settlement of some piers or approaches that does not interfere with normal traffic, provided that repairs can bring the structure back to the original operational capacity.

8.2.1.Performance criteria for concrete structure

Performance criteria for concrete structure are strain limits for concrete and reinforcing steel. The strain varies over the cross-section for flexural members. Assuming that plain section remains plain after bending, strain at a distance of y from neutral axis can be expressed as:

$$\varepsilon = \frac{M}{EI} y \qquad (\text{Eq.}\, 8-1)$$

where E is the elastic modulus of the material; I is the second moment of inertia; M is the bending moment about the neutral axial. The strain-moment relationship can also be obtained from section analysis introduced in Chapter 6. Figure 8-1 & 8-2 illustrates the relationship between maximum strain and moment at different axial force (P) values, for pier concrete and pier rebar. Figure 8-3 illustrates the relationship between maximum strain and moment, for cap beam concrete and rebar.

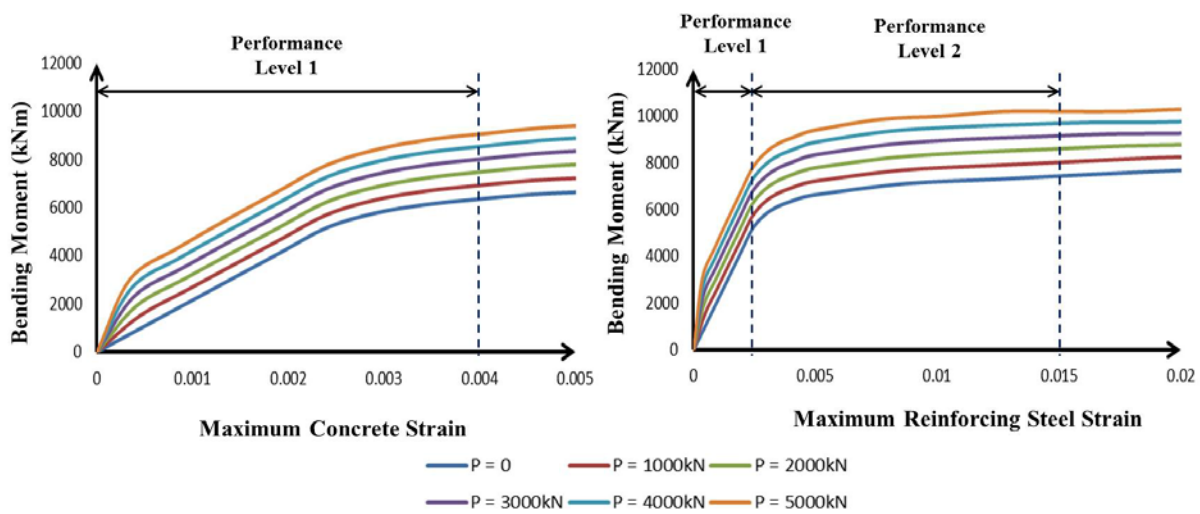

Figure 8-1：Moment-strain relationship for concrete and reinforcing steel at Pier No.1

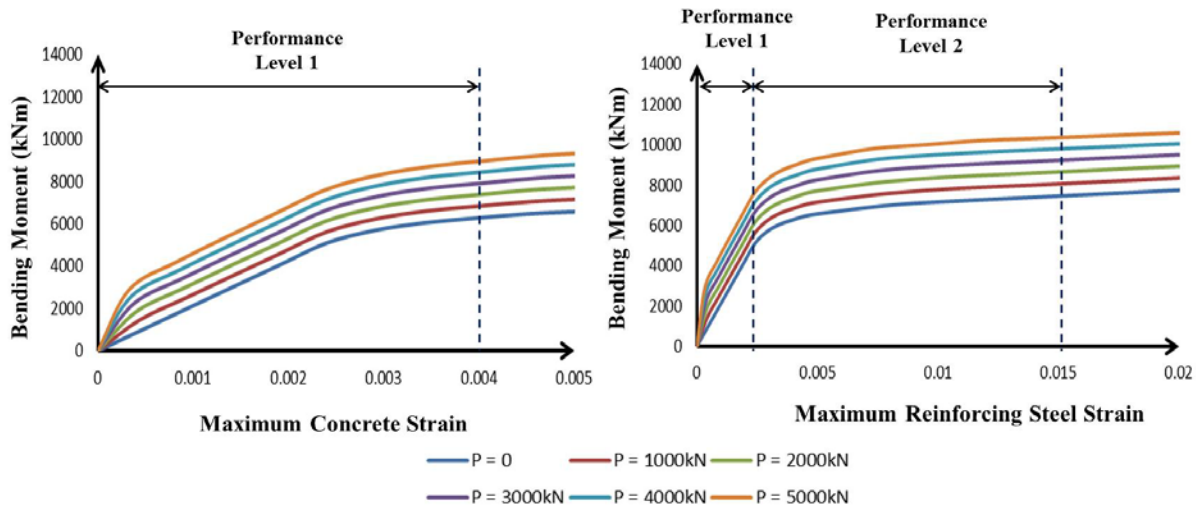

Figure 8-2: Moment-strain relationship for concrete and reinforcing steel at Pier No.2

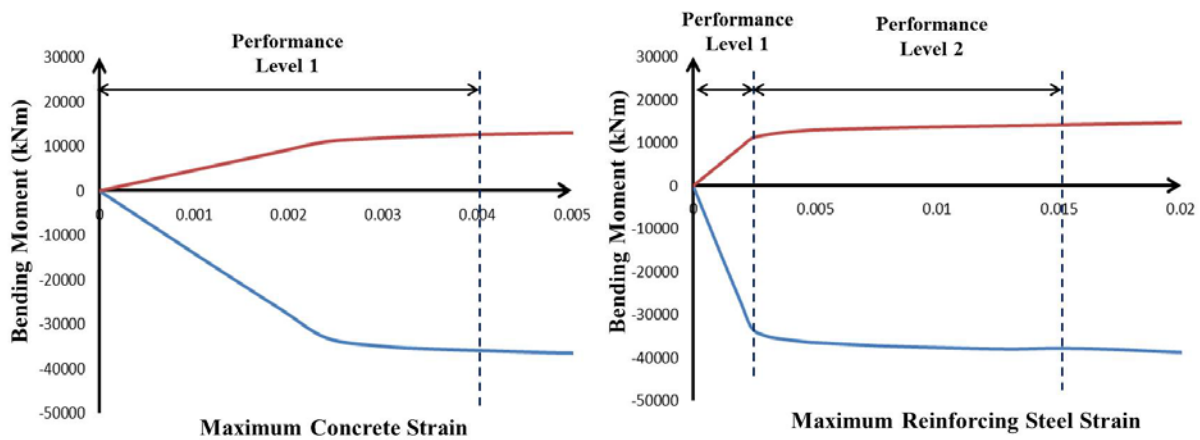

Figure 8-3: Moment-strain relationship for concrete and reinforcing steel at cap beams

Therefore, the strain requirements in the performance criteria can be converted to moment requirement based on the moment-strain curve. Taking the first performance level (Table 8-1) for example, the performance criteria require the maximum concrete compressive strain shall not exceed 0.004 and reinforcing steel strain shall not yield. For piers, the critical bending moments at concrete compressive strain of 0.004 and rebar yield strain are identified at different axial force values. The interaction between the critical bending moments and axial forces is plotted in figure 8-4 & 8-5, for Pier No.1 & 2 respectively. These interaction curves can be regarded as the acceptance criteria for the first performance level and will be compared with the resulted element moment from seismic analysis. For cap beams, axial loads were not considered in the analysis. The critical moments for each performance level are summarized in Table 8-2.

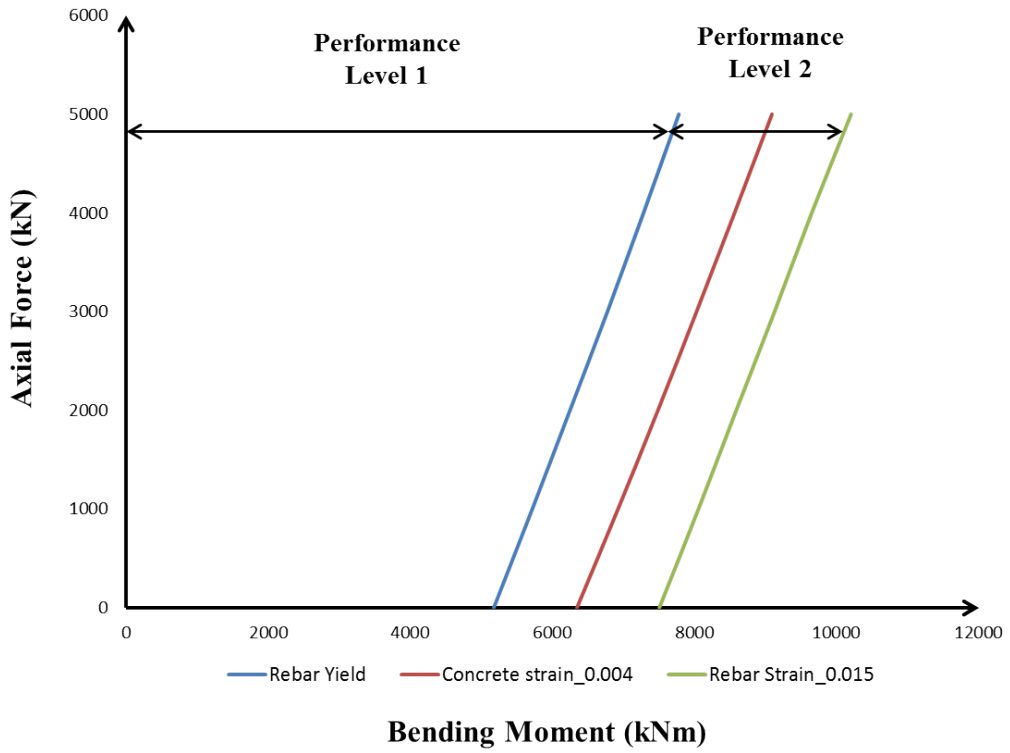

Figure 8-4: Performance levels for pier No.1

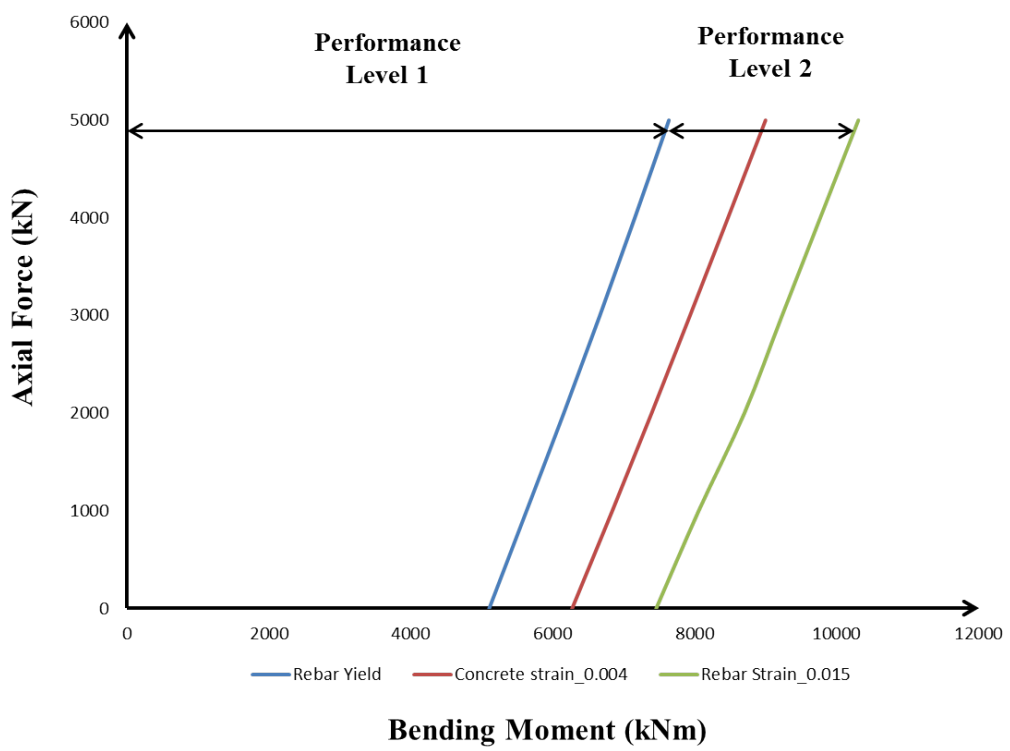

Figure 8-5: Performance levels for Pier No.2

Table 8-2: Critical moments for cap beams (kN•m)

	Performance Level 1	Performance Level 2	
	Rebar Yield	Concrete strain 0.004	Rebar Strain 0.015
Positive	11050	12610	14240
Negative	33100	35800	37800

8.2.2.Performance criteria for other aspects

Steel structure in Portage Creek Bridge, which includes Girders, stringers and floor beams, are all secondary structures. The buckling of steel structure was checked by Euler's critical load ((Timoshenko and Gere 2009):

$$F = \frac{\pi^2 EI}{(KL)^2} \qquad (\text{Eq.}\, 8-2)$$

where F is the expected compressive force on buckling; E is modulus of elasticity; I is area moment of inertia of the cross section; L is the unsupported length of the element and K is the effective length factor. Girders and stringers are all casted together with the concrete decking, which means their unsupported lengths are zero and the buckling fore is infinite large. Floor beams and braces were regarded as fixed-end elements so the K factor was 0.5. Element properties and buckling forces of floor beams and braces are summarized in Table 8-3.

Table 8-3: Buckling force of brace and floor beam

	E (Mpa)	I (mm^4)	L (mm)	F (kN)
Brace	200000	9105150	9485	798
Floor Beam	200000	142800000	2692	155427

*I was taken as the smaller value of that about the two axis.

Primary connections of the bridge are the connections between pier and cap beam as well as the connections between pier and foundation footings. Connections were checked for capacities of sections around them (Figure 8-6) which was determined following the procedure in Section 6.3. Performance of elastomeric bearings, structural displacement and foundation movement was obtained from seismic analysis and evaluated in terms of the criteria in Table 8-1. There is no restrainer in this bridge. The analysis results will be presented in Chapter 9.

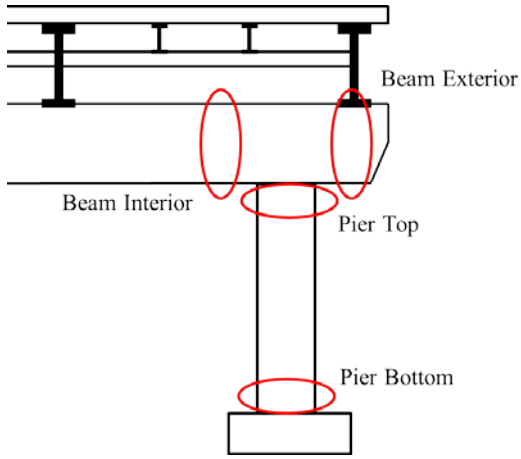

Figure 8-6: Critical sections to be checked

8.3. Performance criteria for force-based design approach

Force-based design (FBD) is the traditional design approach which has been utilized by engineers for hundreds of years. FBD is essentially a comparison between demand and capacity of structural members while the specific design approach varies between different standards. Force-based seismic evaluation was carried out in this study, but the limited evaluation for expansion bearings in performance-based design approach is presented in this section as reference.

Limited evaluation shall be performed according to Section 4.11.5.2 of CSA S06-14. Since there are no longitudinal restrainers or integral connection for the expansion bearings at the west end of Portage Creek Bridge, the seat width shall be checked for a minimum support length *N* given by:

$$N = K\left[200 + \frac{L}{600} + \frac{H}{150}\right]\left[1 + \frac{\Psi^2}{800}\right] \qquad (\text{Eq.}\, 8-3)$$

where *K* is the modification factor, 1.5 for seismic performance category 3; *L* is the length of the bridge deck to the adjacent expansion joint or the end of bridge deck. Since there is only one expansion joint at the west abutment, L is taken as the length of the bridge, 12500mm. *H* is the average height of the columns supporting the bridge deck to the next expansion joint which is taken as (8500+5800)/2 = 7150mm. Ψ is the skew of support measured from a line normal to the span direction, which is 86.9°. Therefore, the minimum support length *N* can be calculated as 783mm. The seat width of the expansion bearings at west abutment is 685.8mm,

which means that the minimum support length requirement is not met for this bridge.

Also, the bearings shall be checked for a force demand not less than 20% of the tributary dead load in the restrained direction. The structural drawings provide the minimum strength of the elastomeric pad which is assumed to dominate the bearing shear capacity in horizontal direction. Table 8-4 summarizes the 20% dead load (DL) and calculated shear capacity for each bearing. The shear demand for each bearing was obtained from seismic analysis and was presented in Chapter 9.

Table 8-4: Minimum force demand and shear capacity of bearings

Bearing Location		20% DL (kN)	Shear Capacity (kN)
West Abutment	Exterior	120.4	1565.773
	Interior	166.8	2562.175
Pier No.1	Exterior	403.4	4697.32
	Interior	563	7686.524
Pier No.2	Exterior	308.4	3558.576
	Interior	434	5337.864
East Abutment	Exterior	89.8	1281.087
	Interior	136.2	1761.495

8.4. Load combination and orthogonal effect

CSA S06-14 requires the seismic evaluation of existing bridges shall be based on following load factor and load combination.

$1.0D + 1.0EQ$

Seismic response resulting from analysis in orthogonal directions shall be combined to ensure that the bridge is capable of resisting earthquake from all possible directions. CSA S06-14 recommends the member shall be designed for “100 percent of prescribed seismic force in one direction plus 30 percent of the seismic force from the perpendicular direction”. However, the percentage combination rule is empirical and could underestimate the design forces in certain members, producing a member design which is relatively weak in

one direction. (Aviram, Mackie, and Stojadinović 2008) In order to obtain a conservative result, three components of ground motion records (longitudinal, transverse and vertical) were included in a single analysis assuming the earthquake from orthogonal directions may occur simultaneously. The input motions were selected based on the Uniform Hazard Spectra indicated in CSA S06-14, which was elaborated in Chapter 7.

8.5. Member Capacity

Flexural resistance was determined based on the section analysis results which have been introduced in Chapter 6. According to CSA S06-14, for non-prestressed elements, the nominal shear resistance, V_r shall be calculated as

$$V_r = V_c + V_s \qquad (\text{Eq.}\, 8-4)$$

where V_c is the shear capacity contributed by concrete, given by

$$V_c = 2.5\beta f_{cr} b_v d_v \qquad (\text{Eq.}\, 8-5)$$

where f_{cr} is the cracking strength given by $0.4\sqrt{f_c^{'}}$ for normal density concrete; b_v and d_v are effective shear depth and width of the section, respectively; β is equal 0.18 for both cap beam and pier according to CSA S06-14; V_s is the shear capacity contributed by transverse reinforcing steel given by

$$V_s = \frac{f_y A_v d_v \cot\theta}{s} \qquad (\text{Eq.}\, 8-6)$$

where f_y is the yield strength of reinforcing steel; A_v is the effective shear area of the section; s is the distance between transverse reinforcing steel layers; θ is taken as 42° for both cap beam and pier.

The shear capacity enhancement by FRP jacket was calculated by equation proposed by Priestly (Priestley, Seible, and Calvi 1996):

$$V_{FRP} = 2.25 t_f f_{FRP} D \qquad (\text{Eq.}\, 8-7)$$

where t_f is the thickness of FRP jacket; f_{FRP} is the tensile strength of FRP and D is the diameter of confined section. The calculated shear capacities of cap beam and pier are summarized in Table 8-5.

Table 8-5: Nominal shear capacity of primary structural elements

	Pier No.1	Pier No.2	Cap Beam
Shear Capacity (kN)	5303	8010	4935

Priestly also proposed an approach for estimating shear capacity of concrete sections, which is widely used in engineering practice. In this approach, the shear capacity enhancement contributed by axial forces is also considered, so the nominal shear capacity, V_r can be expressed as

$$V_r = V_c + V_s + V_p \qquad (\text{Eq.}\, 8-8)$$

where V_c is given by

$$V_c = k\sqrt{f_c'}A_e \qquad (\text{Eq.}\, 8-9)$$

where k can be identified from Figure 8-7 & Figure 8-8, for piers and beams, respectively; A_e is the effective shear area which equals to $0.8A_{gross}$.

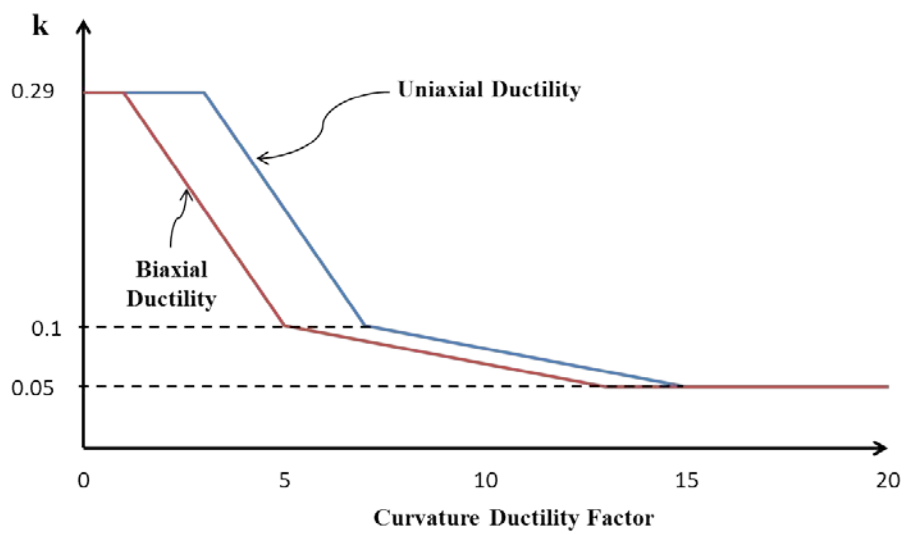

Figure 8-7: k value for estimating shear capacity of pier concrete

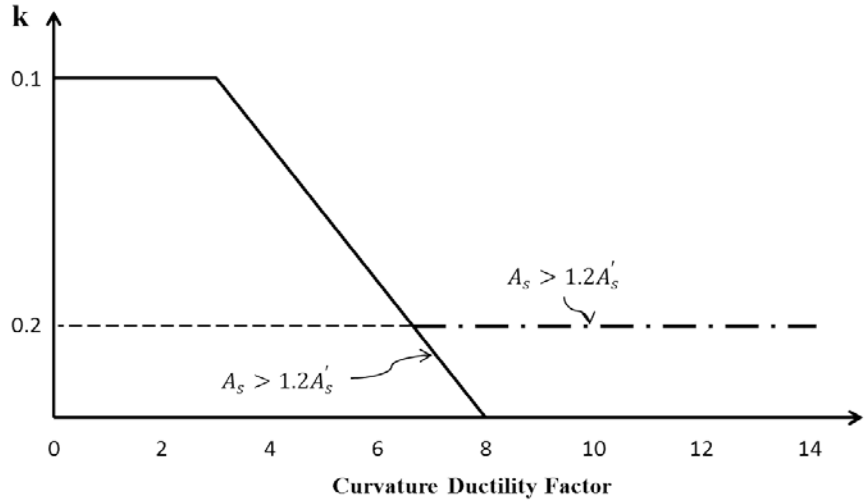

Figure 8-8: k value for estimating shear capacity of beam concrete

The reinforcing steel's contribution to the shear capacity, V_s, is expressed as follows:

For circular section:

$$V_s = \frac{\pi}{2}\frac{f_y A_v D' \cot\theta}{s} \qquad (\text{Eq.}\, 8-10)$$

For rectangular section:

$$V_s = \frac{f_y A_v D' \cot\theta}{s} \qquad (\text{Eq.}\, 8-11)$$

where D' is the core dimension, from center to center of peripheral hoop.

The shear strength enhancement resulting from axial compression is given by

$$V_p = P \tan\alpha \qquad (\text{Eq.}\, 8-12)$$

where α is the angle formed between the column axis and the line joining the centers of flexural compression at the top and bottom of the pier, since pier is considered as double bending in this study. The resulted shear capacity is summarized in Table 8-6.

Table 8-6: Nominal shear capacity of primary structural elements (Priestly)

	Pier No.1	**Pier No.2**	**Cap Beam**
Shear Capacity (kN)	6891	9598	7323

It can be concluded from Table 8-5 & 8-6 that the equations in CSA S06-14 will result in a more conservative estimation of shear capacity. In order to ensure safety of the bridge, the code-based approach was adopted in this study.

Chapter 9: Seismic Analysis

9.1. General

According to Section 4.4.6.3 of CSA S06-14, the assessment of performance levels shall be carried out using nonlinear time-history analysis or static pushover analysis to the design displacement. In this study, nonlinear time history analysis was adopted to evaluate the seismic performance of the bridge while the pushover analysis was also performed.

Prior to perform nonlinear static and dynamic analysis, nonlinear behavior should be defined for the finite element model. Two categories of nonlinear behavior are incorporated in this model to represent the structural response behavior under severe earthquake. The first category is nonlinear behavior of structural elements due to inelastic material stress-strain relationship, as well as the nonlinear behavior of damper, bearing and soil. The second category is geometric nonlinearity which consists of P-Δ effects and stability hazard under large deformation.

In order to model the nonlinear behavior of structure, structural elements which are expected to undergo inelastic excursion should be determined first. In general design practice, superstructure of lifeline-bridge is designed to remain elastic during earthquake to ensure post-disaster serviceability. Therefore, the superstructure is modeled as linear-elastic beam-column element in this model with material properties calibrated based on AVT results. Other structural elements, such as cap beams, piers, abutments and bearings are designed to dissipate energy to protect the superstructure in an earthquake event. Also, the nonlinearity of soil-structure interaction is of great significance when soil condition is not good enough. For Portage Creek Bridge, the nonlinear behaviors of abutments, bearings and soil-structure interaction are difficult to be modeled due to the lack of geotechnical documents and bearing details, so they are also assumed to remain in elastic stage in this study. Instead, viscous damping is defined to represent the energy dissipation induced by nonlinear behavior of these elements. In summary, only the nonlinear behaviors of cap beams and piers are considered in this study. Detailed modeling approaches are presented in following subsections.

9.2. Definition of nonlinear analysis model

Nonlinear behavior of the bridge analysis model was defined by plastic hinge models (model with concentrated plasticity) and assigned to pre-determined locations of the ductile elements. In SAP2000, several modeling options can be employed to define the nonlinear behavior of plastic hinges, which can be summarized into 3 categories: Uncoupled Hinge, Interaction PMM Hinge and Fiber PMM Hinge. Some of the main capabilities and limitations of these models are summarized in Table 9-1. (Aviram, Mackie, and Stojadinović 2008)

Table 9-1: Capacities and limitations of nonlinear models in SAP2000

Nonlinear Option	Couple Behavior M2-M3	Axial-moment interaction P-M2-M3	Degrading behavior	Ductility estimation	Numerical stability	Low computational effort
Uncoupled Hinge			√	√		√
Interaction PMM Hinge	√	√	√	√		√
Fiber PMM Hinge	√	√	√		√	

Uncoupled hinge and interaction PMM Hinge

Uncoupled Hinge was employed for cap beams since axial force can be ignored. Nonlinear behavior of plastic hinge was defined by an idealized moment-curvature relationship obtained from section analysis, which can be illustrated from figure 9-1.

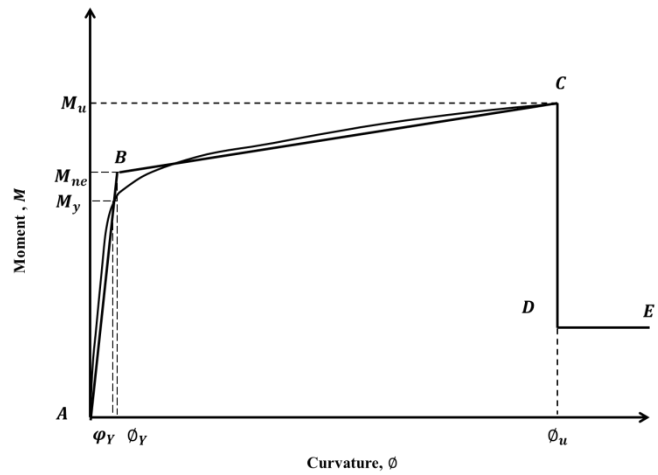

Figure 9-1: Moment-curvature relationship defined for plastic hinge

In the figure above, point B is yield point for which nominal moment capacity, M_{ne} and its corresponding curvature, $\emptyset_y$ shall be used. Point C is the ultimate point for which ultimate moment capacity, M_{ne} and ultimate curvature $\emptyset_u$ was defined. Point D stands for the degraded capacity of the plastic hinge, which can be taken as 20% of the ultimate capacity. However, the consideration of degradation would result in a convergence problem in the analysis so the degradation effect was ignored in this study given the fact that primary members are not expected to reach the ultimate capacity. Point E is the failure point for which a greater value than point D shall be defined. Other than the moment-curvature relationship, the equivalent analytical plastic hinge length shall be defined for the hinge model, which was calculated by following equations recommended in SDC2010 (Caltrans 2010):

$$L_p = 0.08L + 0.022 f_{ye} d_{bl} \qquad \text{(Eq. } 9-1)$$

where f_{ye} is the yield strength of reinforcing steel; d_{bl} is the diameter of reinforcing steel.

For the PMM Interaction Hinge, moment-curvature relationship was defined for several levels of axial load of the piers, following the same procedure described above for uncoupled hinge. The axial load includes the dead load calculated from the gravity analysis as well as several additional levels of axial load with a range between the minimum and maximum axial force expected in the piers. The range of expected axial force was determined from the elastic dynamic analysis. In addition, the normalized PMM interaction diagram was defined using the results from section analysis.

Fiber hinge

Uncoupled Hinge and Interaction PMM hinge have low computational effort but they are only limited to static pushover analysis since convergence problem may occur during the nonlinear time-history analysis. In this study, Fiber Hinge option in SAP2000 was employed to model the plastic hinge in nonlinear time-history analysis. Structural degradation and softening after yielding can be considered by fiber hinge, which makes it more accurate in predicting the nonlinear behavior of structural elements. The fiber hinge automatically computes the moment-curvature relationships in any bending direction for varying levels of axial load through section analysis of discretized fibers in the cross section.

To define the fiber hinge, stress-strain relationship was defined first for confined concrete, unconfined concrete and reinforcing steel with material model introduced in previous chapter. Then the fiber hinge was created as a user-defined displacement control model, with a characteristic length of L_p, given by Eq.9-1. The section was divided into a number of discretized fibers corresponding to the cover, the core, and reinforcing steel, as shown in figure 9-2 for piers. The area, coordinates and material type for each fiber shall be defined.

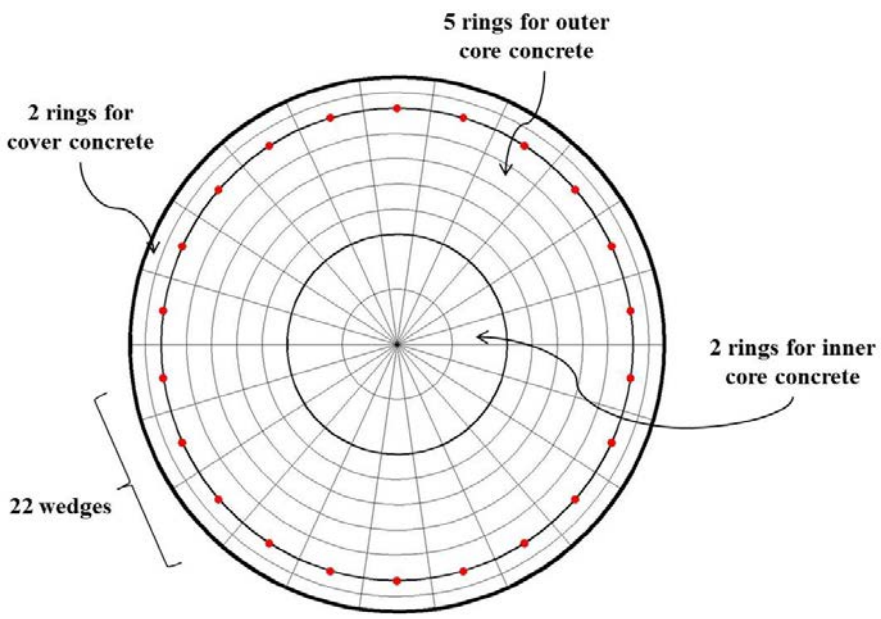

Figure 9-2: Fiber distribution of pier section

Fibers defined for concrete are categorized into inner core, outer core, and cover. The number of each category of fiber is illustrated in Figure 9-2. The number of fibers defined for the inner core was reduced since the cross-sectional behavior in flexure is controlled by the outer rings. One fiber was defined for each

reinforcing bar with its area and coordinate. A sufficient number of fibers are required to represent the cross section configuration with enough accuracy. Also, the values for the hinge area and moment of inertias shall be within 5% difference from the member gross section. (Aviram, Mackie, and Stojadinović 2008) The comparison of properties between fiber hinge and pier section is shown in Table 9-2.

Table 9-2: Comparison of properties between fiber hinge and pier section

Items	Fiber Hinge	Pier Section	Difference (%)
Area (m^2)	2.2167	2.2072	0.4286
Centroid3 (mm)	-0.275	0	—
Centroid2 (mm)	-0.039	0	—
I33 (m^4)	0.3741	0.3877	3.6354
I22 (m^4)	0.3737	0.3877	3.7463

9.3. Pushover analysis

Pushover analysis is a static-nonlinear analysis method where the magnitude of structural loading is increased incrementally following a predefined load pattern until an ultimate condition is reached. Weak links and failure modes can be determined with the continuous loading. Also, the overall strength, maximum displacement and ductility capacity can be obtained from the pushover analysis. Moreover, the pushover analysis can examine the sequence of plastic hinge formation, which could provide an overview of the failure mechanism of the structure.

Displacement capacity was estimated first as the target displacement for pushover analysis. Since it is very difficult to determine the overall displacement capacity of the bridge, local pier displacement capacity was employed instead to control the pushover analysis. In this study, the pier was idealized as two-end-fixed member as presented in Figure 9-3.

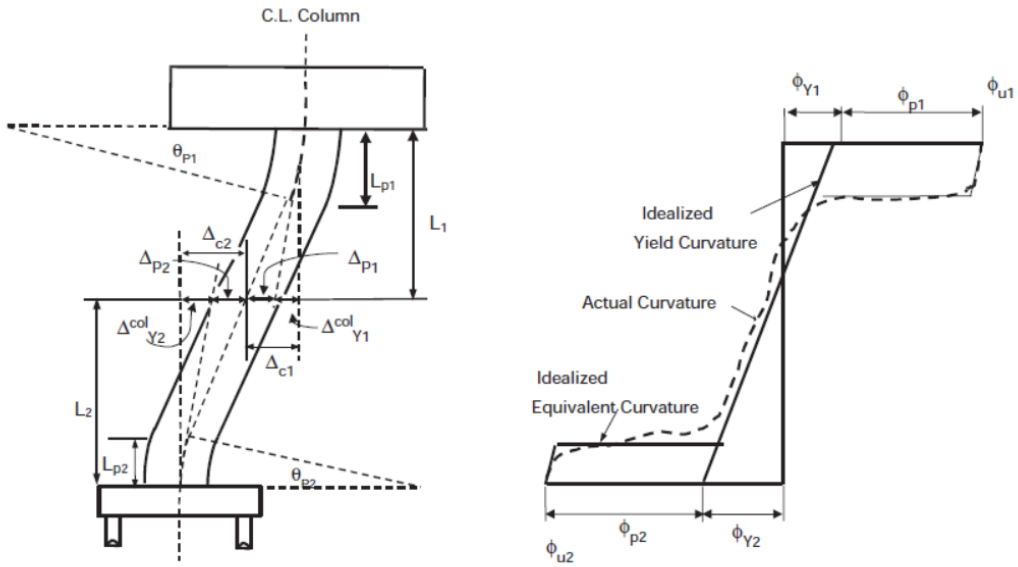

Figure 9-3: Pier displacement capacity (Caltrans 2010)

The pier displacement capacity Δ_c is the summation of Δ_{c1} and Δ_{c2}, which can be estimated by following equations:

$$\Delta_{c1} = \Delta_{Y1}^{col} + \Delta_{p1} \quad , \quad \Delta_{c2} = \Delta_{Y2}^{col} + \Delta_{p2} \qquad (\text{Eq.}\, 9-2)$$

$$\Delta_{Y1}^{col} = \frac{L_1^2}{3} \times \emptyset_{Y1} \quad , \quad \Delta_{Y2}^{col} = \frac{L_2^2}{3} \times \emptyset_{Y2} \qquad (\text{Eq.}\, 9-3)$$

$$\Delta_{p1} = \theta_{p1} \times \left(L_1 - \frac{L_{p1}}{2}\right) \quad , \quad \Delta_{p2} = \theta_{p2} \times \left(L_2 - \frac{L_{p2}}{2}\right) \qquad (\text{Eq.}\, 9-4)$$

$$\theta_{p1} = L_{p1} \times \emptyset_{p1} \quad , \quad \theta_{p2} = L_{p2} \times \emptyset_{p2} \qquad (\text{Eq.}\, 9-5)$$

$$\emptyset_{p1} = \emptyset_{u1} - \emptyset_{Y1} \quad , \quad \emptyset_{p2} = \emptyset_{u2} - \emptyset_{Y2} \qquad (\text{Eq.}\, 9-6)$$

where L is the distance from the point of maximum moment to the point of contra-flexure; L_p is equivalent analytical plastic hinge length; Δ_p is the idealized plastic displacement capacity due to rotation of the plastic hinge; Δ_Y^{col} is the idealized yield displacement of the column at the formation of the plastic hinge; θ_p is the plastic rotation capacity; $\emptyset_Y$, $\emptyset_p$, and $\emptyset_u$ are idealized yield curvature, plastic curvature capacity and ultimate curvature, respectively, as illustrated in Figure 9-3. The characteristic curvatures can be obtained from section analysis introduced in Section 5. The point of contra-flexure was assumed to be the center of pier, so the parameters for upper and lower part were adopted at the same values (Δ_{c1}=Δ_{c2}). The displacement capacity Δ_c and parameters to calculate it are summarized in Table 9-3.

Table 9-3: Pier displacement capacity and related parameters

	L (mm)	L_p (mm)	$\emptyset_Y$ (1/m)	$\emptyset_u$ (1/m)	θ_p (1/m)	Δ_Y^{col} (mm)	Δ_p (mm)	Δ_c (mm)
Pier No.1	4267.5	999.6	0.0026	0.075	0.072	47.35	272.67	**640.04**
Pier No.2	2896	780.16			0.056	21.80	141.54	**326.70**

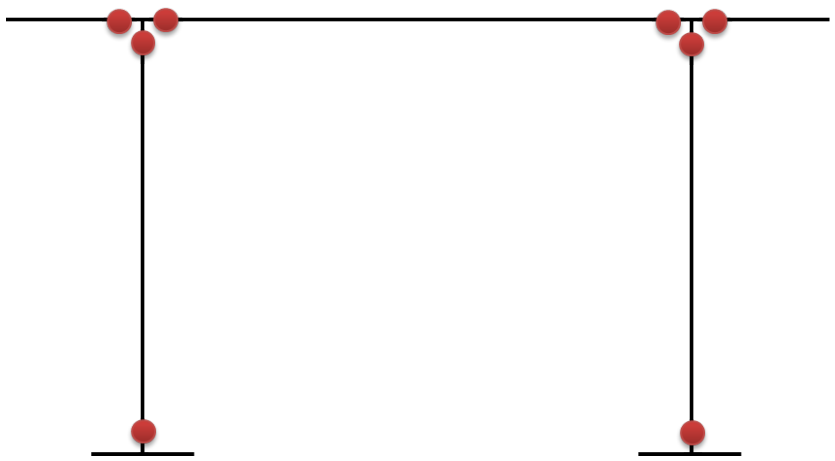

Figure 9-4: Locations of plastic hinges

Pushover analysis was performed in SAP2000 with both longitudinal and transverse loading, with plastic hinges assigned to the locations illustrated in Figure 9-4. For each direction of loading, the analysis was carried out twice with the monitoring point at the top of Pier 1 & Pier 2 (Figure 9-5), respectively. The results for the 4 sets of pushover analysis are presented in Figure 9-6 to 9-9. Overall strength V_b, yield and maximum displacement Δ_Y, Δ_u, as well as ductility factor μ identified from each set of analysis are summarized in Table 9-4. Sequences of hinge formation in both directions are shown in Figure 10 & 11, for transverse and longitudinal direction, respectively

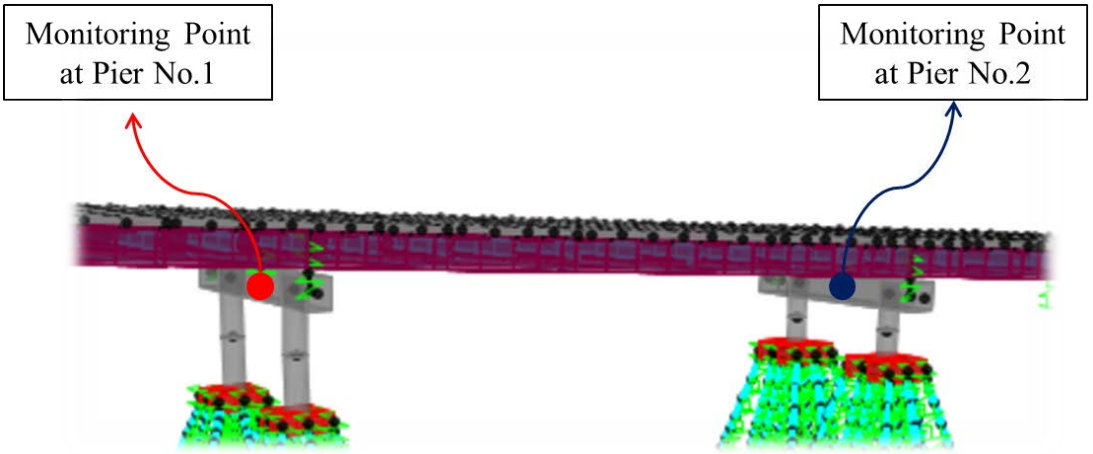

Figure 9-5: Monitoring points for pushover analysis

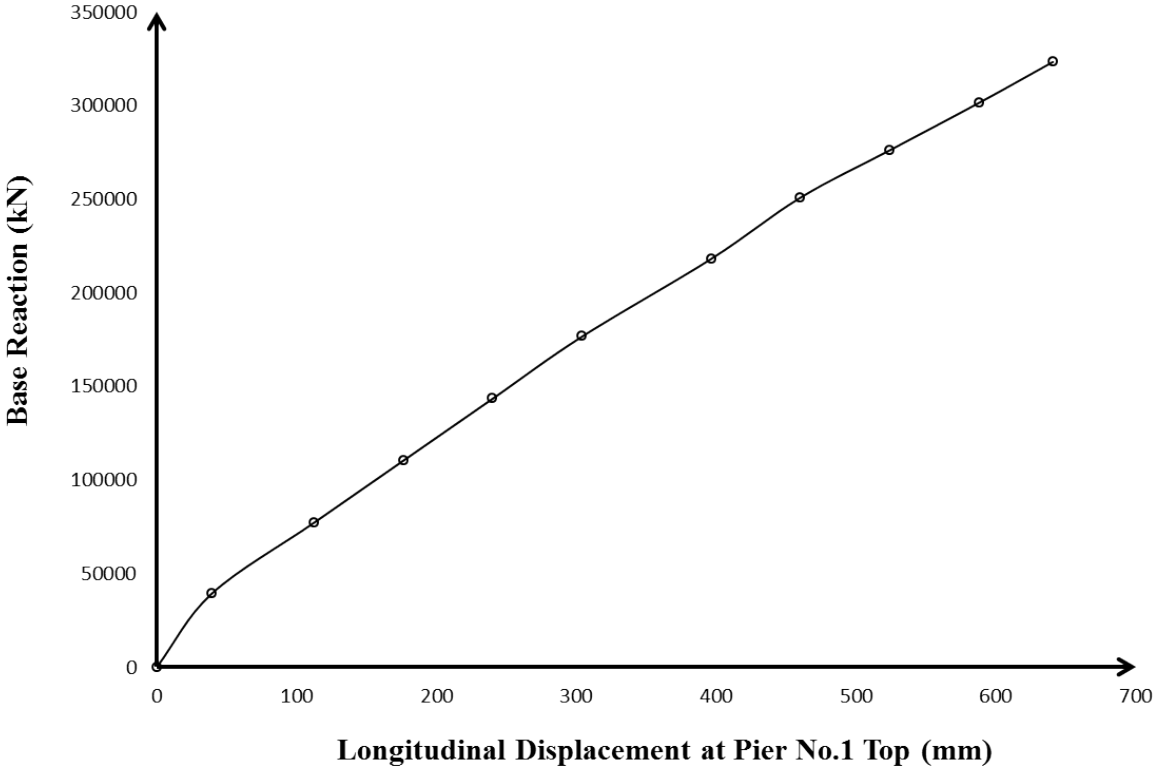

Figure 9-6: Pushover curve in longitudinal direction monitored at Pier No.1 Top

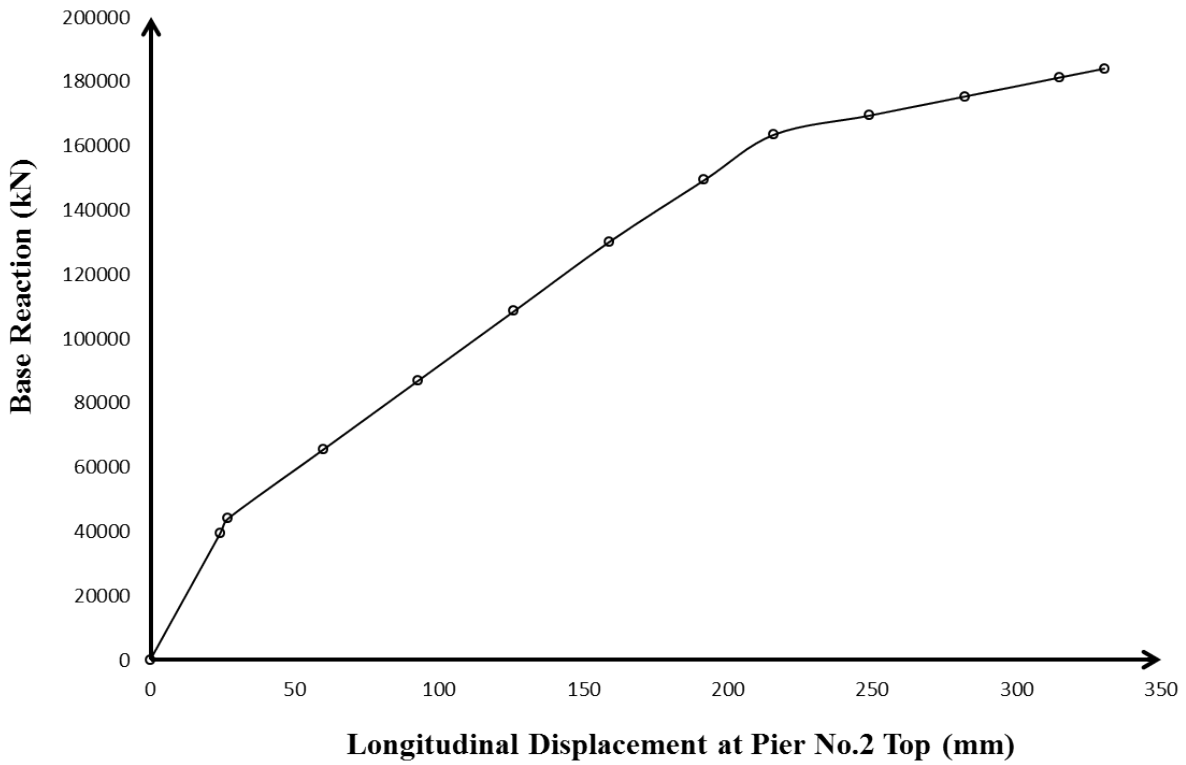

Figure 9-7: Pushover curve in longitudinal direction monitored at Pier No.2 Top

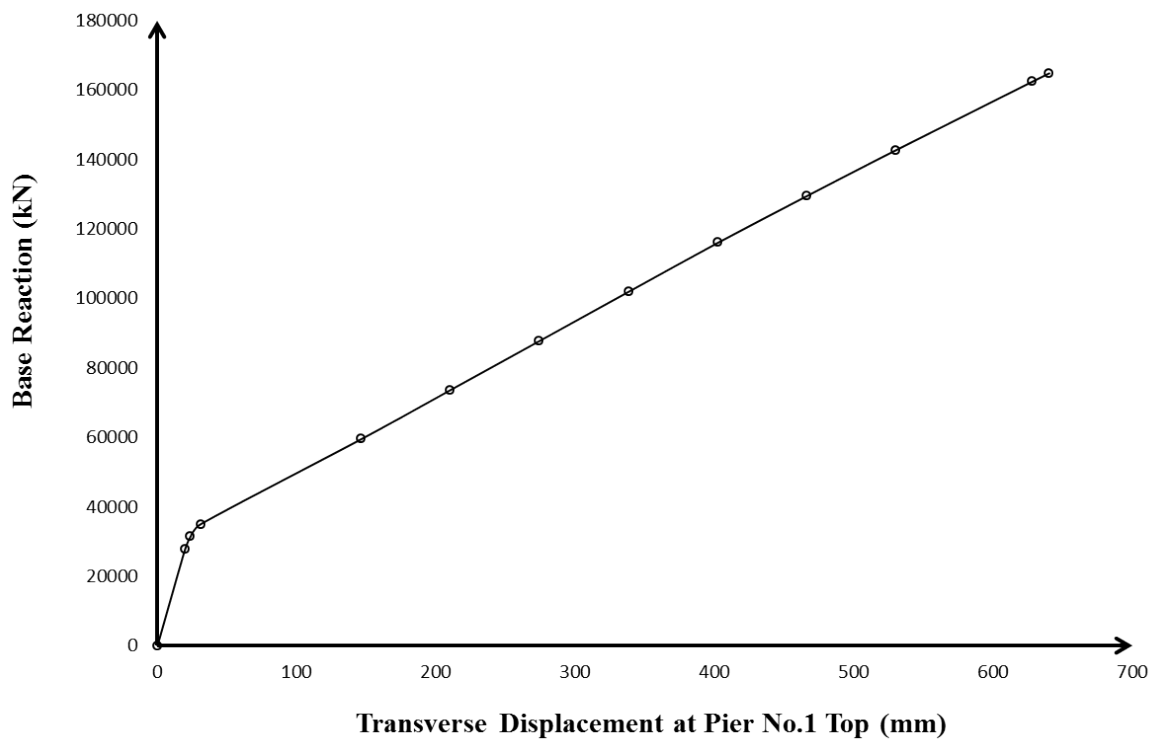

Figure 9-8: Pushover curve in transverse direction monitored at Pier No.1 Top

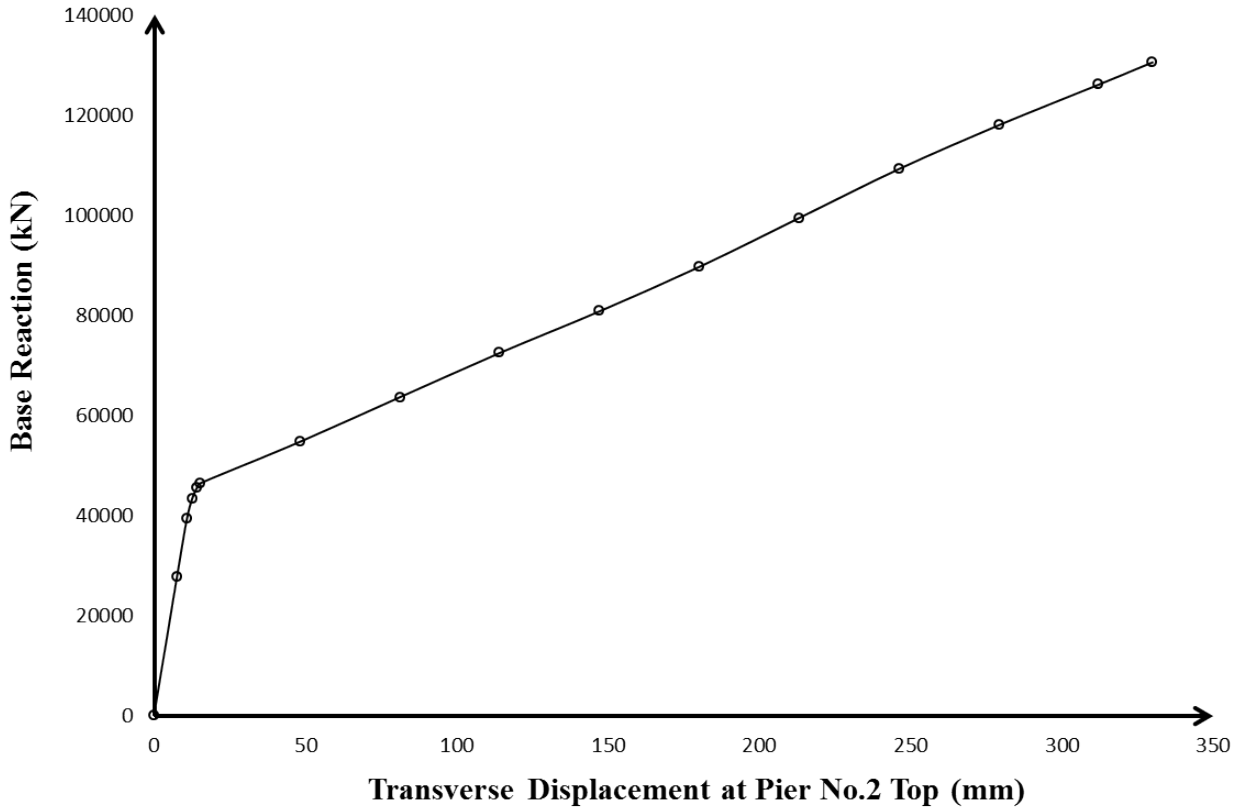

Figure 9-9: Pushover curve in transverse direction monitored at Pier No.2 Top

Table 9-4: Structural capacities estimated from pushover analysis

	Pier No.	Yield V_b	Ultimate V_b	Δ_Y	Δ_u	μ
Longitudinal	1	39271	323223	39.36	640	16.28557
	2	39271	183951	24.17	330	13.65329
Transverse	1	35108	164903	31.036	640	20.62121
	2	46432	130460	15.29	330	21.58273

The figures and table above show that the structural capacities are relevant to the direction of analysis and the location of reference point. However, the yield base shear forces and ductility factors are close for each direction whatever the reference point is. Also, the pushover analysis exhibits that cap beams will not yield before the estimated ultimate displacement.

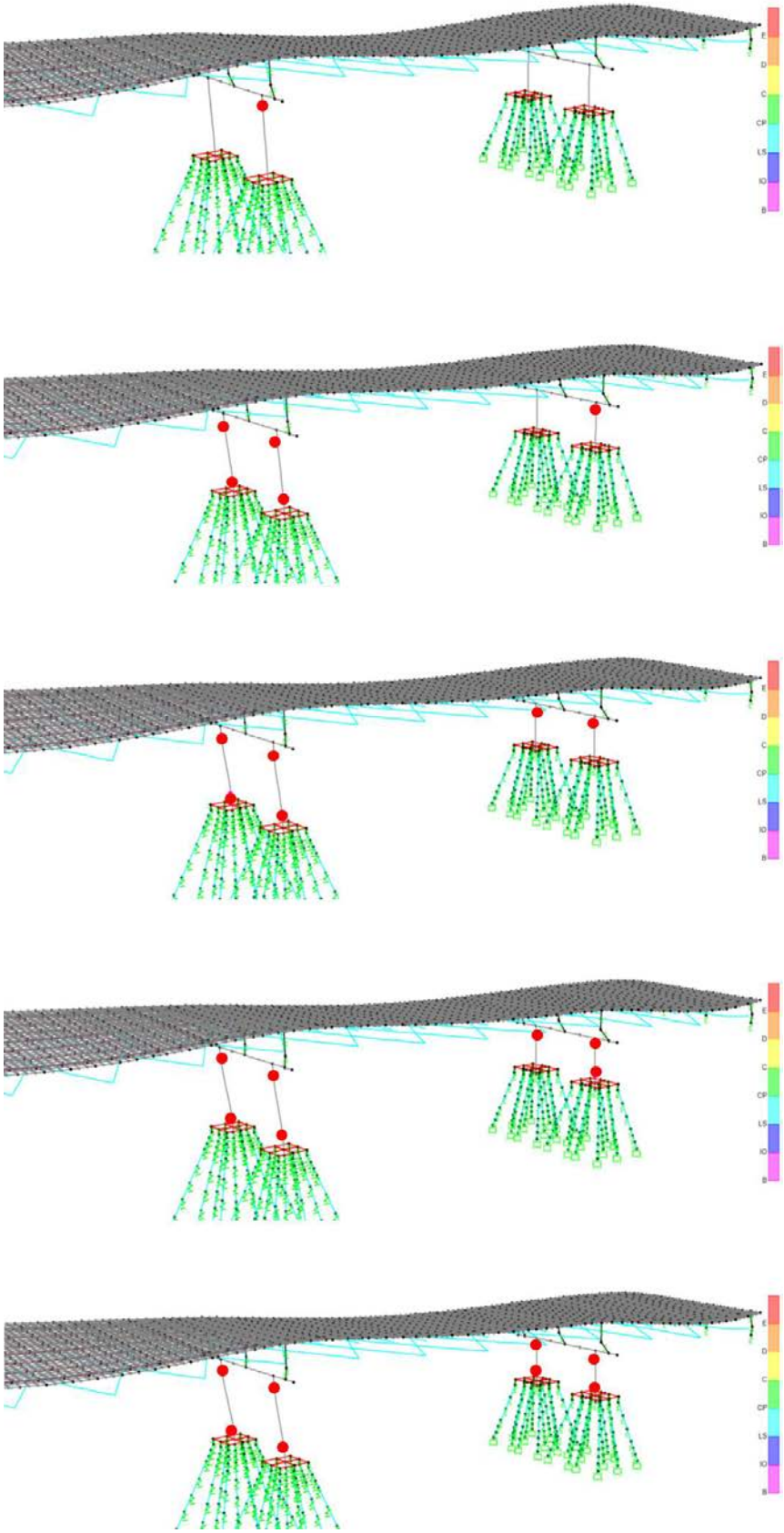

Figure 9-10: Sequence of hinge formation (Transverse direction)

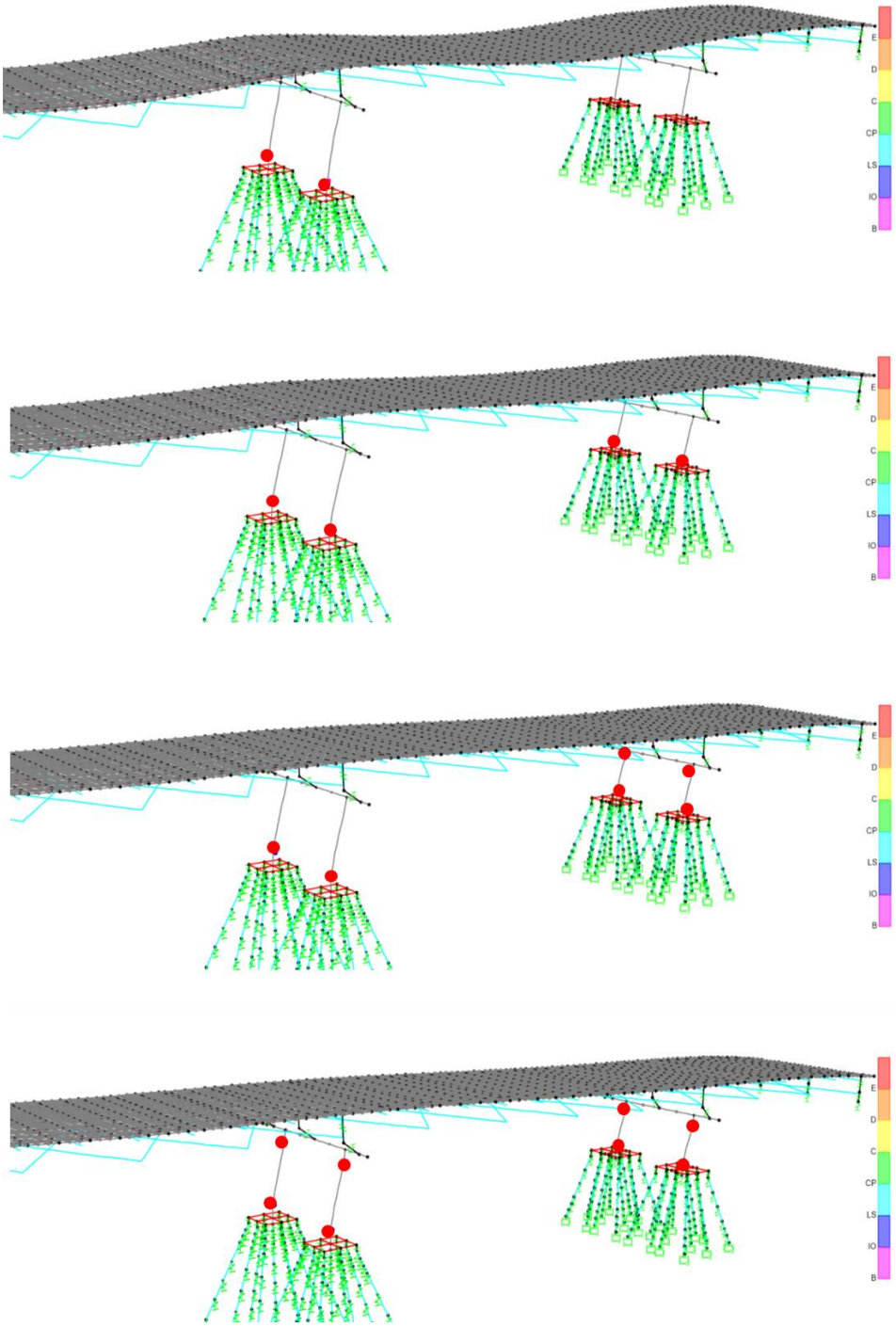

Figure 9-11: Sequence of hinge formation (Longitudinal direction)

9.4. Time-history analysis

9.4.1. General

Time-history analysis is a linear or nonlinear analysis method which provides an evaluation of dynamic structural response under loading which may vary according to the specified time series. The Method is capable of evaluating structural capacities at each time step and allows for the redistribution of internal forces within the structure, which makes it more accurate than the response spectrum analysis. Also, THA does not require establishing a design displacement prior to the analysis which makes it easier to be implemented in engineering practice since the target displacement is difficult to determine with high accuracy and reliability. Therefore, time history analysis was employed in this study to evaluate the seismic response of Portage Creek Bridge.

9.4.2. Solution methods

SAP2000 provides two solution methods for time history analysis: modal method and direct integration method. Both methods are applicable for linear and nonlinear analysis but strength and limitation vary for each solution method.

Modal solution method is recommended for linear elastic analysis with greater efficiency than direct-integration methods and reduced accuracy. (Aviram, Mackie, and Stojadinović 2008) A modal-superposition type of nonlinear analysis is also available in SAP2000 called fast nonlinear analysis (FNA). FNA can significantly reduce the computational and analytical efforts comparing to the direct-integration nonlinear method but is discouraged for bridge structures since it only accounts for nonlinear behavior of Link/Support elements and ignores geometric and material nonlinearity.

Direct-integration method in SAP2000 is a step-by-step solution method which attempt to satisfy dynamic equilibrium at discrete time step. When nonlinear behavior is developed in the structure, the stiffness of the structural system will be recalculated due to the degradation of strength and redistribution of forces. The time-integration methods in SAP2000 include the Newmark's family of methods, Wilson, HHT, Collocation, and Chung and Hulbert, all of which are implicit integration methods so iterations are required at each time step to achieve equilibrium. As recommended by Aviram et al (Aviram, Mackie, and Stojadinović 2008),

Newmark's average acceleration or HHT method shall be used for seismic analysis. In this study, HHT method with α of 0 was adopted initially.

9.4.3. Damping

In time history analysis, damping was defined to represent the energy dissipation of structure. The damping was modeled from the following two sources:

1) Damping matrix applied to the entire structure calculated as a linear combination of the stiffness and mass matrices, which is also referred as Rayleigh damping. Theory of Rayleigh damping can be illustrated in Figure 9-12 and Eq. 9-7. Stiffness and mass proportional damping coefficients was calculated per Eq. 9-8 & 9-9.

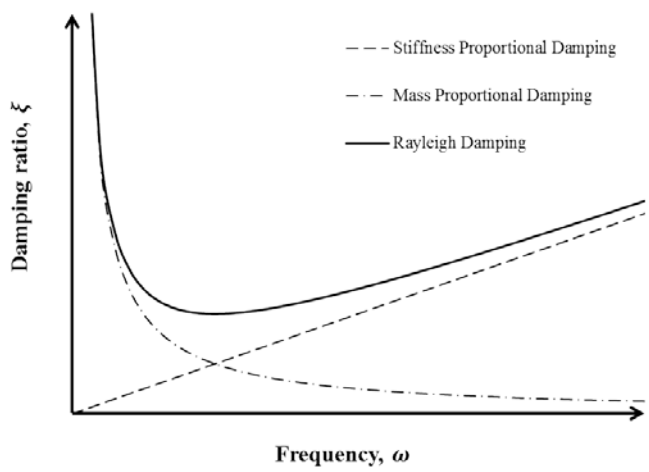

Figure 9-12: Rayleigh damping used for time-history analysis

$$\boldsymbol{C} = \eta \boldsymbol{M} + \delta \boldsymbol{K} \qquad (\text{Eq. } 9-7)$$

where η and δ are given by:

$$\eta = \frac{2\omega_i\omega_j}{\omega_i+\omega_j}\boldsymbol{\xi} \qquad (\text{Eq. } 9-8)$$

$$\delta = \frac{2}{\omega_i+\omega_j}\boldsymbol{\xi} \qquad (\text{Eq. } 9-9)$$

Stiffness proportional damping is linearly proportional to frequency and uses the current tangent stiffness of the structure at each time step. Mass proportional damping is linearly proportional to period. (Chopra 1995)

2) Another source of damping is the damping from nonlinear properties of materials. In SAP2000, stiffness and mass proportional damping can be specified for materials. Also, additional damping can be accounted for through the hysteresis behavior of nonlinear elements, such as plastic hinges and nonlinear Link/Support elements. Therefore, damping ratio defined in terms of proportional damping can be reduced in a nonlinear model. In the analysis model of Portage Creek Bridge, 5% Rayleigh damping was utilized for linear elastic analysis, and 4% damping was adopted for nonlinear analysis because nonlinear structural elements could account for part of energy dissipation. Proportional damping from materials were not included in both analysis types.

9.4.4. Elastic time-history analysis

As mentioned before, fiber hinge requires high computational effort in nonlinear time-history analysis, so hinges at structural elements which are not expected to yield was excluded in nonlinear time-history analysis in order to increase the computational efficiency. Pushover analysis shows that the cap beams will remain elastic before the anticipated ultimate displacement. In order to verify the results from pushover analysis, an elastic time-history analysis was performed though it is not permitted for seismic evaluations. Modal solution method was utilized for elastic time-history analysis so the computation was very fast. Analysis was performed with 11 ground motions and analysis results for primary structural elements are presents below. Flexural responses for piers at each time step are all plotted in Figure 9-13 & 9-14 with the member capacities and performance criteria described in Chapter 8. For shear response of piers and dynamic response of cap beams, only maximum responses at critical sections are identified and summarized in Table 9-5 & 9-6.

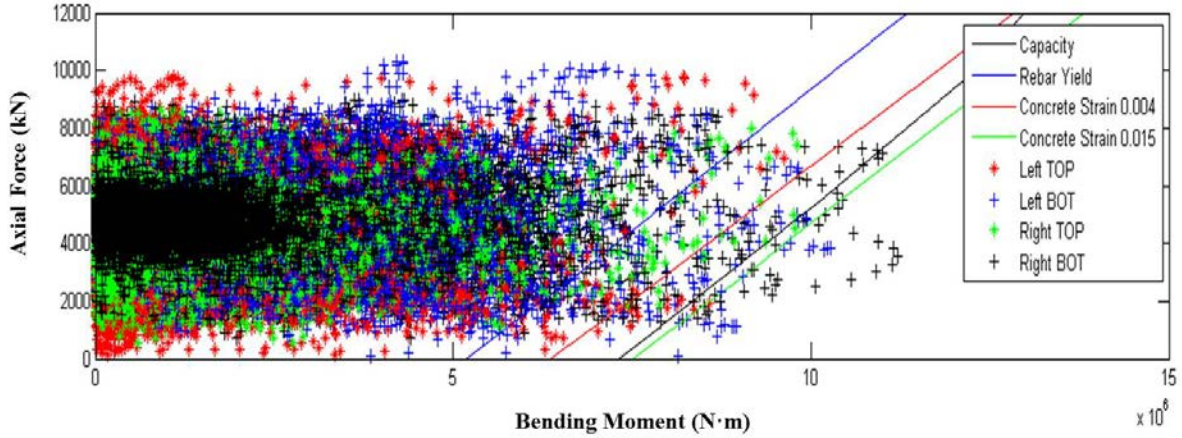

Figure 9-13: Summary of flexural response for Pier No.1 (EDA)

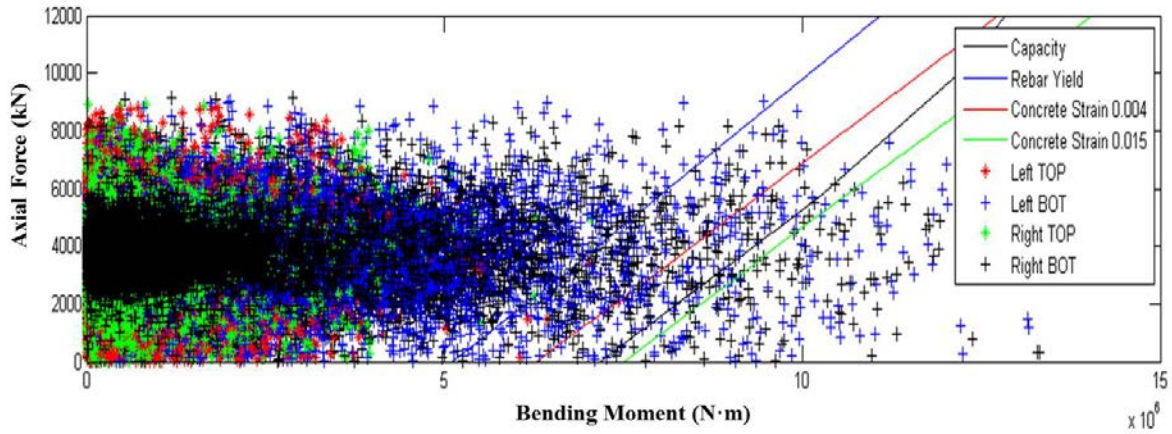

Figure 9-14: Summary of flexural response for Pier No.2 (EDA)

Table 9-5: Summary of shear response for Piers (EDA)

		S22	S33	Max.S	D/C
No.1 Right	TOP	953.02906	2182.6601	2182.6601	**0.41159**
	BOT	1438.81591	1858.3351	1858.3351	**0.350431**
No.1 Left	TOP	1139.32055	2206.769	2206.769	**0.416136**
	BOT	1648.55866	2160.0413	2160.0413	**0.407324**
No.2 Right	TOP	2100.9167	2543.678	2543.678	**0.479668**
	BOT	2630.16446	2085.6118	2630.1645	**0.495977**
No.2 Left	TOP	2149.30758	2464.3167	2464.3167	**0.464702**
	BOT	2674.96252	2543.678	2674.9625	**0.504424**

Table 9-6: Summary of cap beam response (EDA)

		Mmax	D/C	Mmin	D/C	S22	D/C
No.1 Right	Ext	590726.9	0.0414836	-10973874	0.290314	4909.704	0.994874
	Int	6472544.9	0.4545326	-19082561	0.50483	5128.701	1.03925
No.1 Left	Ext	717692.1	0.0503997	-12656439	0.334826	5349.837	1.08406
	Int	2764457	0.1941332	-13021610	0.344487	3620.099	0.733556
No.2 Right	Ext	2569485.8	0.1804414	-11267741	0.298088	4650.627	0.942376
	Int	6130547.9	0.430516	-13149168	0.347862	4162.835	0.843533
No.2 Left	Ext	2028913	0.1424798	-11406508	0.301759	4754.585	0.963442
	Int	3059356.8	0.2148425	-12911658	0.341578	3965.993	0.803646
MAX		**6472544.9**	**0.4545326**	**-10973874**	**0.50483**	**5349.837**	**1.08406**

It can be concluded from the EDA results that piers have a risk of yielding in bending during severe earthquakes while cap beams will remain elastic. Therefore, the plastic hinges at cap beams were not considered in the nonlinear time-history analysis.

9.4.5. Nonlinear time-history analysis

Nonlinear time-history analysis was performed with fiber hinges assigned only at ends of piers. Seismic responses of piers and cap beams are summarized below in the same way with EDA. Since results of NLTHA will be used for seismic evaluation of the bridge, other engineering parameters including bearing response, residual displacements and foundation misalignment are also presented in this section. The mid-point (Figure 9-15) of the bridge was chosen to represent the global displacement because it is expected to undergo the maximum displacement.

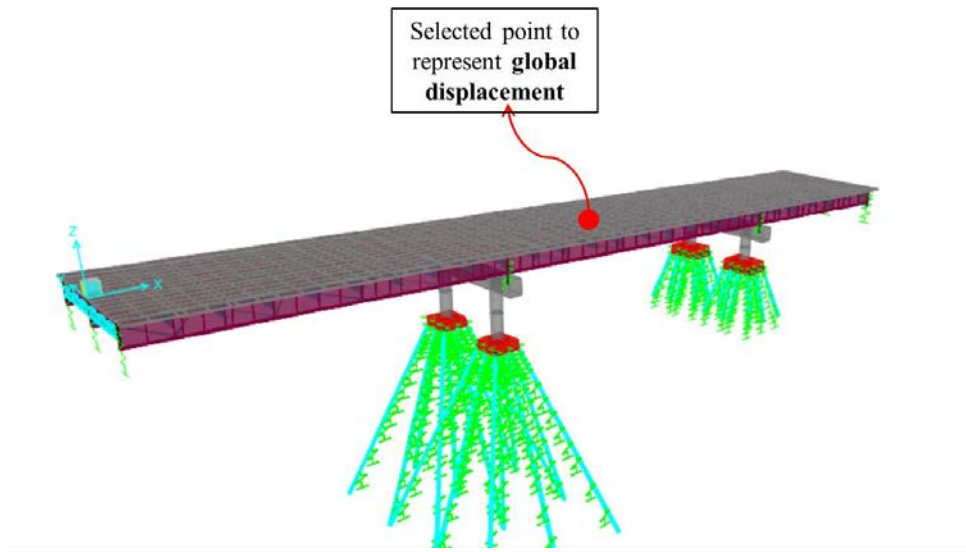

Figure 9-15: Selected point to represent global displacement

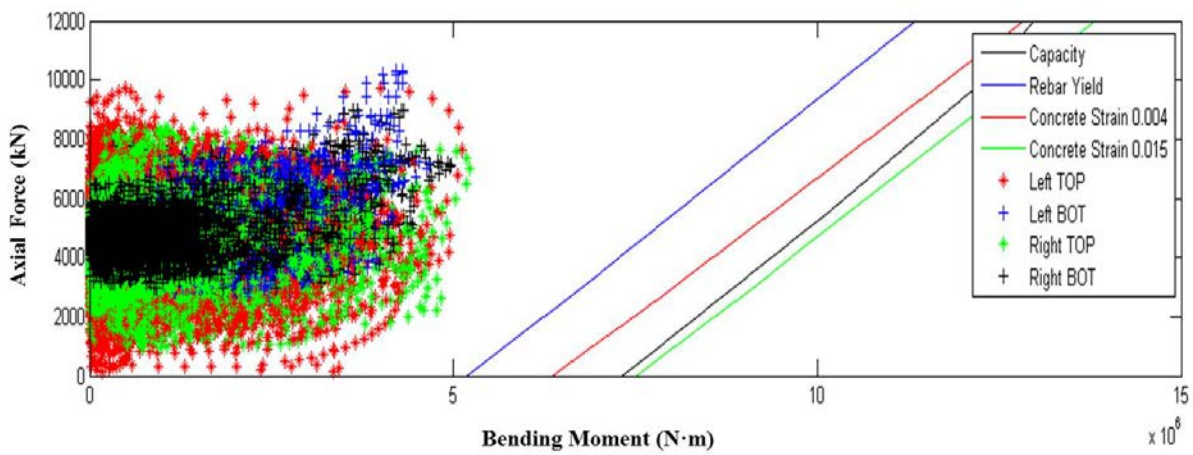

Figure 9-16: Summary of flexural response for Pier No.1 (NLTHA)

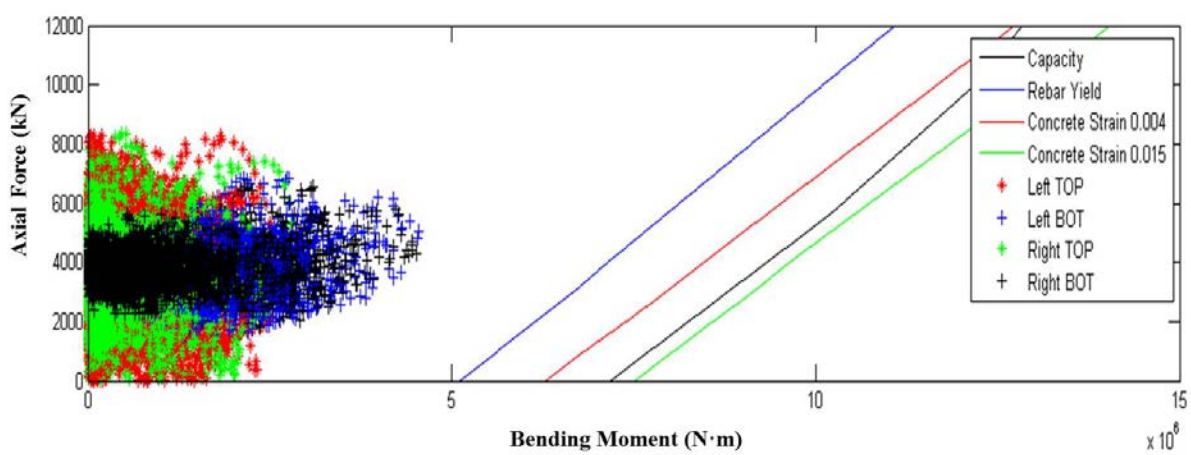

Figure 9-17: Summary of flexural response for Pier No.2 (NLTHA)

Table 9-7: Summary of shear response for piers (NLTHA)

		S22	S33	Max.S	D/C
No.1 Right	TOP	696.21629	1659.2841	1659.2841	**0.312895**
	BOT	959.7736	1361.6674	1361.6674	**0.256773**
No.1 Left	TOP	854.24516	1726.8703	1726.8703	**0.32564**
	BOT	1086.0015	1571.6341	1571.6341	**0.296367**
No.2 Right	TOP	1782.23752	1877.5769	1877.5769	**0.354059**
	BOT	2067.58958	1545.7153	2067.5896	**0.389891**
No.2 Left	TOP	1855.32783	1852.2071	1855.3278	**0.349864**
	BOT	2141.70321	1877.5769	2141.7032	**0.403866**

Table 9-8: Summary of cap beam response (NLTHA)

		Mmax	D/C	Mmin	D/C	S22	D/C
No.1 Right	**Ext**	-88405.5	-0.006208	-10802156	0.285771	4644.691	0.941173
	Int	5449431	0.3826848	-18014237	0.476567	4947.628	1.002559
No.1 Left	**Ext**	428430	0.0300864	-12208318	0.322971	5212.149	1.05616
	Int	1929263.6	0.135482	-13552258	0.358525	3738.516	0.757551
No.2 Right	**Ext**	2319922.1	0.1629159	-10399390	0.275116	4538.77	0.91971
	Int	5481027.9	0.3849036	-13048112	0.345188	4135.602	0.838015
No.2 Left	**Ext**	1552709.6	0.1090386	-10785238	0.285324	4519.619	0.91583
	Int	2036131	0.1429867	-11757735	0.311051	3556.614	0.720692
MAX		**5481027.9**	**0.3849036**	**-10399390**	**0.476567**	**5212.149**	**1.05616**

Table 9-9: Summary of bearing response

	S22	S33	Max.S	D/C
West Right	1775.5601	12383.074	12383.07	7.908601
West Middle	6768.2168	5435.365	6768.217	2.64159
West Left	1705.6671	11850.591	11850.59	7.568525
No.1 Right	631.3156	591.14417	631.3156	0.134399
No.1 Middle	607.44598	597.80438	607.446	0.079027
No.1 Left	580.11601	585.94138	585.9414	0.12474
No.2 Right	576.61104	572.60813	576.611	0.162034
No.2 Middle	575.47762	580.03158	580.0316	0.108664
No.2 Left	530.7032	573.07577	573.0758	0.161041
East Right	3109.8563	9661.6785	9661.679	7.541782
East Middle	3606.607	3082.3011	3606.607	2.047469
East Left	3034.0979	9598.3344	9598.334	7.492336

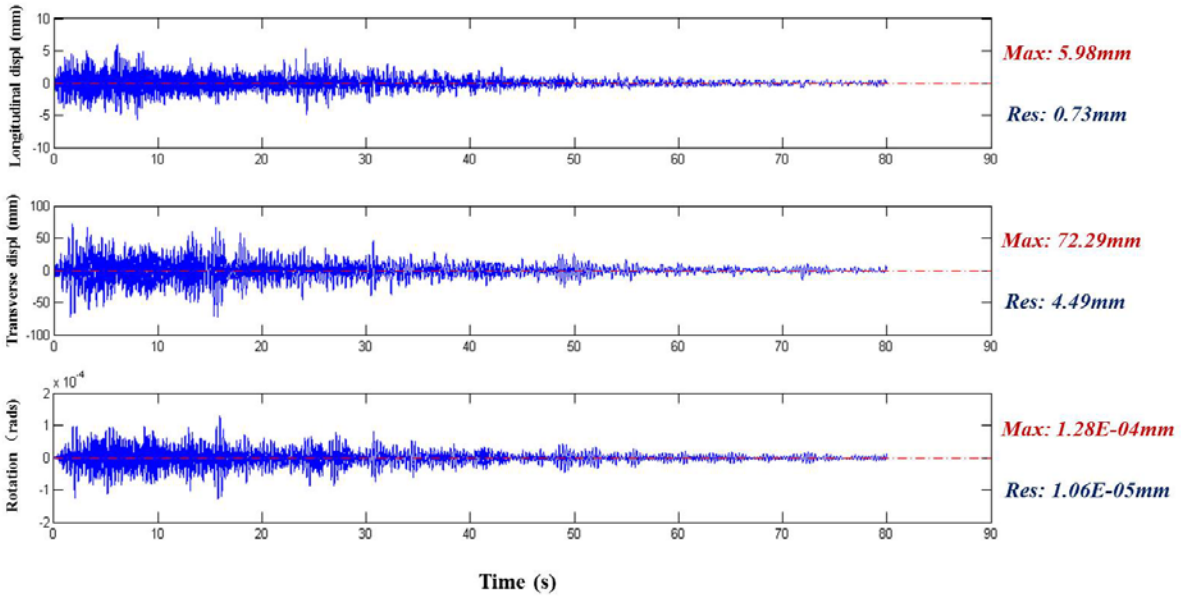

Figure 9-18: Displacement response at mid-point

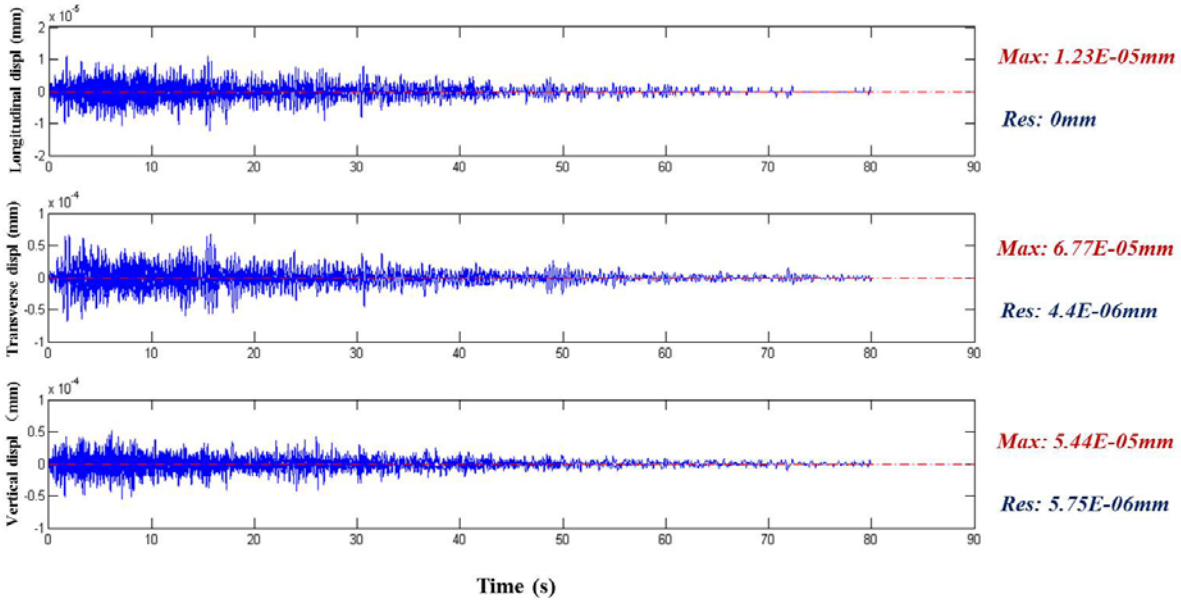

Figure 9-19: Displacement response at west abutment

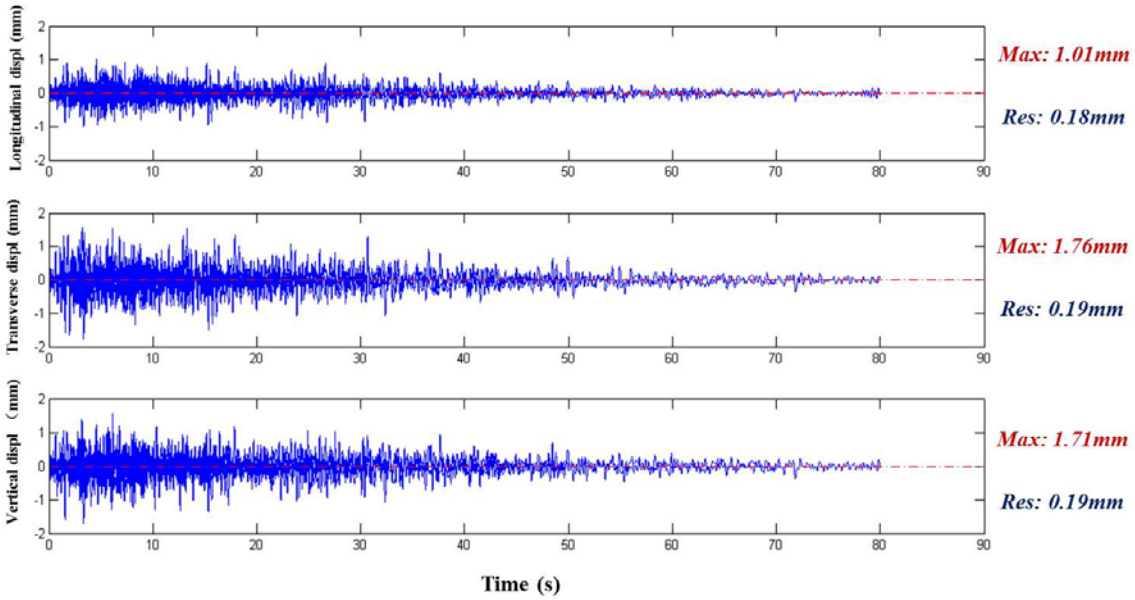

Figure 9-20: Displacement response at the foundation under Pier No.1

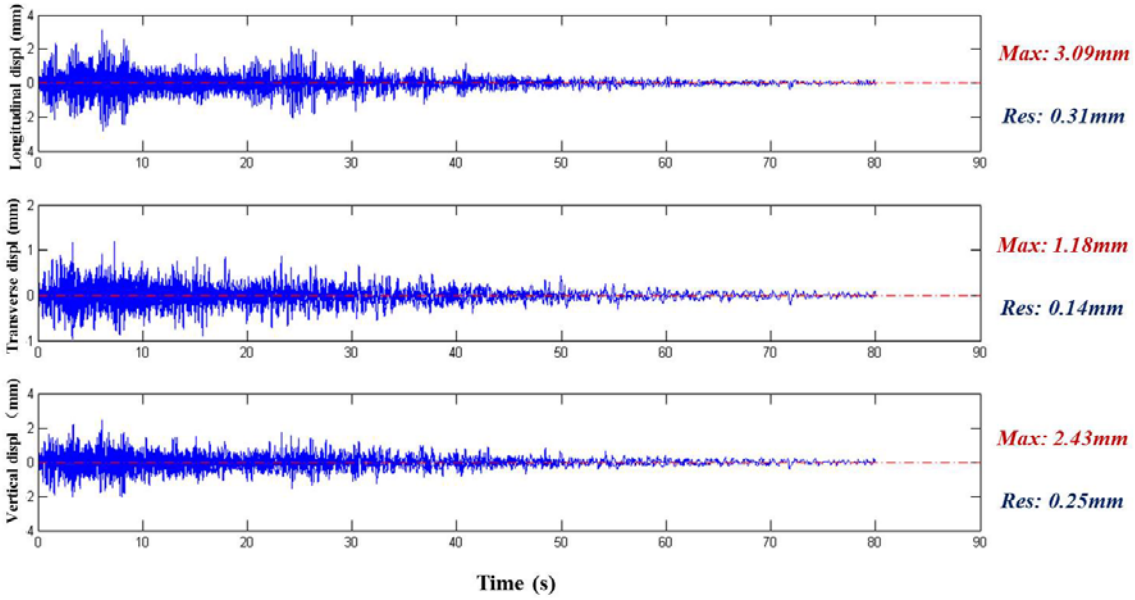

Figure 9-21: Displacement response at the foundation under Pier No.2

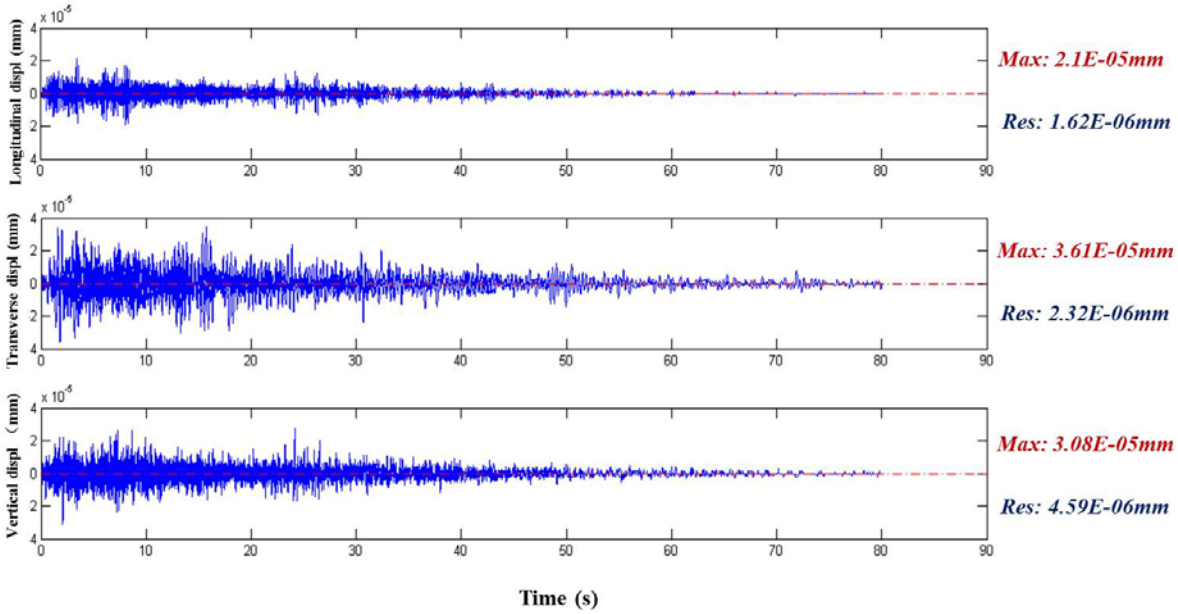

Figure 9-22: Displacement at east abutment

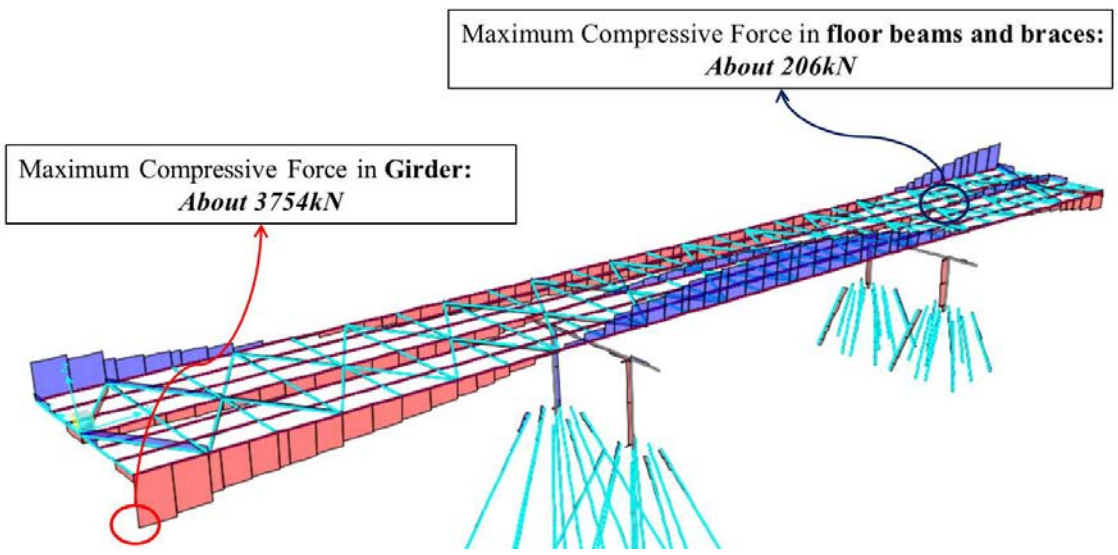

Figure 9-23: Axial force diagram under Tohoku earthquake

9.4.6. Discussion of results

Performance of Portage Creek Bridge can be evaluated in terms of the criteria described in Chapter 8. The evaluation for each structural aspect is presented below:

Concrete structures and connections: Concrete compressive strains do not exceed 0.004 and reinforcing steels do not yield at all the critical sections of substructure, as shown in Figure 9-16 & 9-17 and

Table 9-7 & 9-8. However, the cap beam at Pier No.1 has a risk of failing in shear at its connections with piers. The flexural response is significantly reduced in nonlinear analysis, which could explain why a response reduction factor is required by the code in elastic dynamic analysis.

Steel Structures: Steel structures are all assigned in superstructure so they are secondary members. CSA S06-14 allows the buckling of secondary steel members but the structural instability is not permitted. Since the girders and stringers are casted together with the concrete decking, their stability can be ensured. For the floor beams and braces, the analysis results shows that both of them will not experience large axial forces under major earthquakes, so the instability issues are not possible to occur. Axial force diagram obtained from seismic analysis under Tohoku earthquake records is shown in Figure 9-23 as example. It shows that the maximum axial force in braces and floor beams is only about 200kN which is much smaller than the buckling forces calculated from Euler's equation (See Table 8-3).

Bearings: Elastomeric bearings at east and west abutments shall be replaced while the ones on the pier caps are not damaged, as shown in Table 9-9.

Displacements: Figure 9-14 shows that no obvious permanent offset or residual displacements occur after major earthquakes so the displacement criteria are satisfied.

Foundations: Foundation movements were checked at four points (foundation under west & east abutment, pier No.1&2). The analysis results show that the misalignment or settlement of the foundations under abutments and piers are ignorable, as shown in Figure 9-15 to 9-18. Therefore, the foundation condition is acceptable.

Chapter 10: Conclusions

The results of the study show that during severe earthquake: 1) there will be some inelastic behavior for the primary members (piers, cap beams and girders) of the bridge but the moment capacities of these members meet the demands; 2) the shear capacity of cap beam at Pier No.1 is not adequate. Since shear failure is brittle failure which is not convenient to be repaired in place, the seismic performance of cap beam is not acceptable according to CSA S06-14; 3) elastomeric bearings at east and west abutments will be damaged but can be replaced in place after the earthquake. Thus the conditions of the bridge bearings are acceptable; 4) there are no permanent offsets and residual displacements for both the superstructure and foundation so the displacement-related criteria are satisfied.

Given the fact that the cap beam at Pier No.1 has a high risk of failure in shear which is fatal in severe earthquake and cannot be repaired in place after earthquake, Portage Creek Bridge does not meet the seismic performance criteria specified in Canadian Highway Bridge Design Code. Seismic retrofit is necessary to ensure the safety of this bridge in potential major earthquake.

Future work will include 1) a research of the state of art retrofit techniques which are capable of enhancing the shear capacity of beams in an economical and efficient way; 2) retrofit design of the bridge and re-assessment of seismic performance after the retrofit.

References

Adams, John, and Stephen Halchuk. 2003. Fourth Generation Seismic Hazard Maps of Canada: Values for over 650 Canadian Localities Intended for the 2005 National Building Code of Canada. Geological Survey of Canada.

Akogul, Can, and Oguz C. Celik. 2008. “Effect of Elastomeric Bearing Modeling Parameters on the Seismis Design of RC Highway Bridges with Precast Concrete Girders.” Proceedings of the 14th World Conference on Earthquake Engineering.

Asaei, S. Mohsen S., Tze Liang Lau, Norazura Muhammad Bunnori, and others. 2012. “Experimental and Numerical Verification of the Retrofitted RC Columns Using FRP-A State of the Art Review.” Caspian Journal of Applied Sciences Research 1 (9): 38–55.

Aviram, Ady, Kevin Rory Mackie, and Božidar Stojadinović. 2008. Guidelines for Nonlinear Analysis of Bridge Structures in California. Pacific Earthquake Engineering Research Center.

Brincker, Rune, C. Ventura, and Palle Andersen. 2001. “Damping Estimation by Frequency Domain Decomposition.” IMAC XIX, Kissimmee, USA 9: 72.

Brincker, Rune, Lingmi Zhang, and P. Andersen. 2000. “Modal Identification from Ambient Responses Using Frequency Domain Decomposition.” Proc. of the 18*‘International Modal Analysis Conference (IMAC), San Antonio, Texas.

Caltrans, S. D. C. 2010. “Caltrans Seismic Design Criteria Version 1.6.” California Department of Transportation, Sacramento.

Chadwell, C. B., and R. A. Imbsen. 2004. “XTRACT: A Tool for Axial Force-Ultimate Curvature Interactions.” Struct. ASCE Library.

Chopra, Anil K. 1995. Dynamics of Structures. Vol. 3. Prentice Hall New Jersey.

Das, Braja. 2015. Principles of Foundation Engineering. Cengage learning.

Dj Amar, Bouzid . 2013. “Winkler Springs (p-Y Curves) for Pile Design from Stress-Strain of Soils: FE Assessment of Scaling Coefficients Using the Mobilized Strength Design Concept.” Geomechanics and Engineering 5 (5). doi:10.12989/gae.2013.5.5.379.

Fahmy, Mohamed FM, and Zhishen Wu. 2010. “Evaluating and Proposing Models of Circular Concrete Columns Confined with Different FRP Composites.” Composites Part B: Engineering 41 (3): 199–213.

Habibullah, A., and E. L. Wilson. 1996. “SAP2000 User’s Manual.” Computers & Structures, Inc.

Huffman, Sharlie, Ashutosh Bagchi, Aftab Mufti, Kenneth Neale, Dennis Sargent, and Evangeline Rivera. 2006. “GFRP Seismic Strengthening and Structural Heath Monitoring of Portage Creek Bridge Concrete Columns.”

Kerr, Arnold D. 1964. “Elastic and Viscoelastic Foundation Models.” Journal of Applied Mechanics 31 (3): 491–98.

Lam, L., and J. G. Teng. 2003. “Design-Oriented Stress–strain Model for FRP-Confined Concrete.” Construction and Building Materials 17 (6): 471–89.

Levin, R. I., and N. A. J. Lieven. 1998. “Dynamic Finite Element Model Updating Using Simulated Annealing and Genetic Algorithms.” Mechanical Systems and Signal Processing 12 (1): 91–120.

Love, Augustus Edward Hough. 1888. “The Small Free Vibrations and Deformation of a Thin Elastic Shell.” Philosophical Transactions of the Royal Society of London. A 179: 491–546.

Malvar, L. Javier, John E. Crawford, James W. Wesevich, and Don Simons. 1997. “A Plasticity Concrete Material Model for DYNA3D.” International Journal of Impact Engineering 19 (9): 847–73.

Mander, John B., Michael JN Priestley, and R. Park. 1988. “Theoretical Stress-Strain Model for Confined Concrete.” Journal of Structural Engineering 114 (8): 1804–26.

Marwala, Tshilidzi. 2002. “Finite Element Model Updating Using Wavelet Data and Genetic Algorithm.” Journal of Aircraft 39 (4): 709–11.

———. 2010. Finite Element Model Updating Using Computational Intelligence Techniques: Applications to Structural Dynamics. Springer Science & Business Media.

McGuire, R. 1995. “EZ-FRISK, User’s Manual”, RISK Engineering, Boulder, Co.”

Mindlin, Raymond D. 1951. “Influence of Rotary Inertia and Shear on Flexural Motions of Isotropic Elastic Plates.”

MoHo s.r.l. 2011. “TROMINO User’s Manual.”

Priestley, MJ Nigel, Frieder Seible, and Gian Michele Calvi. 1996. Seismic Design and Retrofit of Bridges. John Wiley & Sons.

Richart, Frank Erwin, Anton Brandtzaeg, and Rex Lenoi Brown. 1928. “A Study of the Failure of Concrete under Combined Compressive Stresses.” University of Illinois Bulletin; v. 26, No. 12.

Solutions, Structural Vibration. 2001. ARTeMIS Extractor: Ambient Response Testing and Modal Identification Software, User’s Manual. Demark.

Tedesco, J. W., J. C. Powell, C. Allen Ross, and M. L. Hughes. 1997. “A Strain-Rate-Dependent Concrete Material Model for ADINA.” Computers & Structures 64 (5): 1053–67.

Timoshenko, Stephen P., and James M. Gere. 2009. Theory of Elastic Stability. Courier Corporation.

Turgay, T., H. O. Köksal, Z. Polat, and C. Karakoc. 2009. “Stress–strain Model for Concrete Confined with CFRP Jackets.” Materials & Design 30 (8): 3243–51.

Venture, NEHRP Consultants Joint. 2011. “Selecting and Scaling Earthquake Ground Motions for

Performing Response-History Analyses." NIST GCR, 11–917.

Wu, Zhaohua, Norden E. Huang, Steven R. Long, and Chung-Kang Peng. 2007. "On the Trend, Detrending, and Variability of Nonlinear and Nonstationary Time Series." Proceedings of the National Academy of Sciences 104 (38): 14889–94.

Appendices

A.1 Details of elastomeric bearings

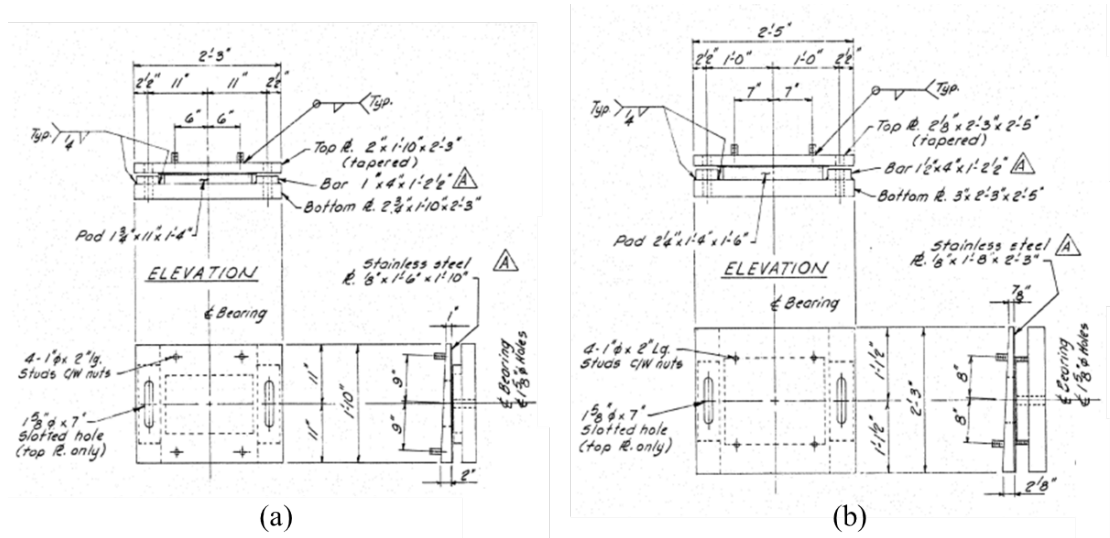

(a) (b)

Figure A-1: Bearing at west abutment under (a) exterior girder (b) interior girder

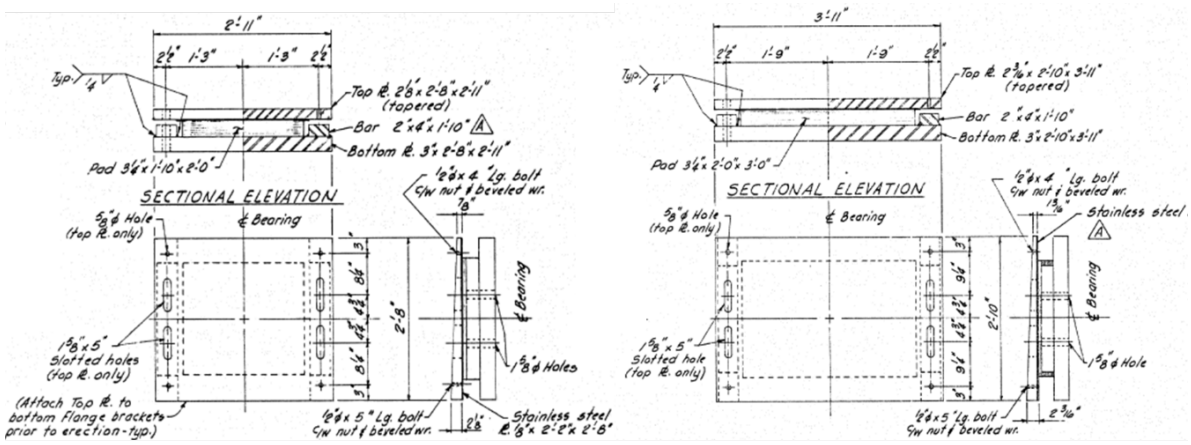

(a) (b)

Figure A-2: Bearing at Pier No.1 under (a) exterior girder (b) interior girder

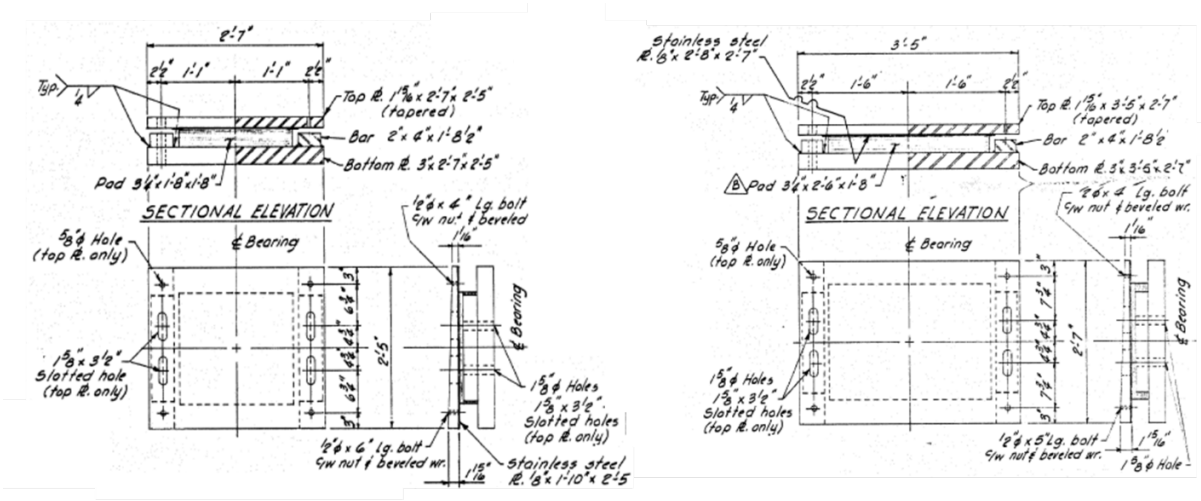

(a) (b)

Figure A-3: Bearing at Pier No.2 under (a) exterior girder (b) interior girder

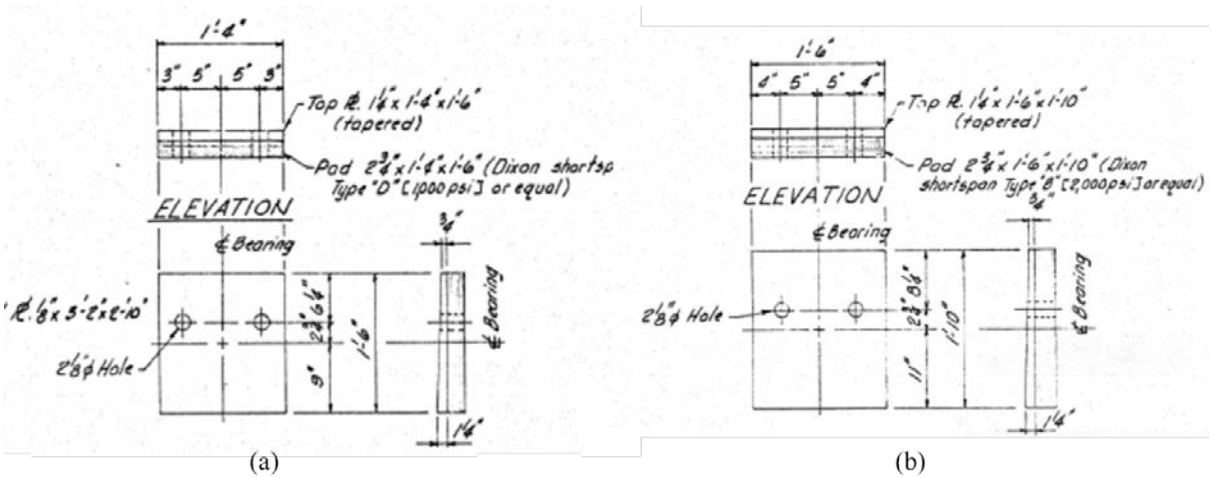

(a) (b)

Figure A-4: Bearing at east abutment under (a) exterior girder (b) interior girder

A.2 Section size of structural steel

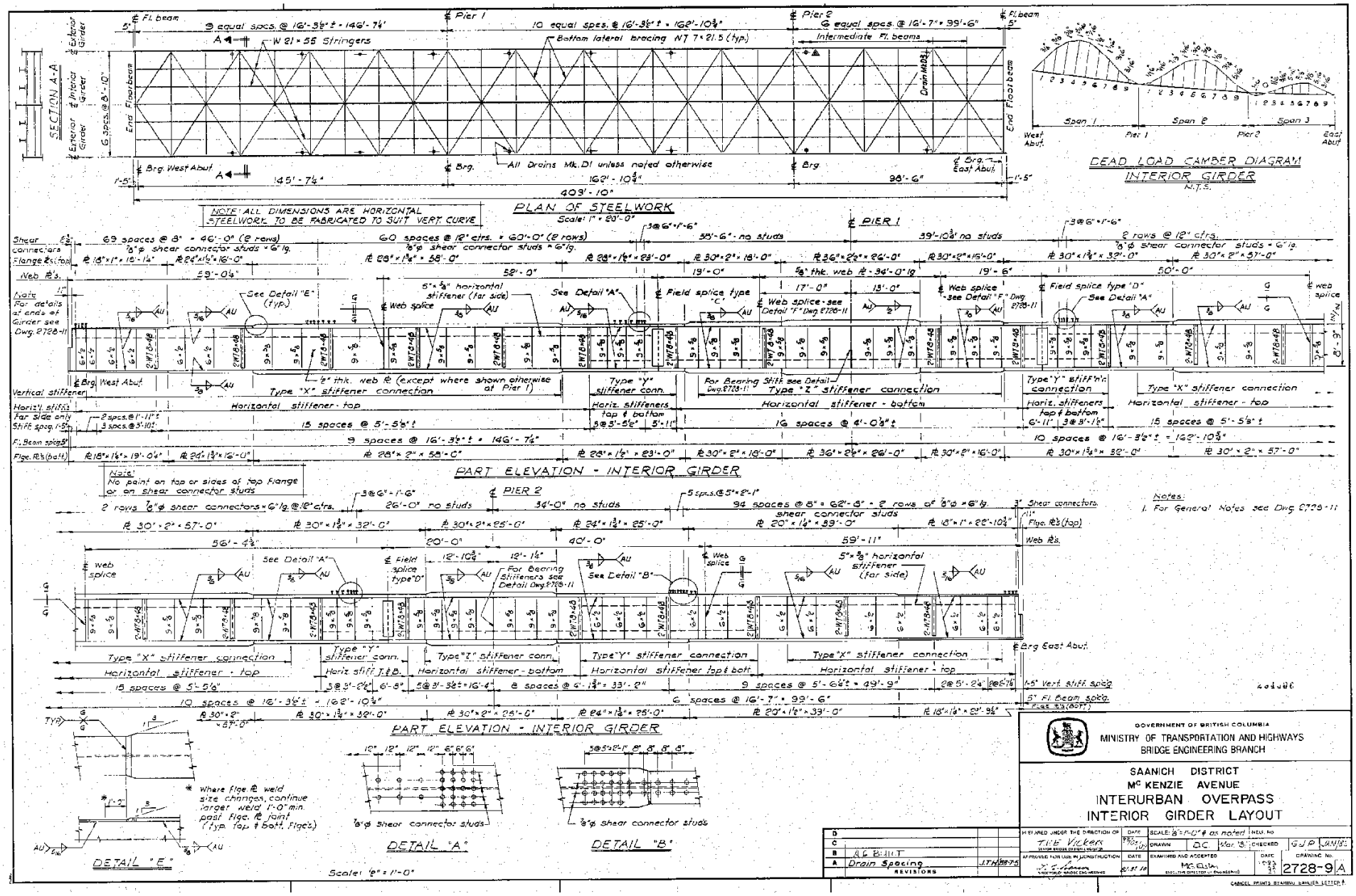

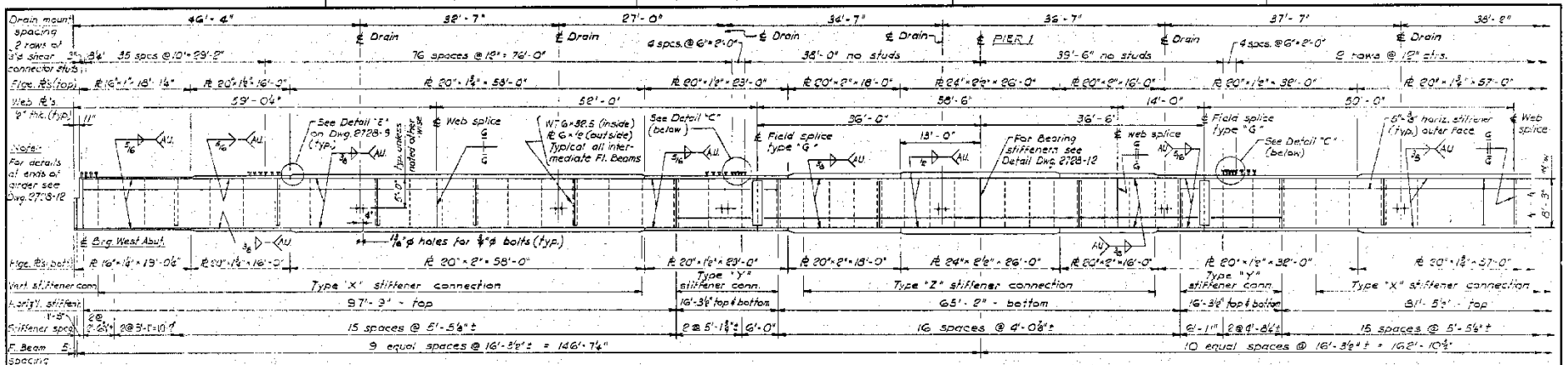

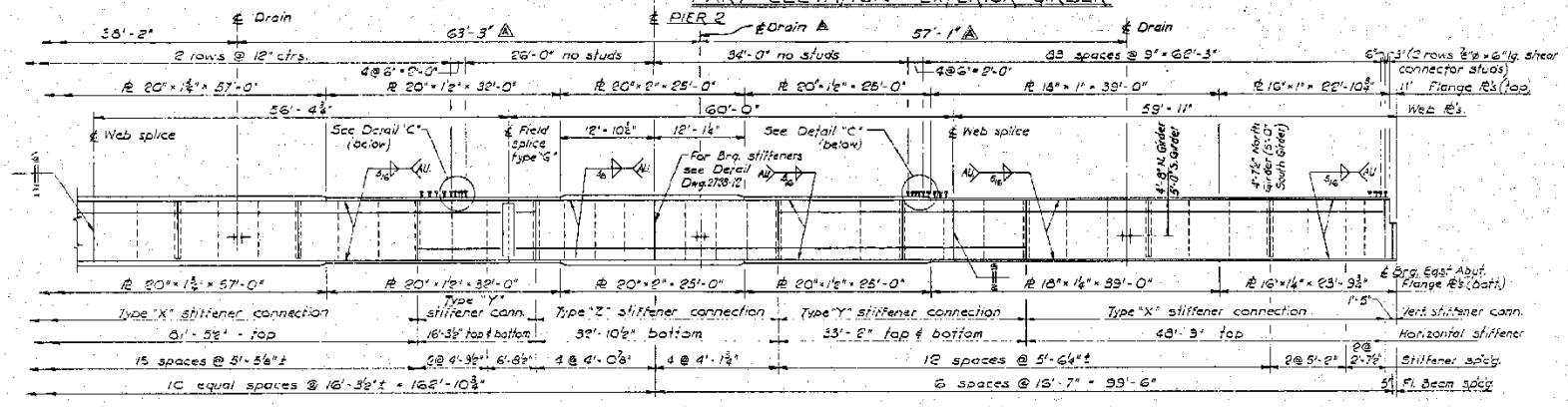

NOTES:
All vertical stiffeners to be PL 6" × ⅜" & to be on inner face of girder except at Floor Beam connections where they are on outer face

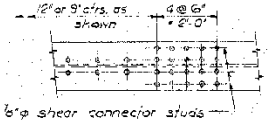

DETAIL "C"
Scale: ⅜" = 1'-0"

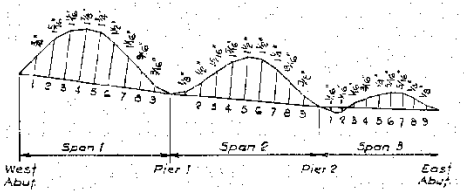

DEAD LOAD CAMBER DIAGRAM
EXTERIOR GIRDERS
N.T.S.

Notes:
For General Notes see Dwg. 2728-11

GOVERNMENT OF BRITISH COLUMBIA
MINISTRY OF TRANSPORTATION AND HIGHWAYS
BRIDGE ENGINEERING BRANCH

SAANICH DISTRICT
McKENZIE AVENUE
INTERURBAN OVERPASS
EXTERIOR GIRDER LAYOUT

D		
C		
B	AS BUILT	
A	Drain Spacing	J.T.H. 88-7-5
	REVISIONS	

PREPARED UNDER THE DIRECTION OF: T.V.E. Vickers, SENIOR BRIDGE DESIGN ENGINEER — DATE: Mar/87
SCALE: ⅛" = 1'-0" & as noted — REG. No.
DRAWN: D.C. Mar/87 — CHECKED: G.J.P. JAN/88
APPROVED FOR USE IN CONSTRUCTION: DIRECTOR OF BRIDGE ENGINEERING — DATE: 88-12-19
EXAMINED AND ACCEPTED: REGIONAL DIRECTOR (ENGINEERING) — DATE
DRAWING No. 2728-10 A

CANCEL PRINTS BEARING EARLIER LETTER